

**POLYPYRROLE AND COMPOSITE MATERIALS FOR
ELECTROCHEMICAL CAPACITORS**

By

SHILEI CHEN, M. ENG., B. ENG.

A Thesis submitted to the School of Graduate Studies in Partially
Fulfillment of the Requirements for the Degree Doctor of Philosophy

McMaster University

© Copyright by Shilei Chen, July 2015

DOCTOR OF PHILOSOPHY (2015)

McMaster University

Department of Materials Science & Engineering

Hamilton, Ontario

TITLE: Polypyrrole and Composite Materials for Electrochemical Capacitors

AUTHOR: Shilei Chen, M. Eng. (Tsinghua University), B. Eng. (Tsinghua University)

SUPERVISOR: Igor Zhitomirsky, Distinguished Professor, Ph.D., P.Eng.

NUMBER OF PAGES: xxv, 155

Abstract

In this research, different anionic dopants were investigated for the fabrication of polypyrrole (PPy) electrode materials for electrochemical capacitors (ECs). Anionic dopants from catechol, salicylic acid and chromotropic acid family allowed for the formation of adherent PPy thin film on stainless steels current collectors by electropolymerization. Comparison between galvanostatic and pulse electropolymerization of PPy thin films was made. Pulse electropolymerization was found to provide improved impregnation of Ni plaque current collectors and formation of nanostructured coating. The electrodes prepared by pulse electropolymerization showed higher porosity, lower electrical resistance, higher capacitance and improved cyclic stability.

In order to overcome the mass loading limitation for thin film PPy electrodes, chemical polymerization of PPy was investigated. The use of fine particles, prepared by the chemical polymerization method, allows impregnation of Ni foams and fabrication of porous electrodes with high materials loading. Moreover, improved capacitive performance and cyclic stability was obtained for PPy electrodes with high materials loading using new anionic dopants.

To further improve the cyclic stability of PPy electrodes, multiwalled carbon nanotubes (MWCNT) were used for the fabrication of PPy-MWCNT composite materials due to their high surface area and excellent conductivity. Different dispersants as well as dispersing methods were studied in order to obtain stable MWCNT suspensions. Among those dispersants, multifunctional anionic dopants were found to benefit the formation of

MWCNT suspension as well as the polymerization of PPy. A conceptually new approach has been developed for the fabrication of PPy coated MWCNT based on the use of multifunctional anionic dopants.

The use of PPy coated MWCNT allowed excellent electrochemical performance for high active mass loadings, required for commercial EC applications. The electrodes and devices made of PPy coated MWCNT showed high capacitance, good capacitance retention at high charge-discharge rates and good cycling stability. The record high capacitance achieved at high charge-discharge rates is promising for the development of high power ECs.

Key words: polypyrrole, carbon nanotubes, dispersion, electropolymerization, chemical polymerization, devices, electrochemical capacitors.

Acknowledgements

The work described in this thesis could not have been finished without the instruction of my supervisor Dr. Igor Zhitomirsky. I deeply appreciate him for his solid expertise, selfless support and patience and tolerance throughout the whole process of my Ph.D. study in McMaster University. I would also like to express my gratitude to the members of my supervisory committee: Dr. Marek Niewczas and Dr. Gu Xu for their support and helpful advises.

I would also like to thank the following people for their technical support for my research: Jim Britten, Steve Koprach, Chris Butcher, Xiaogang Li, Ed McCaffery and Doug Culley. The work cannot go smoothly without their help.

The enormous help from my colleagues in the group: Xin Pang, Yaohui Wang, Mustafa Ata, Yanchao Sun, Lijia Yang, Xiaofei Zhu, Yisong Su, Kaiyuan Shi, Yangshui Liu, Yeling Zhu, Dan Luo, and Tianshi Zhang, Patrick Wojtal, Cameron Wallar are also acknowledged here.

In the end, I would like to dedicate this thesis to my husband, Huaxiang Shen and my parents for their encouragement and support. Your support is the biggest motivation in my life.

Declaration of Academic Achievements

This dissertation was used to fulfill the requirements of Ph.D. degree. The major research project was undertaken from September 2011 to July 2015. The author of this dissertation and the supervisor are the major contributor to the presented materials. As the primary author, contributions included: literature review, proposal and approaches, experiments setup, materials synthesis, sample preparation, materials characterization, electrochemical tests, data analysis, journal paper writing.

The results of this dissertation were published in 8 papers in peer-reviewed journals. The published papers are listed below.

1. Chen S, and Zhitomirsky I. Polypyrrole electrodes doped with sulfanilic acid azochromotrop for electrochemical supercapacitors. *Journal of Power Sources*, 2013. **243**(0): 865-871.
2. Chen S, and Zhitomirsky I. Influence of dopants and carbon nanotubes on polypyrrole electropolymerization and capacitive behavior. *Materials Letters*, 2013. **98**(0): 67-70.
3. Chen S, and Zhitomirsky I. Capacitive behaviour of polypyrrole, prepared by electrochemical and chemical methods. *Materials Letters*, 2014. **125**(0): 92-95.
4. Chen S, and Zhitomirsky I. Polypyrrole coated carbon nanotubes for supercapacitors, prepared using indigo carmine as a dispersant and dopant. *Materials Letters*, 2014. **135**(0): 47-50.

5. Chen S, and Zhitomirsky I. Influence of Additives on Performance of Polypyrrole–Carbon Nanotube Supercapacitors. *Materials and Manufacturing Processes*, 2015: 1-7.

6. Chen S, and Zhitomirsky I. Influence of multifunctional dopants on capacitive behavior of polypyrrole-carbon nanotube ECs. *Materials and Manufacturing Processes*, submitted.

In addition to the work presented here, I co-authored and contributed to 2 peer reviewed publications relevant to this thesis in the course of my graduate studies.

7. Wojtal P, Chen S, Shi K, et al. Electrophoretic deposition of a memory-type flame retardant material. *Materials Letters*, 2015. **153**(0): 106-109.

8. Wojtal P, Luo D, Chen S, Zhitomirsky I. Composite Polymer-Metal Hydroxide Coatings with Flame Retardant Properties. *Materials and Manufacturing Processes*, 2015.

Table of Contents

Chapter 1 Introduction	1
References	6
Chapter 2 Literature review	7
2.1 Brief history of electrochemical capacitors (ECs)	7
2.2 Energy storage mechanisms of electrochemical capacitors	9
2.2.1 Electrochemical double layer capacitors.....	12
2.2.2 Electrochemical capacitors based on pseudocapacitance	14
2.3 Electrode materials for electrochemical capacitors.....	19
2.3.1 Carbon-based electrode materials	20
2.3.2 Transition metal oxides.....	26
2.3.3 Conductive polymers	31
2.3.4 Composite electrodes	36
2.4 Electrolytes.....	38
2.4.1 Organic electrolytes	38
2.4.2 Aqueous electrolytes.....	39
2.4.3 Ionic liquid electrolytes.....	40
2.5 Synthesis methods	40
2.5.1 Electropolymerization.....	40

2.5.2	Chemical polymerization	43
2.6	Influence of dopants	44
2.6.1	Influence of anodic electropolymerization on non-noble metals.....	44
2.6.2	Influence of electrical conductivity of PPy.....	46
2.6.3	Influence of microstructure of PPy	47
2.7	Application of ECs	47
	References	50
Chapter 3	Problem statement and objective.....	67
3.1	Problem statement	67
3.2	Objective and approach	71
	References	72
Chapter 4	Experimental procedures	76
4.1	Starting materials.....	76
4.2	Materials synthesis	76
4.2.1	Electropolymerized PPy and composite films	76
4.2.2	Chemically polymerized PPy and composite powders	79
4.3	Fabrication of electrodes and EC devices using impregnation	81
4.4	Morphology characterization	82
4.5	Adhesion test	82
4.6	Electrochemical characterization of electrodes	83

4.6.1	Cyclic voltammetry study	84
4.6.2	Impedance spectroscopy study	85
4.7	Characterization of capacitive performance for EC devices	86
	References	87
Chapter 5 Influence of dopants and carbon nanotubes on polypyrrole electropolymerization and capacitive behavior.....		
		88
5.1	Electropolymerization of PPy thin films	88
5.2	Morphology study of PPy and PPy-MWCNTs films.....	90
5.3	Capacitive performance of PPy and PPy-MWCNTs films	92
5.4	Conclusions	94
	References	95
Chapter 6 Polypyrrole electrodes doped with sulfanilic acid azochromotrop for electrochemical supercapacitors		
		96
6.1	Electrodeposition of PPy films doped by SPADNS.....	96
6.2	Electrochemical properties of electropolymerized PPy films	98
6.3	Characterization of chemical polymerized porous PPy electrodes	100
6.4	Conclusions	107
	References	108
Chapter 7 Capacitive behaviour of polypyrrole, prepared using pyrocatecholsulfonphthalein by electrochemical and chemical methods.....		
		111
7.1	Electropolymerization of PPy using PS	111

7.2	Comparison between galvanostatic and pulse deposited PPy	114
7.3	Morphology and capacitive behaviour of PPy synthesized by different methods.....	116
7.4	Conclusions	118
	References.....	120
Chapter 8 Influence of tartrazine and brilliant yellow dopants and new dispersants on performance of polypyrrole–carbon nanotube supercapacitors		
8.1	Chemical structures of dopants and dispersants.....	121
8.2	Capacitive performance of PPy doped by TR and BY.....	123
8.3	Characterization of PPy-MWCNT composites, prepared using different dispersants.....	126
8.4	Conclusions	130
	References.....	132
Chapter 9 Polypyrrole coated carbon nanotubes for supercapacitors, prepared using indigo carmine as a dispersant and dopant.....		
9.1	Morphology study of PPy-MWCNT using indigo carmine	133
9.2	Capacitive behavior of PPy-MWCNT electrodes and devices	136
9.3	Conclusions	139
	References.....	141
Chapter 10 Influence of multifunctional dopants on capacitive behavior of polypyrrole-carbon nanotube ECs		
10.1	Chemical structures of multifunctional dopants.....	142

10.2	Capacitive performance of PPy and PPy-MWCNT.....	143
10.3	Morphology study of PPy and PPy-MWCNT.....	148
10.4	Conclusions	151
	References.....	153
	Conclusion and future works	154

List of Figures

Figure 1.1 Ragone plot showing the specific power against specific energy for various electrical energy storage systems	2
Figure 2.1 Difference of discharge and recharge relationships for a capacitor and a battery: potential as function of state of charge, Q	9
Figure 2.2 Working diagram illustrating storage of energy E for a battery at ideally constant charging voltage, and for a capacitor with progressively changing voltage	11
Figure 2.3 Simple RC circuit	11
Figure 2.4 Structure and function of an ideal double-layer capacitor.....	12
Figure 2.5 Models of EDL at a positively charged surface: (a) the Helmholtz model, (b) the Gouy-Chapman model, and (c) the Stern model, showing the inner Helmholtz plane (IHP) and outer Helmholtz plane (OHP)	13
Figure 2.6 Energy vs. charging time for an EDLC and a lithium-ion battery	15
Figure 2.7 Cyclic voltammetry profiles for RuO ₂ in aq. 0.1 M H ₂ SO ₄ taken to a successive series of positive electrode potentials relative to RHE. Sweep rate, 50 mV s ⁻¹ ; 298K.....	17
Figure 2.8 Different types of reversible redox mechanisms that give rise to pseudocapacitance: (a) underpotential deposition, (b) redox pseudocapacitance, (c) intercalation Pseudocapacitance	18
Figure 2.9 Normalized capacitance versus average pore size for TiC-CDC and other carbons from literature tested in the same electrolytes.....	21
Figure 2.10 (a) The crystal structure of graphene (b) Electronic Band structure of graphene.....	24
Figure 2.11 Atomic structure of carbon nanotubes.....	25

Figure 2.12 (a) Cyclic voltammogram for RuO ₂ in 1 M aqueous H ₂ SO ₄ (298K) showing mirror image symmetry along the scanned potential range. (b) Cyclic voltammogram for Pb-PbCl ₂ battery electrode showing typical irreversible process	28
Figure 2.13 Different structures of conducting polymers	31
Figure 2.14 Comparison of charging of (a) double-layer capacitor (carbon) and (b) pseudocapacitor (conducting polymer).....	32
Figure 2.15 Cyclic voltammogram for Ni/PAni at various sweep rates: (a) 25.0 mV s ⁻¹ , (b) 50.0 mV s ⁻¹ , (c) 75.0 mV s ⁻¹ and (d) 100 mV s ⁻¹	34
Figure 2.16 Synthesis of PPy nanostructures by electropolymerization.....	35
Figure 2.17 Comparison of various materials according to their specific parameter for supercapacitor applications.....	36
Figure 2.18 Possible strategies to improve both energy and power densities for electrochemical capacitors	37
Figure 2.19 Polymerization potential of PPy using oxalate and the formation of oxide layer on stainless steel substrate.....	45
Figure 2.20 Potential/time curves for the galvanostatic deposition of polypyrrole on Al 2204-T3 at 1 mA cm ⁻² current density in the presence of Tiron (curve 1) and in the presence of Na- <i>p</i> TS (curve 2)	45
Figure 2.21 Use of ECs in electronic circuits. (a) shows a battery powered device where EC provides power backup of the load in case of disconnection of the battery. (b) shows an AC-voltage powered device involving heavy switching currents. The EC protects the critical load from large voltage drops	48
Figure 2.22 Schematic of driveline of a hybrid electric bus using electrochemical capacitors as storage device for regenerative braking. The arrows indicate the flow of energy	49

Figure 3.1 Induction time during electropolymerization of pyrrole on steel using aqueous electrolyte contains oxalic acid	67
Figure 4.1 Electropolymerization set-up diagram.....	77
Figure 4.2 Electropolymerization of PPy films	78
Figure 4.3 Electropolymerization of PPy-MWCNTs films	78
Figure 4.4 Pulse currents.....	79
Figure 4.5 Full process of chemical polymerization of PPy.....	79
Figure 4.6 Full process of chemical polymerization of PPy-MWCNTs using dopants and dispersants.....	80
Figure 4.7 Synthesis PPy-MWCNTs using multifunctional dopants	81
Figure 4.8 Fabrication process of electrodes	81
Figure 4.9 Construction of EC devices	82
Figure 4.10 Classification of adhesion test results.....	83
Figure 4.11 Three-electrode system.....	84
Figure 5.1 (A) Chemical structures of AQ and AR and potential versus time curves for galvanostatic deposition of PPy from 0.1 M pyrrole solution containing (a) 5 mM AR and (b) 5 mM AQ at a current density of 1 mA cm^{-2} , (B) film mass versus time for PPy films prepared at a current density of 1 mA cm^{-2} from 0.1 M pyrrole solution containing 5 mM AR.....	89
Figure 5.2 (A) CVs at a scan rate of 2 mV s^{-1} and (B) SCs versus scan rate for films of different mass: (a) 0.13, (b) 0.18, (c) 0.23, (d) 0.32 and (e) 0.52 mg cm^{-2} , prepared from 0.1 M pyrrole solutions containing 5 mM AR	90

Figure 5.3 SEM images for films prepared from 0.1 M pyrrole solutions, containing 5 mM AR and (A) 0 and (B) 0.3 gL ⁻¹ MWCNT.....	91
Figure 5.4 (A) SC calculated from CV data versus film mass and (B) C', (C) C'' components of complex capacitance, calculated from AC impedance data, versus frequency for films prepared from 0.1 M pyrrole solutions, containing 5 mM AR and (a) 0 and (b) 0.3 g L ⁻¹ MWCNT	93
Figure 6.1 (A) chemical structure of SPADNS, (B) CVs at a scan rate of 20 mV s ⁻¹ for cycles 1, 2 and 10, (C) electrode potential versus time at a current density of 1 mA cm ⁻² , (D) deposit mass versus deposition time at a current density of 1 mA cm ⁻² for (B,C,D) stainless steel electrodes in 0.1 M pyrrole solution, containing 5 mM SPADNS	97
Figure 6.2 (A) SEM image of a PPy film on a stainless steel substrate and (B,C,D) testing results for the films in the 0.5 M Na ₂ SO ₄ electrolyte: (B) CVs at a scan rate of 2mV s ⁻¹ , (C) C _m and (D) C _s versus scan rate for (a) 0.187 and (b) 0.283 mg cm ⁻² PPy films	99
Figure 6.3 (A) C _s ' and (B) C _s '' versus frequency for (a) 0.187 and (b) 0.283 mg cm ⁻² PPy films on stainless steel substrates in 0.5 M Na ₂ SO ₄ electrolyte.....	100
Figure 6.4 SEM image of PPy powder, prepared by a chemical polymerization method.....	100
Figure 6.5 (A) SEM image of an electrode, fabricated by impregnation of a Ni foam with PPy powder, prepared by a chemical polymerization method and (B,C,D) testing results for the electrodes in 0.5 M Na ₂ SO ₄ electrolyte:(B) CVs at a scan rate of 2 mV s ⁻¹ , (C) C _m and (D) C _s versus scan rate for PPy loadings of (a) 15.3, (b) 22.3, (c) 35.4 mg cm ⁻²	101
Figure 6.6 (a) C _m and (b) C _s at a scan rate of 2 mV s ⁻¹ in 0.5 M Na ₂ SO ₄ electrolyte versus PPy mass loading of Ni foam with PPy powder, prepared by a chemical polymerization method	102
Figure 6.7 (A) C _s ' and (B) C _s '' versus frequency for electrodes with PPy loading of (a) 15.3, (b) 22.3 and (c) 35.4 mg cm ⁻² , fabricated by impregnation of Ni foam with PPy powder,	

prepared by a chemical polymerization method and tested in 0.5 M Na ₂ SO ₄ electrolyte.....	103
Figure 6.8 (A) C _s ' and (B) C _s " versus frequency for electrodes with PPy loading of 20.8 mg cm ⁻² , fabricated by impregnation of Ni foam with PPy powder, prepared by a chemical polymerization method and tested in (a) 0.5 and (b) 0.1 M Na ₂ SO ₄ electrolyte	104
Figure 6.9 Capacitance retention in 0.5 M Na ₂ SO ₄ electrolyte versus cycle number for 0.187 mg cm ⁻² PPy film, prepared by electropolymerization on a stainless steel substrate and 23 mg cm ⁻² PPy electrode, prepared by impregnation of Ni foam with PPy powder, prepared by a chemical polymerization method	105
Figure 7.1 (A) The mass-time curve and chemical structure of PS (inset), (B) SEM image of PPy fabricated by galvanostatic deposition using PS under 1 mA cm ⁻² on Ni foil	111
Figure 7.2 (A) specific capacitance at scan rates from 2 to 100 mV s ⁻¹ and CV at a scan rate of 2 mV s ⁻¹ (inset), (B) electrochemical impedance spectroscopy data and corresponding equivalent circuit (inset), and (C) cyclic stability of PPy fabricated by galvanostatic deposition using PS dopant.....	112
Figure 7.3 (A) SC versus scan rate curves of PPy fabricated by galvanostatic deposition in solution contains different concentration of PS (B) Corresponding Nyquist plots for complex impedance and corresponding equivalent circuit (inset).....	113
Figure 7.4 Deposit mass versus deposition time for (A) galvanostatic electropolymerization and (B) pulse electropolymerization.....	114
Figure 7.5 SEM images of Ni plaques at different magnifications: (A,B) as-received, (C,D) impregnated with PPy by galvanostatic electropolymerization, (E,F) impregnated with PPy by pulse electropolymerization	115
Figure 7.6 (A,B) SEM images at different magnifications of Ni plaques, impregnated with PPy, using slurry of PPy powder, prepared by a chemical polymerization method.....	116

Figure 7.7 (A) CVs at a scan rate of 2 mV s^{-1} , (B) specific capacitance versus scan rate, (C) Nyquist plot of complex impedance, inset shows equivalent circuit used for simulation, (D) capacitance retention versus cycle number at a scan rate of 50 mV s^{-1} for Ni plaque based electrodes, impregnated with PPy: (a) by galvanostatic electropolymerization, (b) by pulse electropolymerization and (c) using slurry of a PPy powder, prepared by chemical polymerization	117
Figure 8.1 Chemical structures of (A) TR and (B) BY dopants	121
Figure 8.2 Chemical structures of BAC, SDS and SCH dispersants	122
Figure 8.3 (A) CVs at a scan rate of 2 mV s^{-1} , (B) specific capacitance, derived from the CV data, versus scan rate, (C) real and (D) imaginary parts of capacitance, derived from the impedance data, versus frequency for the PPy electrodes with the active mass of 30 mg cm^{-2} , prepared using (a) TR and (b) BY dopants	123
Figure 8.4 (A) Areal and (B) gravimetric capacitances, derived from the CV data versus scan rate and (C) real and (D) imaginary parts of differential capacitances, derived from impedance spectroscopy data, versus scan rate for PP electrodes with mass loadings of (a) 22, (b) 30 and (c) 36 mg cm^{-2}	125
Figure 8.5 (A) CVs at a scan rate of 5 mV s^{-1} , (B) specific capacitance, derived from the CV data, versus scan rate, (C) real and (D) imaginary parts of capacitance, derived from the impedance data, versus frequency for the PPy-MWCNT electrodes with the active mass of 30 mg cm^{-2} , prepared using (a) TR and BAC (b) BY and BAC, (c) TR and SDS, (d) TR and SCH	126
Figure 8.6 Cyclic stability of (a) PPy electrodes, prepared using TR and (b) PPy-MWCNT electrodes, prepared using TR and BAC with mass loading of 30 mA cm^{-2}	128
Figure 8.7 SEM images of (A) PPy electrodes, prepared using TR and (B) PPy-MWCNT electrodes, prepared using TR and BAC, arrow shows uncoated MWCNT.....	129

Figure 8.8 (A) Specific capacitance versus discharge current, (B) charge-discharge data at current densities of (a) 2, (b) 5, (c) 10, (d) 20 and (e) 40 mA, (C) cyclic stability for coin cells, shown in the inset of (C), and (D) LED bulbs powered by the coin cells.....	130
Figure 9.1 (A) Chemical structure of IC, (B) 0.2 g L ⁻¹ MWCNT suspensions: (a) without IC and (b) containing 10 mM IC.....	133
Figure 9.2 SEM images (A) PPy and (B-D) PPy-MWCNTs powders, containing (B) 10 (C) 20 (D) 30% MWCNT. Arrows (B) show PPy particles.....	134
Figure 9.3 Synthesis process and reactions of PPy-MWCNT composites	135
Figure 9.4 (A) CVs at a scan rate of 2 mV s ⁻¹ , (B) C _s and C _m , calculated from the CV data versus scan rate, (C) C' _s and (D) C'' _s , calculated from the impedance data versus frequency for (a) PPy and (b-d) PPy-MWCNTs electrodes, containing (b) 10, (c) 20 (d) 30% MWCNT for electrode mass of 30 mg cm ⁻²	136
Figure 9.5 (A) Capacitance retention versus cycle number for (a) PPy and (b) PPy-20%MWCNT electrodes, with electrode mass of 30 mg cm ⁻² , (B) charge-discharge curves for two electrode PPy-20%MWCNT coin cell at currents of (a) 2, (b) 5, (c) 10, (d) 20 and (e) 40 mA, (C) C _m versus current for the coin cells, inset shows coin cells, (D) capacitance retention of a coin cell versus cycle number, inset shows LED bulbs powered by the coin cells.	139
Figure 10.1 Chemical structures of different dopants (a) SB, (b) NAT, (c) TRI and (d) TETRA.....	142
Figure 10.2 (A) CVs at a scan rate of 2 mV s ⁻¹ , (B) C _m and C _s calculated from the CV data versus scan rate, (C) C' _s and (D) C'' _s calculated from the impedance data versus frequency for PPy electrodes with the active mass loading of 30 mg cm ⁻² , prepared using (a) SB, (b) SB with 20% MWCNT, (c) NAT and (d) NAT with 20% MWCNT.....	143
Figure 10.3 (A) CVs at a scan rate of 2 mV s ⁻¹ , (B) C _m and C _s calculated from the CV data versus scan rate, (C) C' _s and (D) C'' _s calculated from the impedance data versus frequency	

for PPy electrodes with the active mass of 30 mg cm^{-2} , prepared using (a) TRI, (b) TRI with 20% MWCNT, (c) TETRA and (d) TETRA with 20% MWCNT	145
Figure 10.4 (A) Capacitance retention versus cycle numbers for (a) PPy doped by SB, (b) PPy-MWCNT doped by SB, (c) PPy doped by NAT and (d) PPy-MWCNT doped by NAT, (B) Capacitance retention versus cycle numbers for (a) PPy doped by TRI, (b) PPy-MWCNT doped by TRI, (c) PPy doped by TETRA and (d) PPy-MWCNT doped by TETRA.....	147
Figure 10.5 SEM image of polypyrrole powders (a) (b) doped by SB (c) (d) doped by NAT....	148
Figure 10.6 SEM images at different magnifications of PPy powders (a, b) doped by TRI and (c, d) doped by TETRA.....	149
Figure 10.7 SEM image of PPy-MWCNT (a) doped by SB and (b) doped by TETRA..	150
Figure 10.8 (A) Specific capacitance versus discharge current, (B) charge-discharge data at current densities of (a) 2, (b) 5, (c) 10, (d) 20 and (e) 40 mA, (C) ragone plot, (D) cyclic stability for coin cells.....	151

List of Tables

Table 2.1 Comparison between EDLCs and pseudocapacitors.	16
Table 2.2 Summary of the various classes of electrode materials investigated.....	19
Table 2.3 Pseudocapacitance and conductivity of selected metal oxides.	30
Table 2.4 Theoretical specific capacitances of conducting polymers.....	33
Table 2.5 Electrical conductivity of PPy using different dopants.....	46

List of Abbreviations and Symbols

A (unit)	Ampere
AC	Activated carbon
APS	Ammonium peroxydisulfate
AR	Alizarin red
AQ	Antraquinone-2-sulfonic acid sodium salt
BAC	Benzyltrimethylhexadecylammonium chloride
BY	Brilliant yellow
C	Capacitor
C (unit)	Coulomb
C_{dl}	Double layer capacitance
C_m	Mass normalized specific capacitance
cm (unit)	Centimeter
CNT	Carbon nanotube
C_s	Area normalized specific capacitance
CV	Cyclic voltammetry
C_φ	Pseudocapacitance
e	Electron
EC	Electrochemical capacitor

EDLC	Electrochemical double layer capacitor
EIS	Electrochemical impedance spectroscopy
Eq.	Equation
ESR	Equivalent series resistance
F	Faraday constant
F (unit)	Farad
g (unit)	Gram
h (unit)	Hour
IC	Indigo carmine
IHP	Inner helmholtz plane
kg (unit)	Kilogram
L (unit)	Liter
LED(s)	Light-emitting diode(s)
Li-ion	Lithium-ion battery
M (unit)	Mole per liter
mM (unit)	Millimole per liter
m (unit)	Meter
mg (unit)	Milligram
min (unit)	Minute

mL (unit)	Millitre
mV (unit)	Millivoltage
MWCNT	Multiwall carbon nanotube
NAT	1,3,(6,7)-Naphthalenetrisulfonic acid trisodium salt hydrate
nm (unit)	Nanometer
OHP	Outer helmholtz plane
PAni	Polyaniline
PEDOT	Poly(3,4-ethylenedioxythiophene)
PPy	Polypyrrole
PTh	Poly(thiophene)
PS	Pyrocatecholsulfonphthalein
Q	Electric charge
R	Ideal gas constant
S (unit)	Siemens
s (unit)	Second
SB	Sodium benzene-1,3-disulfonate
SC	Specific capacitance
SCH	Sodium cholate
SDS	Sodium dodecyl sulfate

SEM	Scanning electron microscopy
SPADNS	Sulfanilic acid azochromotrop
T	Absolute temperature (K)
TETRA	Potassium indigotetrasulfonate
TR	Tartrazine
TRI	Potassium indigotrisulfonate
V (unit)	Voltage
W (unit)	Watt
Wh (unit)	Watt-hour
Ω (unit)	Ohm
π	Pi
ξ	Zeta potential
μm (unit)	Micrometer
μV (unit)	Micro voltage
$^{\circ}\text{C}$ (unit)	Celsius degree

Chapter 1 Introduction

The greenhouse gas emission which lead to the climate change as well as the decreasing availability of fossil fuel has become major concern of sustainable development of global economy and society. As a result, the development and production of renewable energy sources such as sun and wind are increased. However, large fluctuations during electricity generation using such energy sources may introduce many challenges to power grid management and grid stability[1]. In this situation, efficient and reliable electrical energy storage system start to attract more attention and play a more important role.

Lithium-ion batteries, introduced by Sony in 1990, are widely used in vehicles, computers and telecommunication devices due to their relatively high energy density and good performance despite their high cost[2]. However, the slow power delivery and uptake is a major problem, which limits their application. Electrochemical capacitors (ECs) were invented in 1957 by H.I Becker from General Electric[3], but they didn't attract much attention until recently. ECs can provide high power delivery and long cycle life, although their energy density is relatively lower compared to batteries as illustrated in fig. 1.1. Therefore, they can play an important role in complementing or replacing batteries in electrical energy storage field. One of the important applications of ECs is in emergency doors on the Airbus A380 due to their safe and reliable performance[4].

Based on different charge-discharge mechanism, ECs can be classified in two categories. One of them is electrochemical double-layer capacitors (EDLCs), their capacitance generated from the electrostatic charges accumulation at the electrode/electrolyte interface.

Carbon based active materials which have high surface area such as activated carbon, carbon nanotubes, graphene, carbon aerogels are commonly used electrode materials.

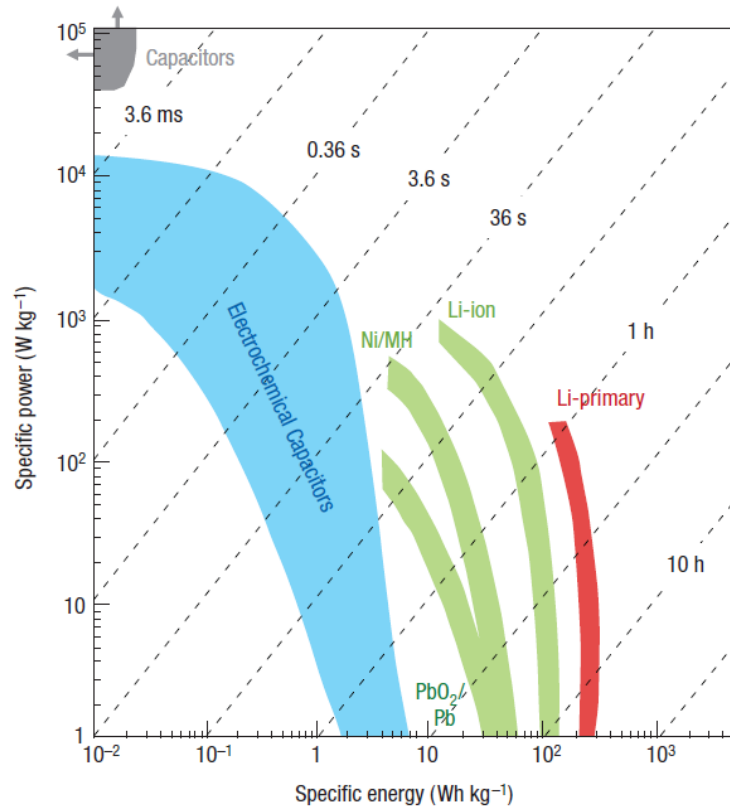


Figure 1.1 Ragone plot showing the specific power against specific energy for various electrical energy storage systems[5]

The other type of ECs is pseudocapacitors, their capacitances result from fast and reversible surface or near-surface faradaic reactions, which take place due to electro-active species. Various transition metal oxides such like RuO₂, MnO₂, V₂O₅ as well as conducting polymers such as polypyrrole and polyaniline are good candidates for electrode materials.[6]

Generally, ECs based on EDLC mechanism can achieve high power density, high conductivity, good environmental stability, and ultra-long cycle life. However, their low

specific capacitance and energy density limits their application. On the contrary, ECs based on pseudocapacitive mechanism have high specific capacitance and enhanced energy storage capacity. Nevertheless, the poor electrical conductivity of metal oxides and mechanical degradation of conducting polymers during redox reaction limit their applications. In this situation, the formation of composite electrode materials was needed in order to combine the advantages of those two types of electrode materials and eliminate those drawbacks.

Polypyrrole is an important material for electrodes of pseudocapacitors due to its high specific capacitance and electrical conductivity, low cost and chemical stability. However, the increase in PPy mass loading resulted in decreasing specific capacitance and increasing impedance. Moreover, the poor cycling stability limits the application of PPy. In attempts to solve such problems, research strategies were focused on the fabrication of PPy-carbon nanotube composites (PPy-CNTs) due to the high conductivity, high surface area of carbon nanotubes. It is important to note that the specific capacitance of CNT is significantly lower, compared to that of PPy[7]. Therefore, the amount of CNT in the composites must be optimized and CNT must be well dispersed in PPy matrix.

In order to optimize the PPy polymerization and CNTs dispersion, the development of anionic dopants and dispersants has been the focus of significant research activity. It was found that anionic dopants can passivate the surface of non-noble electrodes and prevent the oxidation and dissolution during anodic electropolymerization of PPy. Moreover, relatively high electrical conductivity and thermal stability of PPy films were achieved using aromatic anionic dopants. The anionic dopant also showed significant influence on

the size and shape of particles and electrochemical performance of PPy, prepared by chemical polymerization method. Moreover, improved voltage window and cycling stability of PPy were achieved by the use of polyaromatic dopant molecules.

Chemically functionalized CNTs showed improved dispersion and were used for the formation of PPy-CNTs. However, the functionalization strategies introduce defects on the CNTs sidewalls and reduce the electronic conductivity of CNTs. It was found that the use of long chain surfactants for CNTs dispersion generated problems related to PPy deposition on CNTs and coating formation. In this situation, there is a need in the development of new dispersion techniques for the fabrication of PPy-CNTs.

In this investigation, different types of new anionic dopants were used for PPy fabrication through electropolymerization and chemical polymerization. Advanced dispersants and multi-functional dopants were discovered and used for the fabrication of PPy-CNTs composites. The influence of different polymerization methods, concentration of dopant, dispersant and CNTs on the microstructure of PPy were revealed through morphology study. Capacitance measurements through cyclic voltammetry and impedance spectroscopy provided an insight into the effect of chemical structures of new dopants and dispersants on the electrochemical performance of PPy or PPy-CNTs electrodes. One of the important tasks in the ECs technology is the development of efficient electrodes with high active mass loading and large ratio of mass of active materials to mass of current collectors. It was shown that active mass of electrodes must be above [8] 10 mg cm^{-2} for practical applications in manufacturing of ECs. In this research, high capacitance, improved cyclic performance and good capacitance retention at high rates of charge-discharge and

large mass of active material was achieved based on the use of light weight commercial current collectors. Symmetric EC devices were also assembled and showed good electrochemical and capacitive performance as well as acceptable cyclic stability.

References

1. B éguin, F., et al., Carbons and electrolytes for advanced supercapacitors. *Advanced Materials*, 2014. **26**(14): p. 2219-2251.
2. Tarascon, J.M. and M. Armand, Issues and challenges facing rechargeable lithium batteries. *Nature*, 2001. **414**(6861): p. 359-367.
3. Miller, J.R., A brief history of supercapacitors. *Batteries & Energy Storage Technology*, 2007: p. 61-78.
4. Zhang, L.L. and X.S. Zhao, Carbon-based materials as supercapacitor electrodes. *Chemical Society Reviews*, 2009. **38**(9): p. 2520-2531.
5. Simon, P. and Y. Gogotsi, Materials for electrochemical capacitors. *Nature Materials*, 2008. **7**(11): p. 845-854.
6. Zhi, M., et al., Nanostructured carbon-metal oxide composite electrodes for supercapacitors: a review. *Nanoscale*, 2013. **5**(1): p. 72-88.
7. Niu, C., et al., High power electrochemical capacitors based on carbon nanotube electrodes. *Applied Physics Letters*, 1997. **70**(11): p. 1480-1482.
8. Gogotsi, Y. and P. Simon, True performance metrics in electrochemical energy storage. *Science*, 2011. **334**(6058): p. 917-918.

Chapter 2 Literature review

2.1 Brief history of electrochemical capacitors (ECs)

The origin of capacitor can be traced back to the discovery of Leyden jar which showed the principle of charge separation and charge storage on two surfaces of it. However, the mechanism and physical significance of such discovery could not have been fully understood until 1745. Since then, it was known that a charged capacitor can store electrical charge (Q) due to a voltage difference established between two plates, one stored $+Q$, and the other store $-Q$. The stored electrical energy can be calculated by $\frac{1}{2}CV^2$, where C represents capacitance and V represents voltage. The first electrochemical energy storage device applied such principle was reported in 1957 by H.I Becker from General Electric[1]. The device which was later classified as electrochemical double-layer capacitor (EDLC) was described as a porous carbon material immersed in aqueous electrolyte, thus electrical energy was stored by way of the charge held in the interfacial double layer. Based on Becker's work, in 1962, Standard Oil Company of Ohio (SOHIO) started to develop carbon double-layer capacitor devices which provide higher operating voltages (3.4-4.0 V) using high-area carbon materials, but in a non-aqueous electrolyte. Higher charge densities as well as larger specific energy can be stored on such devices due to the use of an organic electrolyte. After that, plenty of researches and many hundreds of journal articles covering all aspects of EDLC technology were reported.

In 1975, a principle different from EDLC was utilized and developed by Conway, so-called 'Pseudocapacitance'. In one type of system, it related to potential dependence of level of

electrochemical H atom adsorption. In the other type of system, which is more commonly used, pseudocapacitance related to solid oxide redox system (e.g. RuO_2) for energy storage. The capacitance arises from oxidation or reduction process. Some continues dependence of charge Q passed faradaically upon electrode potential V , and a derivative dQ/dV corresponded to pseudocapacitance can be measured.

The use of high surface area carbon materials and oxide redox system realizes the development of commercial production of practical high-capacitance electrochemical capacitor devices. In 1975, NEC (a Japanese company) began its investigation and developed a unique design with bipolar construction which can eliminate the need of cell interconnects. It can be described as a stack of six or eight cells in series and sealed the entire device. This approach was subsequently used by other companies like ECOND and ELIT. The first large size capacitor with energy densities exceeding 10 Wh/kg was invented and patented by ESMA company in 1993. It is an asymmetric capacitor using one battery electrode couple with a double layer capacitor electrode. It offers advantages of high specific energy and higher operating voltage, which can be used to power heavy electric vehicles like buses or trucks without gas engines. In 1998, Nippon Chemi-Con (Japan) developed a high energy density line of ECs based on pseudocapacitance energy storage system. It can reach relatively high energy density with lower cycle life compared to double-layer capacitor products, and can be applied in solar-powered lighting as road studs and garden lights.[1]

After nearly 40 years development, electrochemical capacitor technology still has a long way to go to overcome the exiting limitation and accomplish more realistic applications.

2.2 Energy storage mechanisms of Electrochemical Capacitors

Generally, there are two fundamentally different ways to store electrical energy. One of them directly in batteries, where charges can be released to perform electrical work due to the Faradaic oxidation and reduction of electrochemically active reagents. However, chemical interchange of anode and cathode materials (usually phase changes), which is irreversible, takes place during the energy storage process, thus the cycle life of batteries is usually restricted to one to several thousand charge-discharge cycles. On contrary, the electrostatic way in which positive and negative electric charges are stored separately on plates of capacitors allow almost unlimited cycle stability since there isn't any chemical or phase change during the charge-discharge process.

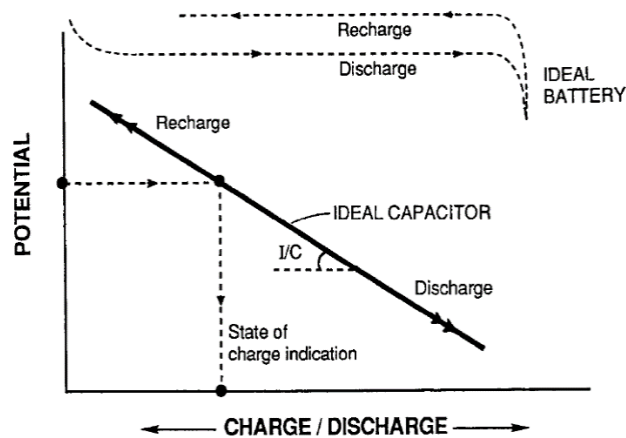


Figure 2.1 Difference of discharge and recharge relationships for a capacitor and a battery: potential as function of state of charge, Q [2].

The different charge-discharge process can be illustrated by curves shown in fig. 2.1. For a battery process, the potential difference of the cell is ideally constant since the thermodynamic potential exists independent of the extent of charge added. But for capacitor

process, for example, charging a pure EDLC, potential difference increase as charge continue accumulated on plates. In this case, electrical work need to be done against the charge density already accumulated on the plates in order to add additional amount of charge.[2]

Due to their different charge-discharge process, the electrical energies stored in batteries and capacitors are different even with the same amount of charges and a given potential difference (see fig. 2.1).[2] For batteries, the stored electrical energy can be calculated by Eq.2.1, while the stored energy for capacitors is expressed in Eq.2.2.

$$E_B = \int_0^Q V_B dQ = VQ \quad (\text{Eq. 2.1})$$

$$E_C = \int_0^Q V_C dQ = \frac{1}{2} \int_0^Q V_B dQ = \frac{1}{2} VQ = \frac{1}{2} CV^2 \quad (\text{Eq. 2.2})$$

Where Q is the total charges stored, C is the capacitance, V is the potential difference. So the power of capacitor which describe the speed of energy delivery or absorption can be calculated through the Eq. 2.3

$$P = \frac{dE}{dt} = \frac{d}{dt} \left(\frac{1}{2} CV^2 \right) = CV(t) \frac{dV}{dt} \quad (\text{Eq. 2.3})$$

It is indicated that the stored energy and power of capacitors is positively proportional to the capacitance and voltage. In order to make the power of ECs more comparable, the concept of maximum power (P_{\max}) instead of power is introduced to identify the energy delivery ability of ECs.

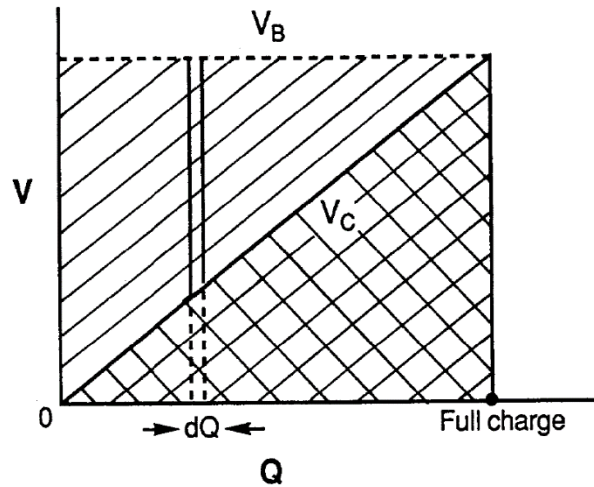


Figure 2.2 Working diagram illustrating storage of energy E for a battery at ideally constant charging voltage, and for a capacitor with progressively changing voltage.[2]

A simple RC circuit is applied (see figure 2.3), where ESR (R_s) is equivalent series resistance corresponding to several components including ionic resistance of electrolyte, resistance of electrode, interface resistance between electrode and current collector, and resistance related to ion penetration through membrane separator (see figure 2.4).

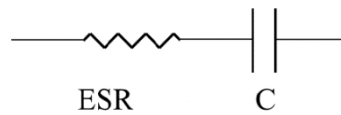


Figure 2.3 Simple RC circuit

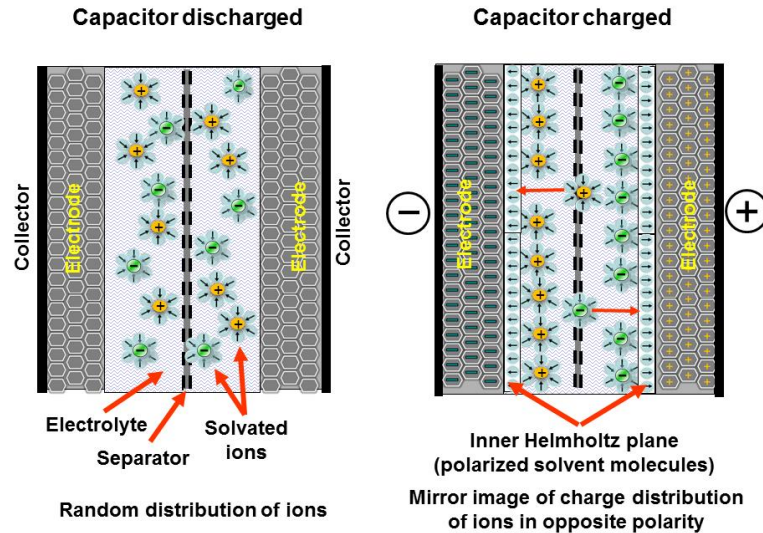


Figure 2.4 Structure and function of an ideal double-layer capacitor.[1]

During the discharging process, the initial voltage will be reduced due to the discharge current. Therefore, the real voltage should be $V=V_i-IR_s$, and the power is $P=VI=V_iI-I^2R_s$. The maximum power can be obtained when $dP/dI=0$, and $I=V_i/2R_s$, so the expression of maximum power is given in Eq. 2.4

$$P = \frac{V_i^2}{4R_s} \quad (\text{Eq. 2.4})$$

2.2.1 Electrochemical double layer capacitors

ECs based on electrochemical double-layer (EDL) mechanism can provide much higher energy storage compare to traditional capacitors due to the atomic range of charge separation distance and large interfacial area. The EDL model was first described by Von Helmholtz in the 19th century when he studied the distribution of opposite charges at the interface of colloidal particles.[3] In this simple model, EDL was described as a positively

charged layer and a negatively charged layer were separated by an atomic distance at the electrode-electrolyte interface (shown in fig. 2.5a).

This original model was then developed by Gouy[4] and Chapman[5] on consideration of diffusion layer in which a continuous distribution of ions in the electrolyte was driven by thermal motion (see fig. 2.5b). Later, the Helmholtz model was combined with Gouy-Chapman model by Stern[6] to clearly identify two region of ion distribution: the inner region called Stern layer or compact layer, and the outer layer called the diffusion layer (shown in fig. 2.5c).

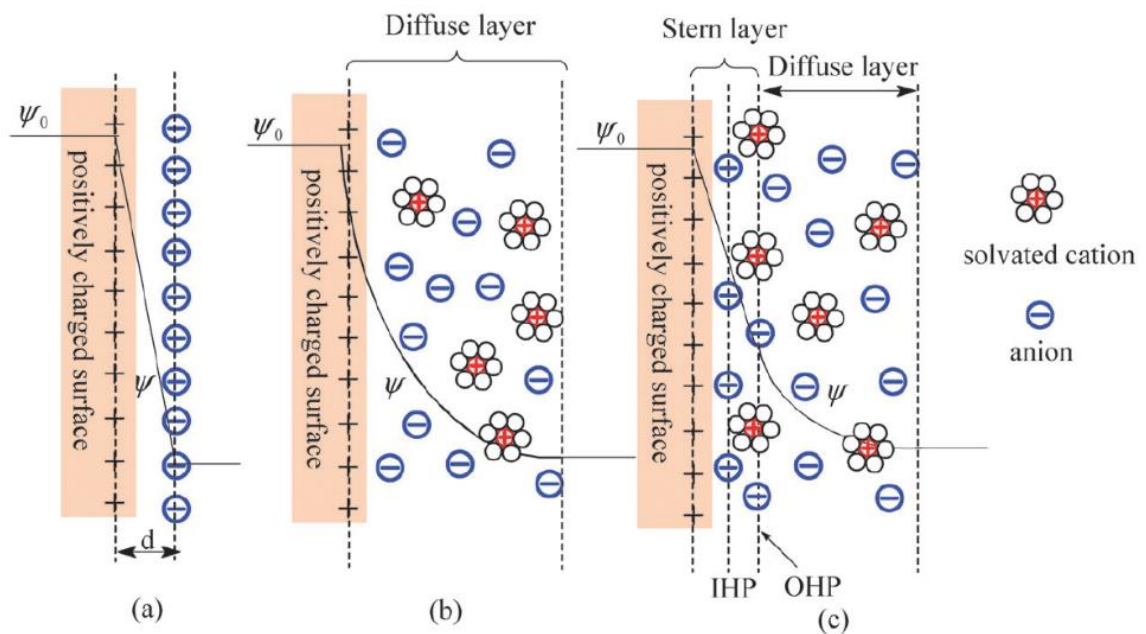


Figure 2.5 Models of EDL at a positively charged surface: (a) the Helmholtz model, (b) the Gouy-Chapman model, and (c) the Stern model, showing the inner Helmholtz plane (IHP) and outer Helmholtz plane (OHP). [7]

In the compact layer, two concepts were introduced to distinguish two types of adsorbed ions. The inner Helmholtz plane (IHP) and outer Helmholtz plane (OHP) are corresponding

to the different distances of closest approach related to anion or cation at the electrode surface. Beyond the compact layer, the diffuse layer exists as Gouy-Chapman described.

The capacitance of EDL (C_{dl}) can be considered as two capacitances from two regions combined, the C_H of compact layer and the C_{diff} of the diffuse layer. Therefore, C_{dl} can be expressed by Eq. 2.5

$$\frac{1}{C_{dl}} = \frac{1}{C_H} + \frac{1}{C_{diff}} \quad (\text{Eq. 2.5})$$

Since the capacitance of diffuse layer is much larger than the capacitance of compact layer, so the contribution of C_{diff} is negligible. Therefore, equation for the capacitance of EDLC is similar to that of traditional capacitor

$$C = \frac{\epsilon_r \epsilon_0}{d} A \quad (\text{Eq. 2.6})$$

Where ϵ_r is the electrolyte dielectric constant, ϵ_0 is the permittivity of vacuum, d is the effective thickness of EDL, and A is the specific area of electrode surface. Other factors that may influence the C_{dl} include the applied electrical field, types of ions in electrolyte, chemical affinity between ions and electrode surface, and the solvent.

2.2.2 Electrochemical capacitors based on pseudocapacitance

Another type of ECs is pseudocapacitors in which fast and reversible redox reaction takes place at the surface of active materials. The pseudocapacitance arises due to thermodynamics reason and shows a derivative relationship between charges acceptance and change of potential in terms of $C=dq/dV$, which has been studied by Conway in 1975[2].

The main difference between EDLC and pseudocapacitor is that the latter is faradaic in origin, while the former only involves non-faradaic process.

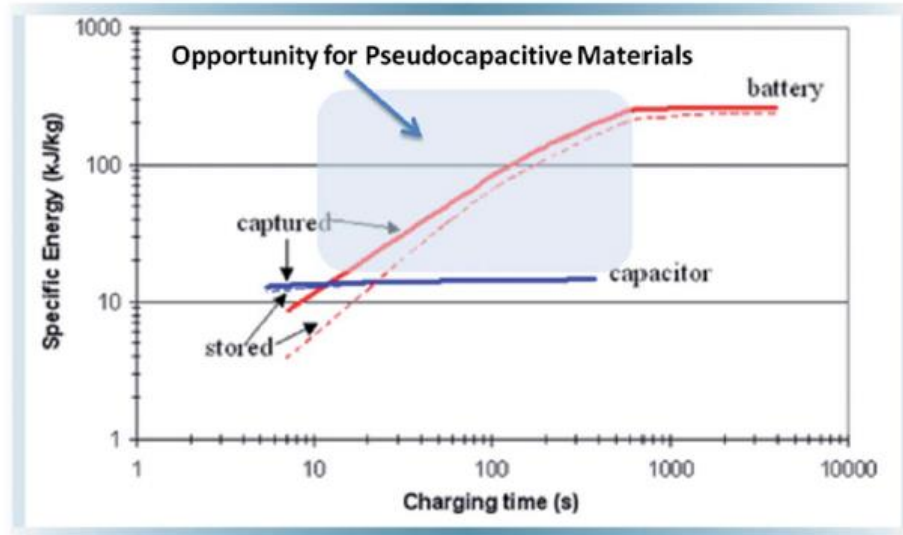


Figure 2.6 Energy vs. charging time for an EDLC and a lithium-ion battery.[7]

The energy versus charging time for EDLC, pseudocapacitor and lithium-ion battery is shown in fig. 2.6. It indicates that though its energy density is relatively high, a lithium-ion battery needs more than 10 minutes charging time to exhibit constant energy density. When look at the shorter timescales, the energy decreases due to various resistive losses within a battery cell, which may lead to serious safety problems like thermal runaway due to heat generation. [8] On the contrary, EDLCs perform constant energy density under all timescales without considering any safety issue, however, their total stored energy is low. In between the best performance of lithium-ion batteries and EDLCs, there is a region represents the time domain (10 s to 10 minutes) where is the opportunity for pseudocapacitors. The aims of studying the pseudocapacitors is to develop an energy

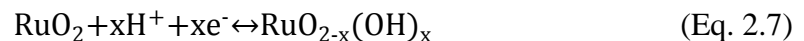
storage mechanism which can deliver both high energy density and high power density.

Table 2.1 Comparison between EDLCs and pseudocapacitors

EDLCs	Pseudocapacitors
Non-faradaic	Involves faradaic process
20-50 $\mu\text{F cm}^{-2}$	2000 $\mu\text{F cm}^{-2}$ for single-state process; 200-500 $\mu\text{F cm}^{-2}$ for multi-state, overlapping processes
C fairly constant with potential except through the p.z.c.	C fairly constant with potential for RuO_2 ; for single-state process, exhibits marked maximum
Highly reversible charging/discharging	Quite reversible but has intrinsic electrode-kinetic rate limitation determined by R_f
Has restricted voltage range	Has restricted voltage range
Exhibits mirror-image voltammograms	Exhibits mirror-image voltammograms

Ruthenium oxide is the first materials in which pseudocapacitive behavior has been discovered[9]. The protons from electrolyte was stored on the RuO_2 thin film electrode and resulted in a faradaic charge-transfer reaction. The cyclic voltammetry (CV) curve of such materials was that of a capacitor, in a rectangular shape (see fig. 2.7). Subsequent studies reported a specific capacitance over 700 F g^{-1} with porous[10], nanoscale architecture[11].

The storage of protons by RuO_2 can be expressed as:



When $x=2$, this results in a maximum theoretical capacitance of 1450 F g^{-1} of RuO_2 over a 1 V window.

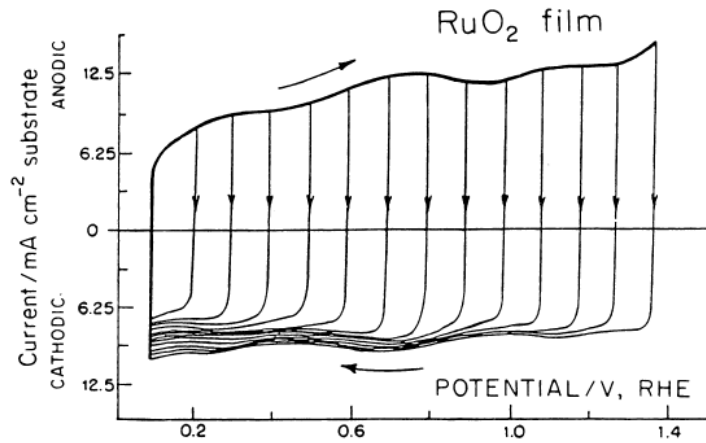


Figure 2.7 Cyclic voltammetry profiles for RuO_2 in aq. 0.1 M H_2SO_4 taken to a successive series of positive electrode potentials relative to RHE. Sweep rate, 50 mV s^{-1} ; 298K[12]

There are three types of pseudocapacitive mechanism (see fig. 2.8) due to different physical process and with different types of materials identified by Conway[2]:

- (1) Underpotential deposition. It takes place when a monolayer formed by metal ions was adsorbed on a different metal's surfaces under a potential higher than their redox potential. One example is lead on the surface of a gold electrode[13].
- (2) Redox pseudocapacitance (e.g. RuO_2). It occurs when ions are adsorbed electrochemically on the surface of a material with simultaneously faradaic charge transfer taking place.
- (3) Intercalation pseudocapacitance. It occurs when ions intercalate into tunnels or layers formed by redox-active materials with simultaneously faradaic charge transfer taking place and without any crystallographic phase change.

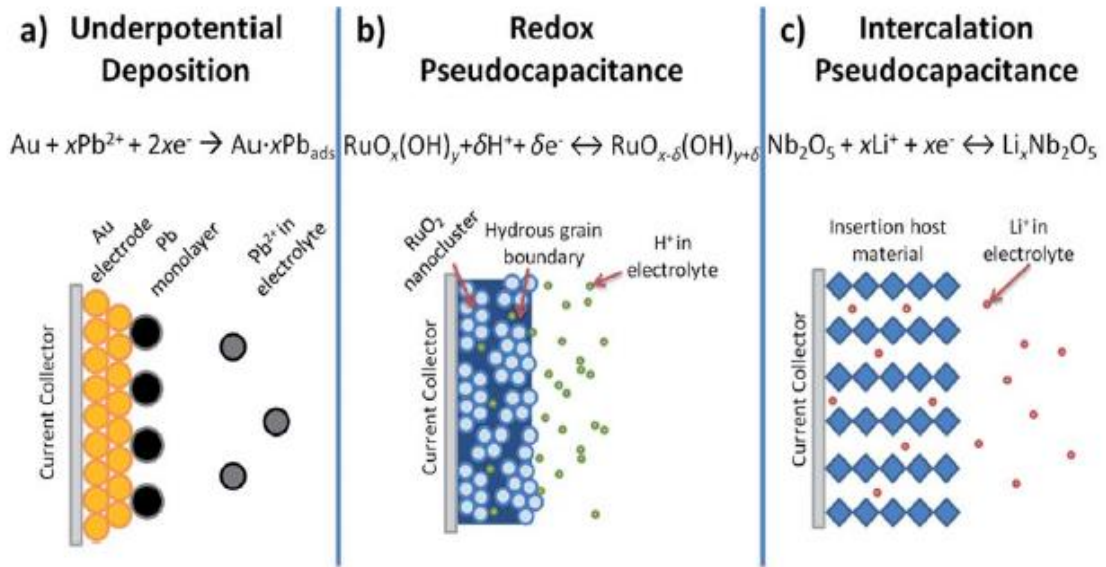


Figure 2.8 Different types of reversible redox mechanisms that give rise to pseudocapacitance: (a) underpotential deposition, (b) redox pseudocapacitance, (c) intercalation Pseudocapacitance.[14]

These three types of mechanism have similar relationship between potential and the extent of charges stored or released due to the adsorption/desorption process at the electrode/electrolyte interface[14], and it is expressed as the following way:

$$E \sim E^0 - \frac{RT}{nF} \ln \left(\frac{X}{1-X} \right) \quad (\text{Eq. 2.8})$$

Where E is the potential, R is the ideal gas constant ($8.134 \text{ J mol}^{-1} \text{ K}^{-1}$), T is the temperature, n is the number of electrons, F is the Faradaic constant (96485 C mol^{-1}), and X is the extent of fractional coverage of surface[15].

According to Eq. 2.8, the capacitance can be defined in the region where plot E vs X shows linear relationship:

$$C = \left(\frac{nF}{m}\right) \frac{X}{E} \quad (\text{Eq. 2.9})$$

Here m is the molecular weight of active material. The capacitance of pseudocapacitor is not always constant since the E vs X plot is not entirely linear.

2.3 Electrode materials for electrochemical capacitors

The electrode material is the major factor which influences the capacitance and energy storage of electrochemical capacitors. Accordingly, investigate and develop proper electrode materials with high capacitance and improved performance is the best way to overcome the limitation of ECs.

Table 2.2 Summary of the various classes of electrode materials investigated[16]

	Electrode material	electrolyte	Working voltage (V)	Specific capacitance (F/g)
Carbon-based	Activated carbon	1M Et ₄ NBF ₄ +PC	1.5	40
	Graphite	1M Et ₄ NBF ₄ +PC	3.0	12
	Multi-walled CNTs	1.96M TEMABF ₄ +PC	2.5	13
Metal oxides	RuO ₂	0.5M H ₂ SO ₄	1.0	650
	MnO ₂	0.5M K ₂ SO ₄	0.8	261
	V ₂ O ₅	2M KCl	0.7	262
Conductive polymer	Poly (3-methylthiophene)	PYR ₁₄ TFSI	3.6	25
	Polypyrrole	0.5M Pyrrole+ 0.5M β-NSA	0.9	345

Generally, three types of electrode materials can be applied in ECs: (1) carbon materials with high surface area[17, 18], they are mainly used in EDLCs, (2) metal oxides, such like RuO₂, MnO₂, and V₂O₅[19, 20], and (3) conducting polymers, such as polypyrrole[21, 22].

Metal oxides and conducting polymers are commonly used in pseudocapacitors. Some examples of these different types of electrode materials are given in table 2.2.

2.3.1 Carbon-based electrode materials

Due to their high chemical stability, rich in nature, non-toxic nature, relatively low cost, good electronic conductivity, wide application temperature range, variety of carbon-based materials such as activated carbon[23], carbon nanotubes[24, 25], graphene[26, 27], carbon aerogels[28, 29], graphite[18, 30] and other nano-structured carbon materials[31-33] have been widely investigated for their use as electrode materials of ECs. Normally, carbon materials store charges by electrochemical double-layer mechanism, in which charges are stored at the surface of electrode instead storing in the bulk of materials.

Therefore, the specific surface area, pore-size distribution, as well as pore shape and structure are important factors which can influence the capacitive performance of carbon materials[34]. Among those factors, the specific surface area and pore-size distribution play the most important roles affecting the performance.

Different methods such as heat treatment, alkaline treatment, steam activation, and plasma surface treatment with NH_3 have been investigated to increase the specific surface area[35-39]. However, a problem exist for high surface area carbon materials because not all the BET surface area can take part in the charge storage process, since some of the surface area is not electrochemically accessible when in contact with electrolyte. Therefore, the gravimetric capacitance of carbon materials does not always increase linearly with the specific surface area. In order to understand this phenomenon, many studies focus on the

pore-size distribution of carbon materials. Such studies draw more and more attention.

At first, scientists thought more contribution was made by mesopores (2-50 nm wide) than by micropores (<2 nm wide) to capacitance due to the long-held axiom that pores smaller than twice the size of solvated electrolyte ions are incapable to contribute to charge storage[40]. In this case, many studies developed template synthesis route which has been proved as an effective method to control the pore size to fabricate carbon materials with mesopores (2 to 10 nm). Although the measured specific capacitances of those templated carbon materials were slightly higher than standard carbon materials, they didn't show a large increase.

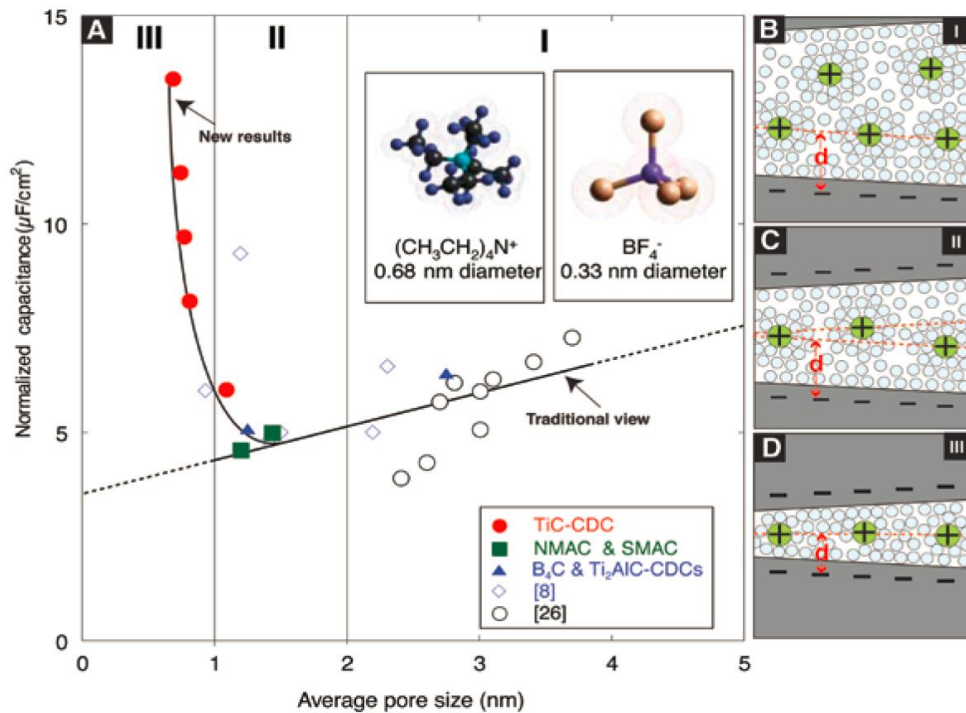


Figure 2.9 Normalized capacitance versus average pore size for TiC-CDC and other carbons from literature tested in the same electrolytes[41].

At the same time, some scientists reported surprising results that much higher specific

capacitance can be achieved by carbon materials with microporous structure (see fig. 2.9). It indicates that the normalized capacitance decreased as the average pore size decrease in accord with traditional view until the pore size reach a critical value. The pores smaller than 1 nm, make great contribution to the normalized capacitance which might be attributed to a closer approach of the solvation ion to carbon surface due to the distortion of ion solvation shell[41]. Other studies also suggested that the pore size of 0.4 or 0.7 nm may be suitable for aqueous electrolytes while for organic electrolytes, pore size of 0.8 nm could be better. Therefore, the key point of designing advanced structure of carbon materials is the match between pore size and ion size to achieve the maximum capacitance.

Apart from high surface area and proper pore size, surface functionalization has also been proved as an effective way to improve the capacitive performance of carbon materials[42-47]. Functional groups and heteroatoms such as nitrogen, boron, and sulfur are believed to help the adsorption of ions, improve hydrophilicity/lipophilicity of carbon materials and facilitate rapid ion transport within micropores. Moreover, those functional groups on the surface of carbon materials can induce redox reactions result in a 5-10% total capacitance increase. However, there are drawbacks of surface functionalization such as high intrinsic electrical resistance due to the bonded heteroatoms, or increased risk of electrolyte decomposition induced by active functional groups.

2.3.1.1 Activated carbon

Due to its large surface area, relatively good electrical conductivity, and moderate cost, activated carbons (ACs) are the most widely used electrode materials for ECs. Normally,

various types of carbonaceous materials such as wood or coal are used to produce ACs through thermal or chemical treatment.

The thermal activation is usually carried out at a temperature range of 400-700 °C, and phosphoric acid, potassium hydroxide or sodium hydroxide are used as activating agents. The thermal activation is normally conducted at a higher temperature (from 700-1200 °C), in the presence of oxidizing gas. ACs possess high surface area and various physicochemical properties depending on different activating treatment and different carbon precursors. Therefore, they can be commercially used as electrode materials for ECs[35, 48-50].

However, ACs' applications are still restricted due to its limited energy storage and rate capability. Although ACs have relatively high surface area, their pore size distribution and pore structures are not easy to control, and this is a really big challenge for AC application in ECs.

2.3.1.2 Graphene

Graphene is another type of carbon materials which incurred great interest since its free standing form was discovered in 2004[51], and it recently has been considered as a promising electrode material for EDLCs. Compare to activated carbon, graphene not only has high surface area, but it also exhibits faster electron mobility and higher conductivity due to its two-dimensional one-atom-thick planar structure (see fig. 2.10). Therefore, it is believed that EDLCs with high energy and power density can be achieved by using graphene based electrodes.

Since the properties of graphene are highly dependent on its fabrication process, the synthesis method of graphene is a heavily researched topic. There are many synthesis methodologies of graphene such as exfoliation (physical, mechanical or chemical)[52, 53], reduction of sugars[54], the unzipping of CNTs, and epitaxial growth via chemical vapor deposition (CVD)[55].

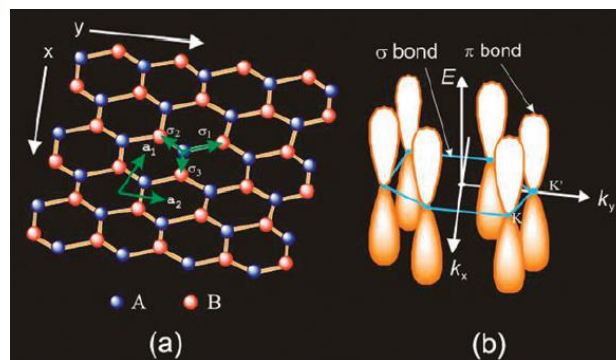


Figure 2.10 (a) The crystal structure of graphene (b) Electronic Band structure of graphene[26]

Although graphene has made a significant impact for the development of EDLCs, there are still some limitation of its application such as the current high cost, reproducibility, and scalability which means more appropriate experiments and comparison need to be developed and conducted.

2.3.1.3 Carbon nanotubes

Carbon nanotubes (CNTs) have great advantages such as good mechanical and thermal stability, excellent electrical properties, and easily accessible surface area due to its unique pore structure, which draw a great deal of attention for EDLCs electrode applications (see fig. 2.11) for high power delivery[56-58]. CNTs are produced by the catalytic

decomposition of certain hydrocarbons and can be classified as single-walled carbon nanotubes (SWCNTs) and multi-walled carbon nanotubes (MWCNTs) based on the layers of rolled graphene sheets.

It has been reported that the specific capacitance of CNTs based electrodes for ECs varies from 15-102 F g⁻¹ with surface areas range from 120-430 m² g⁻¹ depending on different morphology and purity[36, 40, 59]. And chemical activation has been considered to be an efficient way to increase the energy density of CNTs by increasing their specific surface area, the only concern is regarding the balance between the porosity and the conductivity, in order to achieve both high capacitance and good rate performance.

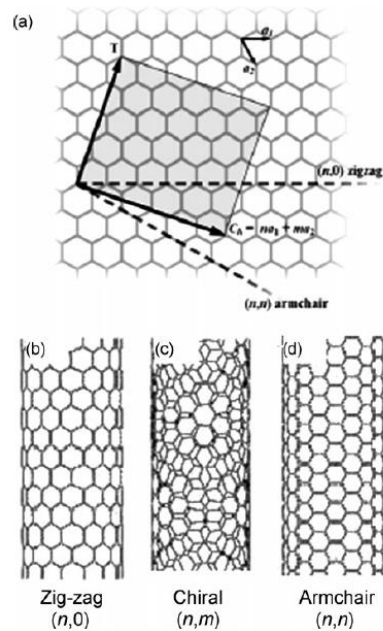


Figure 2.11 Atomic structure of carbon nanotubes[60]

The main drawback of CNTs is its limited surface area which restrict its application of high energy performance EDLCs. Moreover, the high cost of the production and difficulty

purification of CNTs also need to be taken into account when utilizing CNTs as electrode materials of ECs.

2.3.1.4 Other carbon structures

Recently, other carbon materials such as carbon fibers, carbon aerogels and carbon onions have also been investigated for EDLCs applications. It has been reported that carbon fibers can exhibit a high specific capacitance value of 371 F g^{-1} after activation. However, a long term stability problem may be incurred due to high surface area of such materials together with surface functional groups[61]. Carbon aerogels attracted significant attention due to their ultralight weight, highly porous structure and possibility of usage without binding substance. However, small improvement of energy storage capacity has been made although the total surface area was increased significantly (from 592 to $2371 \text{ m}^2 \text{ g}^{-1}$)[62]. It was found that the high internal resistance of the carbon aerogels limited their applications. Therefore, a new type of carbon nanotube aerogels with remarkable specific surface area and a special textural porosity with almost equal amounts of mesopores and micropores seems to be a promising electrode materials despite the difficulty of production[62].

2.3.2 Transition metal oxides

Transition metal oxides are considered as promising electrode materials for ECs with higher energy density compared to traditional carbon materials. Those selected metal oxides should have good electrical conductivity, as well as two or more oxidation states coexist in a continuous range without phase changes involving. Such oxidation states allow

them to store energy not only in an electrostatic way, but they also exhibit faradaic reactions between electrodes and ions within appropriate voltage windows[63]. Among those metal oxides, RuO_2 is considered as the most promising candidate for ECs due to its high specific capacitance, good conductivity, good electrochemical reversibility and high rate capacity[64]. However, the lack of abundance and the high cost of precious metal Ru limited its commercial production. Therefore, other transition metal oxides like MnO_2 , NiO , and V_2O_5 are recently under investigation as alternative materials for RuO_2 .

2.3.2.1 Ruthenium oxides

RuO_2 was first reported as electrode material for ECs by Trasatti and Buzzanca in 1971[9]. For ECs using RuO_2 electrodes, only 10% of accumulated charges are contributed by electrochemical double-layer charging, the rest of them are contributed by redox pseudocapacitance mechanism. Those redox reactions involved in pseudocapacitance are highly reversible, which means that in appropriate voltage range, the resulting cyclic voltammogram (CV) for one direction of potential sweep is nearly mirror image of that generated for the opposite direction of sweep, an equilibrium situation is maintained at all states of charges across CV or along the charging curves. In contrast, redox reaction involved in battery is highly irreversible, different range of potentials are required for oxidation compared to that for its reduction (see fig. 2.12)[65].

The mechanism of pseudocapacitive behavior in acidic electrolytes can be described according to equation 2.10, a rapid reversible electron transfer is combined with electroadsorption of protons on the surface of RuO_2 , and the Ru states change from Ru(II) to Ru(IV)[66-70].

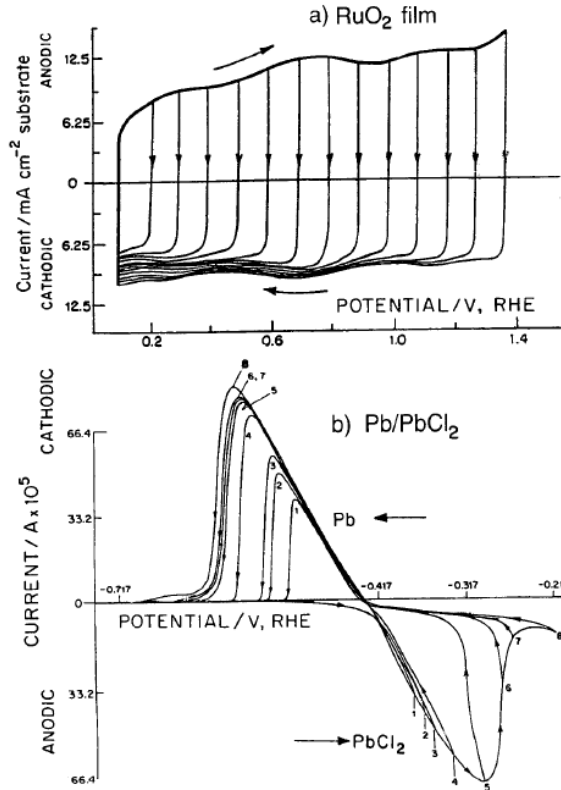


Figure 2.12 (a) Cyclic voltammogram for RuO₂ in 1 M aqueous H₂SO₄ (298K) showing mirror image symmetry along the scanned potential range. (b) Cyclic voltammogram for Pb-PbCl₂ battery electrode showing typical irreversible process[65].

Several factors play important roles in electrochemical behavior of RuO₂ such as specific surface area, the water content hydrated in RuO₂, and the size of RuO₂ particles. By optimizing those factors, the specific capacitance of RuO₂ can be increased from 720 to 1340 F g⁻¹ accompany with a significantly decreased charge-discharge time from 8 to 1 minute, which is quite close to the theoretical capacitance value of 1500 F g⁻¹[10, 71]. Although RuO₂ exhibits high energy storage and power delivery as an electrode material of ECs, its scarcity and high cost are still prohibitive for large scale commercial production,

only military application can be considered.

2.3.2.2 Manganese oxides

MnO_x was discovered by Lee and Goodenough as an alternative electrode material for ECs in 1999[72], since then, it draw more and more attention due to its high theoretical capacities ranging from 1100-1300 F g⁻¹, relatively low cost, and environmental safety[73-76]. The capacitance of MnO_x arises from pseudocapacitive mechanism, in which the reversible redox reactions involving the exchange of protons or cations between electrode and electrolyte accompany with the states change between Mn(III)/Mn(II), Mn(IV)/Mn(III), Mn(VI)/Mn(IV) within appropriate voltage window[77, 78]. This mechanism can be described by the following equation[79, 80]:



Here C⁺ signifies protons or alkali metal cations such as Li⁺, Na⁺, and MnO_α(OC)_β and MnO_{α-β}(OC)_{β+α} denote MnO₂·nH₂O in different oxidation states.

The pseudocapacitive performance of Mn oxides is highly dependent on its physical and chemical properties. For example, the specific capacitances of Mn oxides electrodes are mainly controlled by their chemically hydrous state, and their cyclic stability are governed by their microstructures[81-83].

Moreover, there are several challenges need to be addressed in order to realize the commercial application of Mn oxides for ECs, such as the dissolution problems, low surface area, poor electronic conductivity and ionic conductivity[84, 85].

2.3.2.3 Other oxides

Other metal oxides which also have been under investigation of electrode materials for ECs including Co_3O_4 , SnO_2 , ZnO , TiO_2 , V_2O_5 , Fe_2O_3 , NiO , and etc[86, 87]. The theoretical capacitance values as well as the charge storage reactions of typical metal oxides are listed in table 2.3.

Table 2.3 Pseudocapacitance and conductivity of selected metal oxides[88]

Oxide	Electrolyte	Charge storage reaction	Theoretical capacitance (F g^{-1})	Conductivity (S cm^{-1})
MnO_2	Na_2SO_4	$\text{MnO}_2 + \text{M}^+ + \text{e}^- = \text{MMnO}_2$	1380 (0.9V)	10^{-5} - 10^{-6}
NiO	KOH , NaOH	$\text{NiO} + \text{OH}^- = \text{NiOOH} + \text{e}^-$	2584 (0.5V)	0.01-0.32
Co_3O_4	KOH , NaOH	$\text{Co}_3\text{O}_4 + \text{OH}^- + \text{H}_2\text{O} = 3\text{CoOOH} + \text{e}^-$ $\text{CoOOH} + \text{OH}^- = \text{CoO}_2 + \text{H}_2\text{O} + \text{e}^-$	3560 (0.45V)	10^{-4} - 10^{-2}
V_2O_5	NaCl , Na_2SO_4	$\text{V}_2\text{O}_5 + 4\text{M}^+ + 4\text{e}^- = \text{M}_2\text{V}_2\text{O}_5$	2120 (1V)	10^{-4} - 10^{-2}
RuO_2	H_2SO_4 , Na_2SO_4	$\text{RuO}_2 + x\text{H}^+ + x\text{e}^- = \text{RuO}_{2-x}(\text{OH})_x$	1200-2200 (1.23V)	1 - 10^3

It is indicated that compare to carbon materials, metal oxides electrodes can exhibit one order of magnitude higher specific capacitance. However, those large capacitance can only be delivered at slow scan rate or low current density. Therefore, the metal oxides are hardly to be applied alone as electrodes for ECs because of some limitations including very low electronic conductivity (most metal oxides except RuO_2), poor long term stability (electrodes crack during charge-discharge due to strain development), difficulty in tailoring the surface area as well as the pore size distribution[88].

2.3.3 Conductive polymers

Conducting polymers are considered as another group of potential electrode materials for ECs based on pseudocapacitive mechanism. They have been widely investigated since they were first reported to be utilized for ECs in 1990s due to their low cost, high theoretical capacitance, good conductivity, and ease of fabrication. Therefore, ECs devices with low equivalent series resistance, high power and high energy density can be developed with conducting polymer based electrodes[89].

Conducting polymers exhibits good conductivity due to its conjugated bond system along the polymer backbone. Typically, they are fabricated through chemical or electrochemical oxidation of monomers. The oxidation of monomers and oxidation of polymers with the insertion of counter ion take place simultaneously during the fabrication process[90].

Various conducting polymers structures are shown in fig. 2.13.

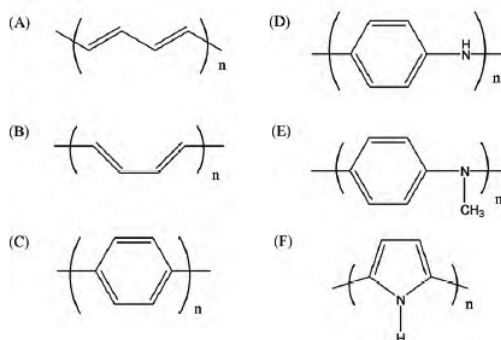
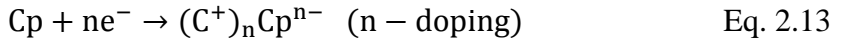
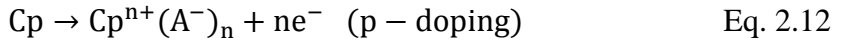


Figure 2.13 Different structures of conducting polymers[91]

Different conducting polymers have different doping types, they can be p-doped with anions during oxidation reaction or n-doped with cations during reduction reaction. The charging process can be described by simplified equations:



Where A^- denotes anion, C^+ denotes cation. The discharging process is along the opposite direction of above equations. Based on the charging mechanism, conducting polymers can achieve much higher specific capacitance due to the bulk of materials can take part in the charging-discharging process compare to carbon materials whose capacitance can only arise from the surface of electrode (see figure 2.14).

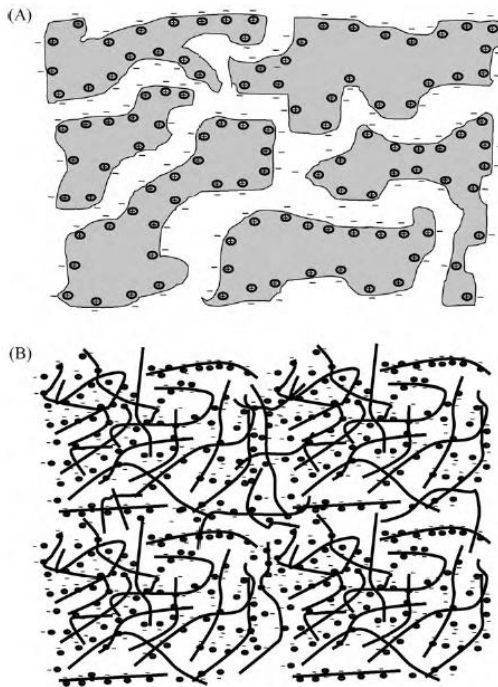


Figure 2.14 Comparison of charging of (a) double-layer capacitor (carbon) and (b) pseudocapacitor (conducting polymer)[91]

Typically, the doping level of conducting polymers is around 0.3 to 0.5, which means 2-3 monomer units per dopant. The theoretical specific capacitance of conducting polymers can be estimated by the following equation (Eq. 2.14)[92]. The theoretical specific

capacitances and conductivity of different conducting polymers are listed in Table 2.4.

$$C_{ts} = \alpha \cdot F / (\Delta E \cdot M) \quad \text{Eq. 2.14}$$

Where C_{ts} denotes theoretical specific capacitance, α denotes doping level, F is the faraday constant ($=96485 \text{ C mol}^{-1}$), M is the molecular mass of the monomer unit, and ΔE is the potential window.

Table 2.4 Theoretical specific capacitances of conducting polymers[93-95]

Conducting polymer	Mw (g mol⁻¹)	Dopant level	Potential range (V)	Conductivity (S cm⁻¹)	Theoretical capacitance (F g⁻¹)
Polyaniline	93	0.5	0.7	0.1-5	750
Polypyrrole	67	0.33	0.8	10-50	620
Polythiophene	84	0.33	0.8	300-400	485
PEDOT	142	0.33	1.2	300-500	210

2.3.3.1 Polyaniline

Polyaniline (PAni) has been widely studied as supercapacitor or battery materials due to its high electroactivity, high doping level, good environmental stability and high specific capacitance. It can only be p-doped, since the potential required for its n-doping process is too negative to reach[96-98].

PAni can be fabricated by both chemical and electrochemical polymerization methods with various substrates such like nickel, stainless steel, etc. It has been reported that PAni-based ECs exhibit a wide range of specific capacitance from 30 to 3000 F g⁻¹, since the properties of PAni can be influenced by many factors, such as polymerization process, dopant concentration, ionic diffusion length of the electroactive materials and structural morphology[96, 99-102]. The cyclic voltammogram of PAni-based electrode is shown in

figure 2.15.

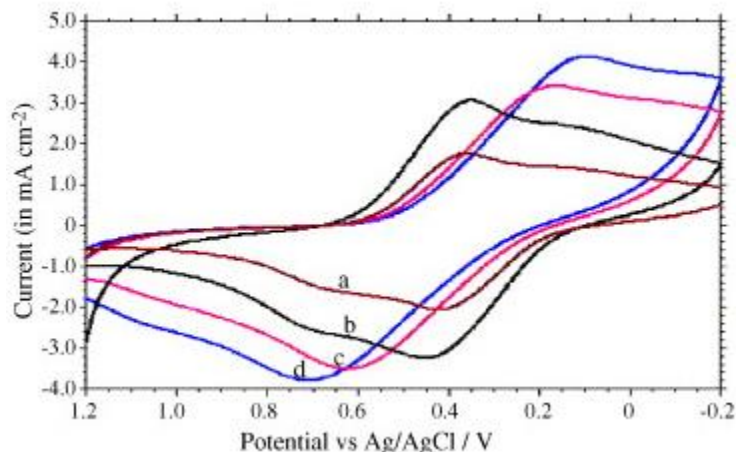


Figure 2.15 Cyclic voltammogram for Ni/PAni at various sweep rates: (a) 25.0 mV s^{-1} , (b) 50.0 mV s^{-1} , (c) 75.0 mV s^{-1} and (d) 100 mV s^{-1} [101].

A major disadvantage limits the application of PAni is that it requires a protic solvent, an acidic solution or a protic ionic liquid to work as electrolyte, since it needs a proton to be properly charged and discharged. Therefore, it increases the cost and lowers the environmental safety of PAni-based ECs[103]. Additionally, the relatively low mechanical stability and limited cycle life also constraint its performance.

2.3.3.2 Polypyrrole

Polypyrrole (PPy) is one of the most important p-doped conducting polymer for EC application, due to its unique features such like high specific capacitance and electrical conductivity, fast charge-discharge mechanism, good thermal and chemical stability, and low cost. Similar to PAni, PPy can be fabricated through both electrochemical and chemical oxidation reactions and different microstructure can be obtained by controlling synthetic

conditions (see fig. 2.16). The electrochemical property of PPy also depends on the synthesis route used, the amount and type of binders and dopants, and the thickness of electrode materials.

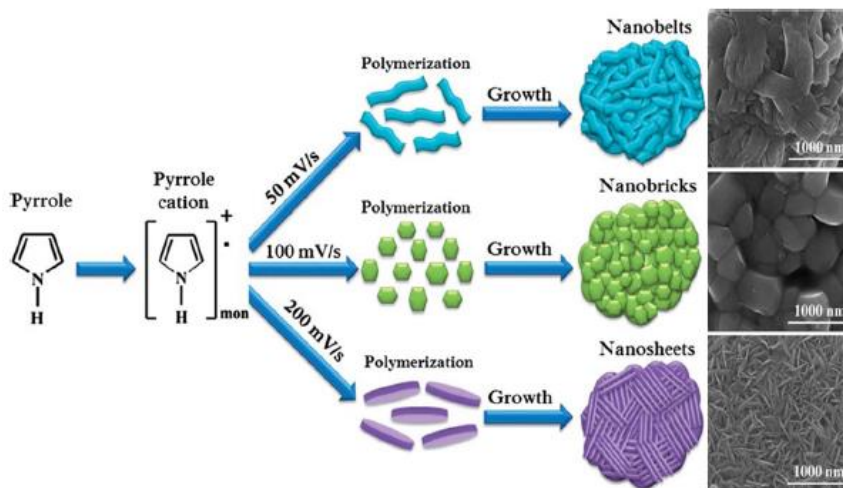


Figure 2.16 Synthesis of PPy nanostructures by electropolymerization[104].

PPy is typically doped by single charge likes Cl^- , ClO_4^- , SO_3^- or multiple charge anions like SO_4^{2-} . Some studies indicated that PPy doped with multiple charge anions result in physical crosslinking of polymers. Therefore, high capacitance can be achieved by cross-linked PPy due to its high ion diffusivity and porosity of active materials. It has also been reported that PPy with great density exhibits high capacitance per unit volume like $400\text{-}500 \text{ F cm}^{-3}$. However, the dense and thick growth of PPy limited the access of dopant ion to the interior sites of polymer backbone, thus, the capacitance per gram is reduced significantly for thicker coating film on electrode substrate. Additionally, the limited cyclic stability due to degradation and swelling of the polymer also need to be addressed for application of PPy-based ECs.

2.3.3.3 Other polymers

Different from PANi and PPy, polythiophene (PTh) and its derivatives such like poly(3,4-ethylenedioxythiophene) (PEDOT), poly(3-(fluorophenyl)thiophene) (PFPT), poly(3-methylthiophene) (PMeT), and poly(ditheno(3,4-b:3',4'd) thiophene) (PDTT) can be both p-doped and n-doped which will give them advantage of wide application[93, 105]. However, compared to n-doped PTh and its derivatives, p-doped polymers not only exhibit higher electrical conductivity, better capacitive performance, but they are also highly stable in air and humidified environment. It has been reported that p-doped PDTT electrode showed a capacitance of 106.4 mF cm^{-2} , while n-doped PDTT electrode exhibits 43.2 mF cm^{-2} . It was found that, n-doped polymers have higher self-discharge and shorter cycle life, which limit their development and application for ECs[106, 107].

2.3.4 Composite electrodes

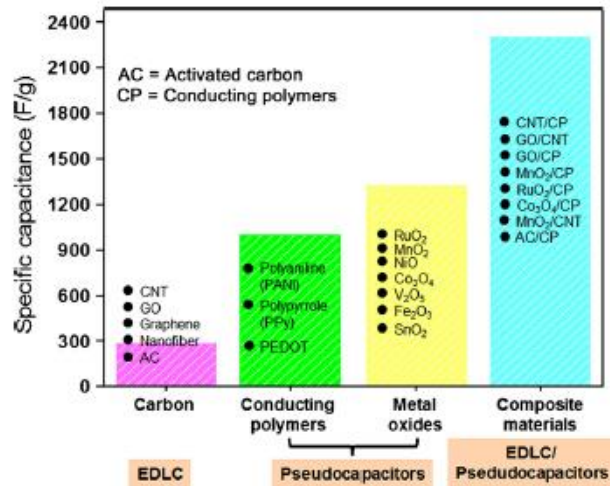


Figure 2.17 Comparison of various materials according to their specific parameter for supercapacitor applications[108].

Generally, electrode materials based on double-layer capacitive mechanism (carbon materials) can achieve high power density, high conductivity, good environmental stability, and ultra-long cycle life. However, their low specific capacitance and energy density limit their application. On the contrary, electrode materials based on pseudocapacitive mechanism (metal oxides or conducting polymers) have high specific capacitance and enhanced energy storage capacity. Nevertheless, the poor electrical conductivity of metal oxides and mechanical degradation of conducting polymers during redox reaction impede their application.

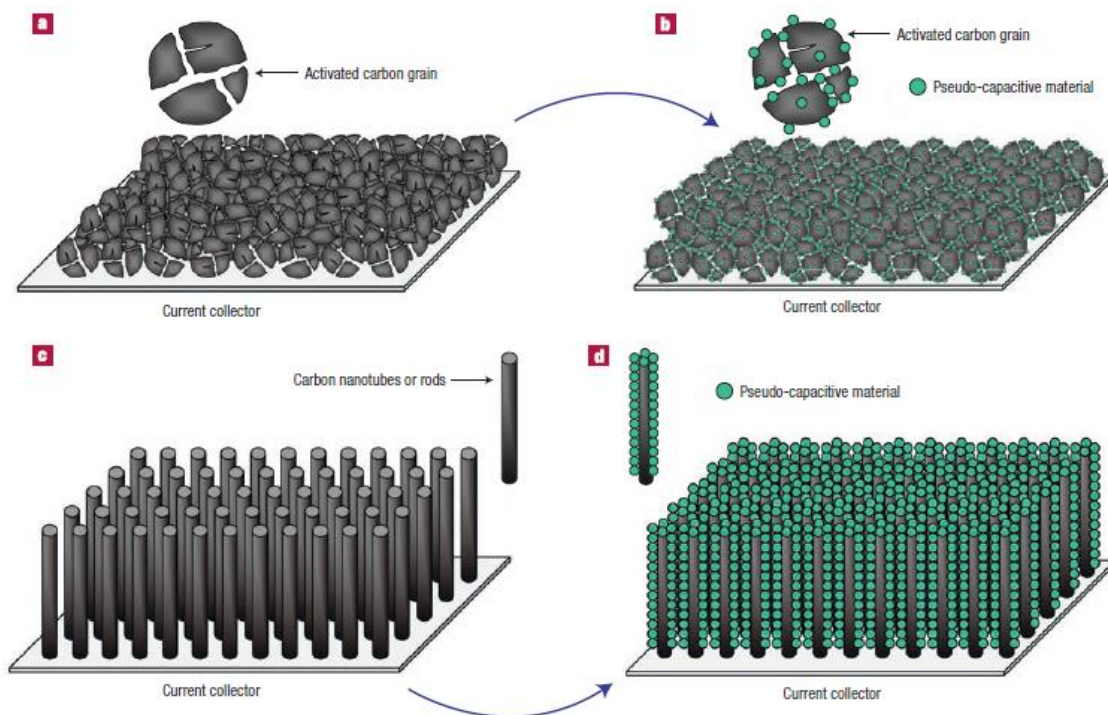


Figure 2.18 Possible strategies to improve both energy and power densities for electrochemical capacitors[61].

In this situation, a concept of composite electrode materials was proposed in order to

combine the advantages of those two types of electrode materials and eliminate the drawbacks. Using carbon materials as support not only can improve the electrical conductivity and mechanical strength of conducting polymers, but the cyclic stability and capacitance value of such electrode materials can also be enhanced (see fig. 2.17). Therefore, more and more studies, focused on composite electrode materials, have been carried out [109-111]. The possible strategies of design of composite electrode materials are described in fig 2.18. Pseudocapacitive materials like PPy can be deposited on the activated carbon grain particles or carbon nanotubes or rods to improve its electrical conductivity, surface area, and mechanical strength which may result in promising composite electrode materials with high energy density, high power density and good cyclic stability.

2.4 Electrolytes

Another important factor which can significantly influence the capacitive performance of EC device is electrolyte. There are two major criteria for the selection of an electrolyte. One is its electrochemical stability window, which is important to achieve higher energy density. The other is ionic conductivity, which can influence the power delivery. There are three types of electrolytes applied in EC device, which are organic, aqueous electrolyte and ionic liquid.

2.4.1 Organic electrolytes

The advantage of an organic electrolyte is it can help to achieve much higher voltage, which can benefit the energy storage of EC, since the maximum stored energy of EC is proportional to the square of cell voltage. Normally, organic electrolytes allow for a cell

voltage range from 2.3 to 2.7 V according to electrolyte with different water content[60]. In order to target even higher voltage, extreme purification procedures as well as protective coating for corrosion resistance of carbon electrode are required for application. On the other hand, organic electrolytes exhibit significantly higher resistance and result in lower power delivery. In addition to that, the high cost, low dielectric constant as well as safety concern such like flammability and toxicity of organic electrolytes still limit their applications.

2.4.2 Aqueous electrolytes

Different from organic electrolytes, aqueous electrolytes limit the cell voltage of EC to typically 1 V due to their low electrochemical stability[112], thus the energy density is reduced. However, aqueous electrolytes exhibit excellent conductivity (up to 1 S cm^{-1}) and allow higher power delivery to be achieved. In addition, the less stringent purification and drying process result in a much lower cost for production. In order to increase the voltage window, electrolytes with neutral pH instead of acid electrolytes were investigated. It has been reported that, symmetric AC cell can achieve up to 2 V with good charge-discharge cycle life in Na_2SO_4 and Li_2SO_4 [113]. Moreover, compare to organic electrolytes, aqueous electrolytes with neutral pH have much less safety issues and are more environmental friendly, which can also benefit EC for commercial applications[113-115].

2.4.3 Ionic liquid electrolytes

Another type of electrolytes is ionic liquids, which are also known as room temperature molten salts- ionic liquids are considered to be next generation electrolytes due to their high thermal stability, non-toxicity, non-flammability, high electrochemical stability and various combination of choices of cations and anions[60]. Commercial devices based on carefully chosen ionic electrolyte can achieve 1000 F within 3 V window[116]. However, the low ionic conductivity of ionic liquids at room temperature still affect their performance, since ECs are mainly used in the temperature range from -30 to 60 °C. In this case, develop ionic liquids with high ionic conductivity and large voltage window (more than 4 V) for practical application is still challenging.

2.5 Synthesis methods

In order to obtain high quality PPy to fabricate electrodes for ECs, fabrication method play a very important role. There are two major methods for the fabrication of PPy, one is electropolymerization method and the other is chemical polymerization method.

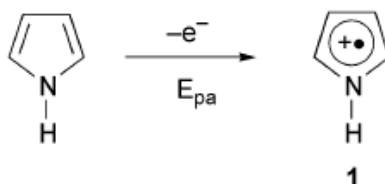
2.5.1 Electropolymerization

In the electropolymerization method, the pyrrole monomer, dissolved in a solvent, containing an anionic dopant, is oxidized at the electrode surface by the applied anodic potential to form a polymer film. The selection of solvent is important, since it has to be stable at oxidation potential of monomer and provide an ionic conductive medium. For those polymer who requires very large potential window to achieve electropolymerization,

organic solvents like acetonitrile is a good choice. But for polypyrrole, electropolymerization is capable to be carried out in aqueous solvent due to the relatively low oxidation potential of pyrrole.

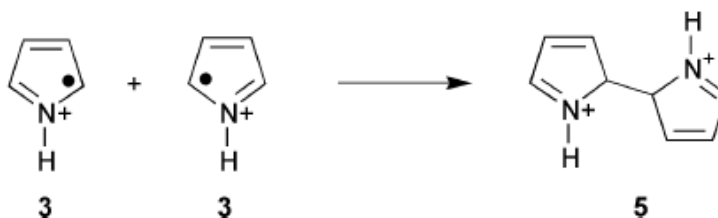
The anode can be made of different materials like platinum, gold, glassy carbon, and tin or indium-tin oxide (ITO) coated glass[117]. The electropolymerization process can be achieved by either galvanostatic (constant current) or potentiostatic (constant potential) methods. During this process, monomers are initially oxidized, then cation radical of monomers are formed and react with other monomers to form oligomeric products and finally the polymer. The synthesis and doping of polymer are generally take place at the same time. The detailed mechanism of electropolymerization has been investigated many years, but there is still no one mechanism can be universally accepted due to some controversial point like the way of beginning the reaction, proton transfer and direct radical pyrrole formation. Here, the Diaz's mechanism which is the one mostly referred to in the literature is used to illustrate the process for electropolymerization of pyrrole.

In the first step, monomers are oxidized at the surface of electrode to form cation radical (see scheme 1).



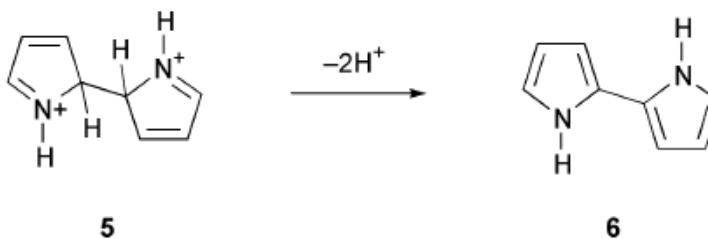
Scheme 1

After that, cation radicals are coupled and result in the formation of a bond between them and the formation of the dication (see scheme 2).



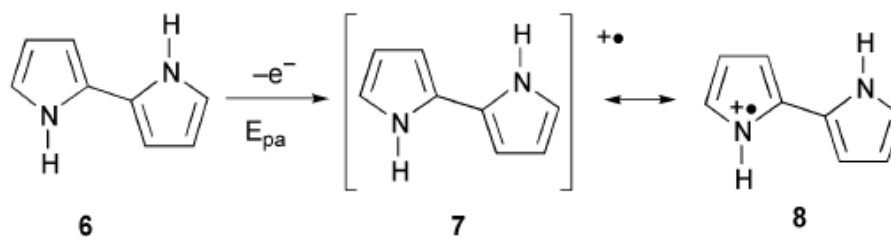
Scheme 2

In the third step, two dications lose two protons and form the aromatic dimer (see scheme 3).



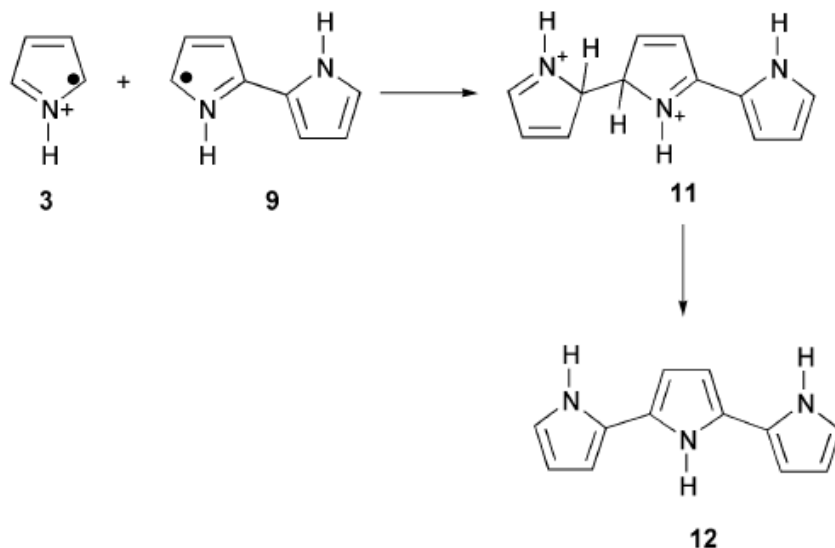
Scheme 3

After that, the dimer is oxidized into the cation radical (shown in scheme 4).



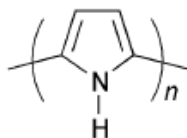
Scheme 4

In the step 5, the cation radical of dimer and cation radical of monomer coupled result in the formation of aromatic trimer (see scheme 5).



Scheme 5

The final polypyrrole product (see scheme 6) can be obtained by the reaction propagation via the same sequence: oxidation, coupling, and deprotonation.



Scheme 6

2.5.2 Chemical polymerization

Different from the electropolymerization method, in which the oxidation process takes place at the surface of an electrode, the chemical polymerization method allows for the formation of PPy powders by the oxidation of pyrrole monomers in the bulk solutions in

the presence of oxidants and dopants. Relatively strong chemical oxidants are used, such as ammonium peroxydisulfate (APS), permanganate or bichromate anions, ferric ions, or hydrogen peroxide[118]. These oxidants can oxidize pyrrole monomer in proper solvent resulting in chemically activated cation radical of monomers. Similar to electropolymerization method, the chemical polymerization process follows sequence likes oxidation of monomers, cation radicals coupled and deprotonation and form dimer, then trimer and so on. And the resulting polymers precipitate as insoluble solids in the solvent. The major factors influence the properties of obtained PPy are the concentration of solution components, the concentration of oxidants and dopants, and the treatment temperature.

2.6 Influence of dopants

The choice of the dopant is of particular importance for the fabrication of PPy since film adhesion, conductivity and microstructure are influenced by the dopant molecules.

2.6.1 Influence of anodic electropolymerization on non-noble metals

It was shown that anionic dopants can passivate the surface of non-noble electrodes and prevent their oxidation and dissolution during anodic electropolymerization of PPy[119]. Adherent films were obtained on stainless steel from aqueous oxalate solutions[119]. However, the formation of the non-conductive and non-capacitive iron oxalate layer[120] can result in increasing charge transfer resistance and reduced electrochemical capacitance of the PPy electrodes (see fig. 2.19).

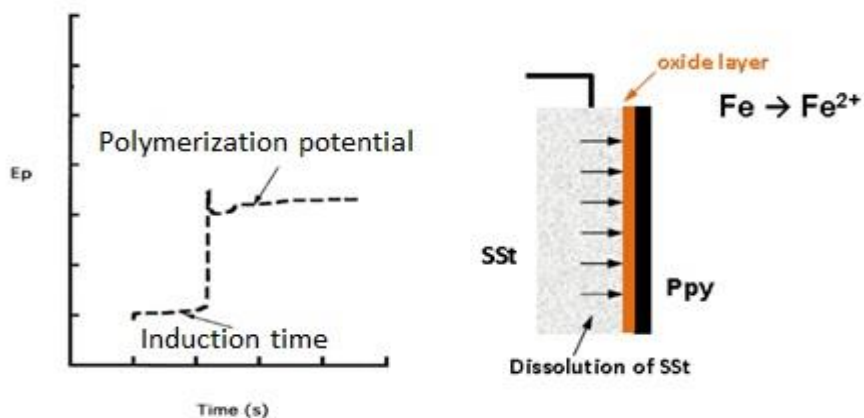


Figure 2.19 Polymerization potential of PPy using oxalate and the formation of oxide layer on stainless steel substrate[119].

Another strategy is based on the use of aromatic molecules. It was found that Tiron promoted charge transfer during electropolymerization, reduced electropolymerization potential and prevented dissolution of Al substrates during electropolymerization (see fig. 2.20) [121].

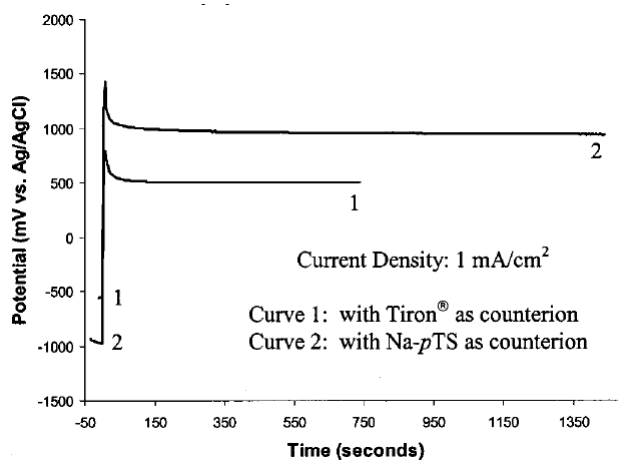


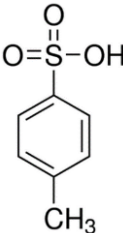
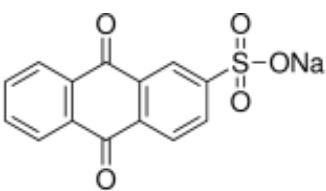
Figure 2.20 Potential/time curves for the galvanostatic deposition of polypyrrole on Al 2204-T3 at 1 mA cm⁻² current density in the presence of Tiron (curve 1) and in the presence of Na-pTS (curve 2)[121]

Therefore, the choice of proper aromatic dopant is a promising way to achieve electropolymerization of PPy on non-noble substrates without the formation of oxide layer.

2.6.2 Influence of electrical conductivity of PPy

Relatively high electrical conductivity of PPy films can also be achieved using aromatic anionic dopants[122]. It was found that aromatic dopants promote preferred orientation of pyrrole ring parallel to the electrode or growth surface[123]. The anisotropic film growth resulted in enhanced conductivity. It was reported that with the variation of the dopant anion, the conductivity of the PPy thin films can differ by three orders of magnitude[124]. Electrical conductivity of PPy, doped with different inorganic dopants and aromatic dopants was shown in table 2.5.

Table 2.5 Electrical conductivity of PPy using different dopants[124]

Dopants	PPy-Cl ⁻	PPy-HSO ₄ ⁻	PPy-TS ⁻	PPy-AQS ⁻
Conductivity σ (S/cm)	1.59	3.08	7.10	120
Molecular formula or structure	FeCl ₃	(NH ₄) ₂ S ₂ O ₈		

The comparison of the experimental data for different aromatic molecules, containing anionic sulfonic groups, showed that the conductivity also increased with increasing charge/volume ratio of the molecules[123].

2.6.3 Influence of microstructure of PPy

Not only the conductivity, but also the structure of PPy can be influenced by the dopant molecules[125]. The anionic dopant showed significant influence on the size and shape of particles and electrochemical performance of PPy, prepared by chemical polymerization method[126, 127]. It was found that PPy nanoparticles, nanofibers and nanorods can be obtained by the variation of dopant concentration[128]. Improved conductivity and thermal stability of PPy nanofibers was achieved using aromatic dopants[128, 129].

Moreover, the voltage window and cycling stability of PPy films can be improved by the use of polyaromatic dopant molecules[130]. The large polyaromatic molecules were considered[130] as “fixed” bulky dopants, which provided improved cycling stability of the ES electrodes. However, the limited mobility of the large dopants can result in restricted doping levels and reduced conductivity of films prepared by electropolymerization[123].

2.7 Application of ECs

ECs are electrochemical energy sources with advantages of high power delivery and uptake with an ultra-long cycle life, non-toxicity and environmental compatibility. They are ideal energy sources for those applications which demanding energy in the time range from 10^{-2} s to 10^2 s.

Recently, small EC with a few faradas capacity is the largest part sold in the market. They are widely used for power buffer application or as memory back-up in consumer electronic products such as cameras, video recorders, toys. In these products, there is a primary source which normally provides an energy. When power outages due to disconnection or contact

problem take place, the EC can supply energy to the critical consumers[131, 132]. The basic design is shown in fig. 2.21.

ECs can also be used as the main power source. One or several large current pulse of several ms to several s can be delivered by such devices. For example, cordless tools such as electric cutters and screwdrivers using ECs have already been produced. They can be fully charged or discharged in less than 2 min, and the cycle life of EDLC is much longer than that of tools[61].

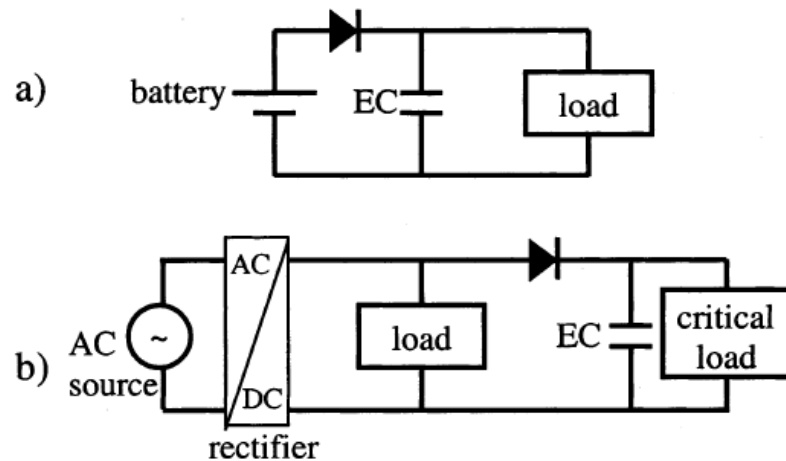


Figure 2.21 Use of ECs in electronic circuits. (a) shows a battery powered device where EC provides power backup of the load in case of disconnection of the battery. (b) shows an AC-voltage powered device involving heavy switching currents. The EC protects the critical load from large voltage drops[133].

The main market targeted by ECs for the upcoming year is the transportation market, such as the hybrid electric vehicles, electrical vehicles, metro trains and tramways. In these applications, ECs can also work independently as main power or energy source, or it can cooperate with gasoline or batteries to improve the energy efficiency and lower the cost. In

some cases, ECs work as a short time energy storage devices with high power deliverability and can store energy from braking. The stored energy can be reused for next acceleration and boost it. In this case, the size of main power source like batteries, internal combustion engine can be reduced, and they can be operated in optimized conditions. Additionally, aircraft and ships can also apply similar energy system design to reuse the braking energy during next acceleration. A possible design of a drive system is shown in fig. 2.22.

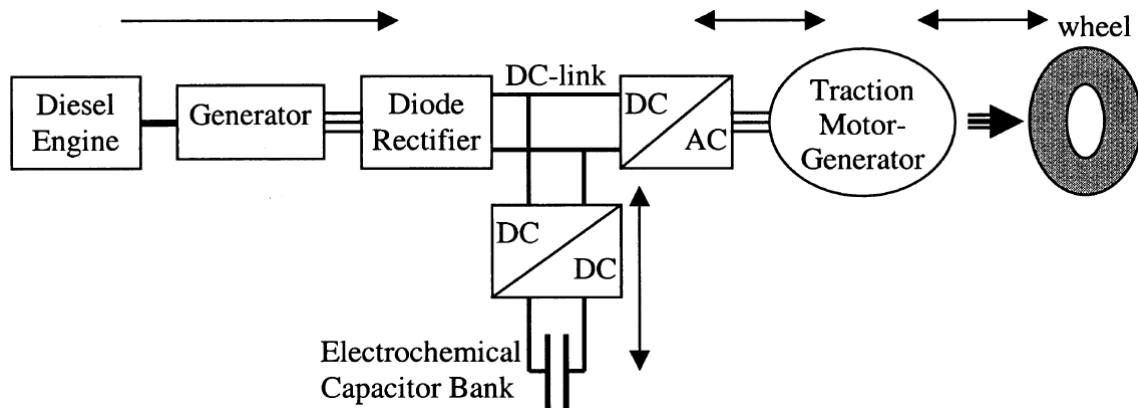


Figure 2.22 Schematic of driveline of a hybrid electric bus using electrochemical capacitors as storage device for regenerative braking. The arrows indicate the flow of energy[133].

In addition to these applications, ECs can be used as alternating power sources. For example, solar watch, the electric load is supplied by solar cells during the daytime, which also recharge the ECs. And these stored energy will be delivered by ECs during the night for watch to continue working.

References

1. Miller, J.R., A brief history of supercapacitors. *Batteries & Energy Storage Technology*, 2007: p. 61-78.
2. Conway, B.E., *Electrochemical supercapacitors: scientific fundamentals and technological applications*, 1999, Kluwer Academic: New York.
3. Helmholtz, H.V., On the modern development of Faraday's conception of electricity, *Journal of the Chemical Society*, 1881. **39**: p. 277-304.
4. Gouy, M., Sur la constitution de la charge électrique à la surface d'un électrolyte. *Journal de physique Archives*, 1910. **9**: p. 457-468.
5. Chapman, D.L., A contribution to the theory of electrocapillarity. *Philosophical Magazine*, 1913. **25**: p. 475-481.
6. Stern, O., Zur theorie der elektrolytischen doppelschicht. Nachtrag zu *Z. Elektrochem.*, 1924. **30**(21-22): p. 508-516.
7. Miller, J.R. and A.F. Burke, Electrochemical capacitors: challenges and opportunities for real-world applications. *The Electrochemical Society Interface*, 2008. **17**(1): p. 53-57.
8. Braun, P.V., et al., High power rechargeable batteries. *Current Opinion in Solid State and Materials Science*, 2012. **16**(4): p. 186-198.
9. Trasatti, S. and G. Buzzanca, Ruthenium dioxide: A new interesting electrode material. Solid state structure and electrochemical behaviour. *Journal of Electroanalytical Chemistry and Interfacial Electrochemistry*, 1971. **29**(2): p. A1-A5.

10. Zheng, J.P., P.J. Cygan, and T.R. Jow, Hydrous ruthenium oxide as an electrode material for electrochemical capacitors. *Journal of The Electrochemical Society*, 1995. **142**(8): p. 2699-2703.
11. Long, J.W., et al., Voltammetric characterization of ruthenium oxide-based aerogels and other RuO₂ solids: the nature of capacitance in nanostructured materials. *Langmuir*, 1999. **15**(3): p. 780-785.
12. Conway, B.E. and W.G. Pell, Double-layer and pseudocapacitance types of electrochemical capacitors and their applications to the development of hybrid devices. *Journal of Solid State Electrochemistry*, 2003. **7**(9): p. 637-644.
13. Herrero, E., L.J. Buller, and H.D. Abruña, Underpotential deposition at single crystal surfaces of Au, Pt, Ag and other materials. *Chemical Reviews*, 2001. **101**(7): p. 1897-1930.
14. Conway, B.E., Two-dimensional and quasi-two-dimensional isotherms for Li intercalation and up processes at surfaces. *Electrochimica Acta*, 1993. **38**(9): p. 1249-1258.
15. Augustyn, V., P. Simon, and B. Dunn, Pseudocapacitive oxide materials for high-rate electrochemical energy storage. *Energy & Environmental Science*, 2014. **7**(5): p. 1597-1614.
16. Zhang, Y., et al., Progress of electrochemical capacitor electrode materials: A review. *International Journal of Hydrogen Energy*, 2009. **34**(11): p. 4889-4899.
17. Huang, X.W., et al., Electric double layer capacitors using activated carbon prepared from pyrolytic treatment of sugar as their electrodes. *Synthetic Metals*, 2003. **135-136**(0): p. 235-236.

18. Gomibuchi, E., et al., Electrode properties of a double layer capacitor of nano-structured graphite produced by ball milling under a hydrogen atmosphere. *Carbon*, 2006. **44**(5): p. 983-988.
19. Yang, X.-h., et al., Interfacial synthesis of porous MnO₂ and its application in electrochemical capacitor. *Electrochimica Acta*, 2007. **53**(2): p. 752-757.
20. Lao, Z.J., et al., Synthesis of vanadium pentoxide powders with enhanced surface-area for electrochemical capacitors. *Journal of Power Sources*, 2006. **162**(2): p. 1451-1454.
21. Muthulakshmi, B., et al., Electrochemical deposition of polypyrrole for symmetric supercapacitors. *Journal of Power Sources*, 2006. **158**(2): p. 1533-1537.
22. Balducci, A., et al., Cycling stability of a hybrid activated carbon/poly(3-methylthiophene) supercapacitor with N-butyl-N-methylpyrrolidinium bis(trifluoromethanesulfonyl) imide ionic liquid as electrolyte. *Electrochimica Acta*, 2005. **50**(11): p. 2233-2237.
23. Wang, H., et al., From symmetric AC/AC to asymmetric AC/graphite, a progress in electrochemical capacitors. *Journal of Power Sources*, 2007. **169**(2): p. 375-380.
24. Honda, Y., et al., Aligned MWCNT sheet electrodes prepared by transfer methodology providing high-power capacitor performance. *Electrochemical and Solid-State Letters*, 2007. **10**(4): p. A106-A110.
25. Katakabe, T., et al., Electric double-layer capacitors using “Bucky Gels” consisting of an ionic liquid and carbon nanotubes. *Journal of The Electrochemical Society*, 2005. **152**(10): p. A1913-A1916.

26. Brownson, D.A.C., D.K. Kampouris, and C.E. Banks, An overview of graphene in energy production and storage applications. *Journal of Power Sources*, 2011. **196**(11): p. 4873-4885.
27. Miller, J.R., R.A. Outlaw, and B.C. Holloway, Graphene double-layer capacitor with ac line-filtering performance. *Science*, 2010. **329**(5999): p. 1637-1639.
28. Fang, B. and L. Binder, Enhanced surface hydrophobisation for improved performance of carbon aerogel electrochemical capacitor. *Electrochimica Acta*, 2007. **52**(24): p. 6916-6921.
29. Liu, X.-m., et al., Impedance of carbon aerogel/activated carbon composites as electrodes of electrochemical capacitors in aprotic electrolyte. *New Carbon Materials*, 2007. **22**(2): p. 153-158.
30. Wang, H. and M. Yoshio, Graphite, a suitable positive electrode material for high-energy electrochemical capacitors. *Electrochemistry Communications*, 2006. **8**(9): p. 1481-1486.
31. Sivakkumar, S.R., et al., Performance evaluation of CNT/polypyrrole/MnO₂ composite electrodes for electrochemical capacitors. *Electrochimica Acta*, 2007. **52**(25): p. 7377-7385.
32. Xu, B., et al., Activated carbon fiber cloths as electrodes for high performance electric double layer capacitors. *Electrochimica Acta*, 2007. **52**(13): p. 4595-4598.
33. Kim, S.-U. and K.-H. Lee, Carbon nanofiber composites for the electrodes of electrochemical capacitors. *Chemical Physics Letters*, 2004. **400**(1-3): p. 253-257.

34. Wang, G., L. Zhang, and J. Zhang, A review of electrode materials for electrochemical supercapacitors. *Chemical Society Reviews*, 2012. **41**(2): p. 797-828.
35. Raymundo-Piñero, E., et al., Relationship between the nanoporous texture of activated carbons and their capacitance properties in different electrolytes. *Carbon*, 2006. **44**(12): p. 2498-2507.
36. Frackowiak, E., et al., Enhanced capacitance of carbon nanotubes through chemical activation. *Chemical Physics Letters*, 2002. **361**(1-2): p. 35-41.
37. Raymundo-Piñero, E., et al., High surface area carbon nanotubes prepared by chemical activation. *Carbon*, 2002. **40**(9): p. 1614-1617.
38. Lozano-Castelló, D., et al., Preparation of activated carbons from spanish anthracite: I. activation by KOH. *Carbon*, 2001. **39**(5): p. 741-749.
39. An, K.H., et al., Supercapacitors using single-walled carbon nanotube electrodes. *Advanced Materials*, 2001. **13**(7): p. 497-500.
40. Pandolfo, A.G. and A.F. Hollenkamp, Carbon properties and their role in supercapacitors. *Journal of Power Sources*, 2006. **157**(1): p. 11-27.
41. Chmiola, J., et al., Anomalous increase in carbon capacitance at pore sizes less Than 1 nanometer. *Science*, 2006. **313**(5794): p. 1760-1763.
42. Momma, T., et al., Electrochemical modification of active carbon fiber electrode and its application to double-layer capacitor. *Journal of Power Sources*, 1996. **60**(2): p. 249-253.

43. B éguin, F., et al., A self-supporting electrode for supercapacitors prepared by one-step pyrolysis of carbon nanotube/polyacrylonitrile blends. *Advanced Materials*, 2005. **17**(19): p. 2380-2384.
44. Raymundo-Pi ñero, E., F. Leroux, and F. B éguin, A high-performance carbon for supercapacitors obtained by carbonization of a seaweed biopolymer. *Advanced Materials*, 2006. **18**(14): p. 1877-1882.
45. Leitner, K., et al., Nomex-derived activated carbon fibers as electrode materials in carbon based supercapacitors. *Journal of Power Sources*, 2006. **153**(2): p. 419-423.
46. Hulicova, D., et al., Supercapacitors prepared from melamine-based carbon. *Chemistry of Materials*, 2005. **17**(5): p. 1241-1247.
47. Hulicova, D., M. Kodama, and H. Hatori, Electrochemical performance of nitrogen-enriched carbons in aqueous and non-aqueous supercapacitors. *Chemistry of Materials*, 2006. **18**(9): p. 2318-2326.
48. Qu, D. and H. Shi, Studies of activated carbons used in double-layer capacitors. *Journal of Power Sources*, 1998. **74**(1): p. 99-107.
49. Hu, C.-C., et al., Design and tailoring of the nanotubular arrayed architecture of hydrous RuO₂ for next generation supercapacitors. *Nano Letters*, 2006. **6**(12): p. 2690-2695.
50. Zhang, H., et al., Growth of manganese oxide nanoflowers on vertically-aligned carbon nanotube arrays for high-rate electrochemical capacitive energy storage. *Nano Letters*, 2008. **8**(9): p. 2664-2668.

51. Novoselov, K.S., et al., Electric field effect in atomically thin carbon films. *Science*, 2004. **306**(5696): p. 666-669.
52. Pan, D., et al., Li storage properties of disordered graphene nanosheets. *Chemistry of Materials*, 2009. **21**(14): p. 3136-3142.
53. Guo, H.-L., et al., A green approach to the synthesis of graphene nanosheets. *ACS Nano*, 2009. **3**(9): p. 2653-2659.
54. Zhu, C., et al., Reducing sugar: new functional molecules for the green synthesis of graphene nanosheets. *ACS Nano*, 2010. **4**(4): p. 2429-2437.
55. Li, X., et al., Transfer of large-area graphene films for high-performance transparent conductive electrodes. *Nano Letters*, 2009. **9**(12): p. 4359-4363.
56. Niu, C., et al., High power electrochemical capacitors based on carbon nanotube electrodes. *Applied Physics Letters*, 1997. **70**(11): p. 1480-1482.
57. Futaba, D.N., et al., Shape-engineerable and highly densely packed single-walled carbon nanotubes and their application as super-capacitor electrodes. *Nature Materials*, 2006. **5**(12): p. 987-994.
58. Frackowiak, E., et al., Nanotubular materials for supercapacitors. *Journal of Power Sources*, 2001. **97-98**(0): p. 822-825.
59. Frackowiak, E., et al., Nanotubular materials as electrodes for supercapacitors. *Fuel Processing Technology*, 2002. **77-78**(0): p. 213-219.
60. Zhang, L.L. and X.S. Zhao, Carbon-based materials as supercapacitor electrodes.

Chemical Society Reviews, 2009. **38**(9): p. 2520-2531.

61. Simon, P. and Y. Gogotsi, Materials for electrochemical capacitors. *Nature Materials*, 2008. **7**(11): p. 845-854.

62. Fang, B. and L. Binder, A modified activated carbon aerogel for high-energy storage in electric double layer capacitors. *Journal of Power Sources*, 2006. **163**(1): p. 616-622.

63. Zhao, D.-D., et al., Preparation of hexagonal nanoporous nickel hydroxide film and its application for electrochemical capacitor. *Electrochemistry Communications*, 2007. **9**(5): p. 869-874.

64. Kim, I.-H. and K.-B. Kim, Electrochemical characterization of hydrous ruthenium oxide thin-film electrodes for electrochemical capacitor applications. *Journal of The Electrochemical Society*, 2006. **153**(2): p. A383-A389.

65. Conway, B., *Electrochemical supercapacitors: scientific fundamentals and technological applications*. 1999, New York: Kluwer Academic.

66. Trasatti, S., Physical electrochemistry of ceramic oxides. *Electrochimica Acta*, 1991. **36**(2): p. 225-241.

67. Hu, C.C., C.H. Lee, and T.C. Wen, Oxygen evolution and hypochlorite production on Ru-Pt binary oxides. *Journal of Applied Electrochemistry*, 1996. **26**(1): p. 72-82.

68. Ramani, M., et al., Synthesis and characterization of hydrous ruthenium oxide-carbon supercapacitors. *Journal of The Electrochemical Society*, 2001. **148**(4): p. A374-A380.

69. Ferro, S. and A. De Battisti, Electrocatalysis and chlorine evolution reaction at

ruthenium dioxide deposited on conductive diamond. *The Journal of Physical Chemistry B*, 2002. **106**(9): p. 2249-2254.

70. Wen, T.C. and C.C. Hu, Hydrogen and oxygen evolutions on Ru-Ir binary oxides. *Journal of The Electrochemical Society*, 1992. **139**(8): p. 2158-2163.

71. Hu, C.-C., W.-C. Chen, and K.-H. Chang, How to achieve maximum utilization of hydrous ruthenium oxide for supercapacitors. *Journal of The Electrochemical Society*, 2004. **151**(2): p. A281-A290.

72. Lee, H.Y. and J.B. Goodenough, Supercapacitor behavior with KCl electrolyte. *Journal of Solid State Chemistry*, 1999. **144**(1): p. 220-223.

73. Devaraj, S. and N. Munichandraiah, High capacitance of electrodeposited MnO₂ by the effect of a surface-active agent. *Electrochemical and Solid-State Letters*, 2005. **8**(7): p. A373-A377.

74. Toupin, M., T. Brousse, and D. Bélanger, Charge storage mechanism of MnO₂ electrode used in aqueous electrochemical capacitor. *Chemistry of Materials*, 2004. **16**(16): p. 3184-3190.

75. Pang, S.C., M.A. Anderson, and T.W. Chapman, Novel electrode materials for thin-film ultracapacitors: comparison of electrochemical properties of sol-gel-derived and electrodeposited manganese dioxide. *Journal of The Electrochemical Society*, 2000. **147**(2): p. 444-450.

76. Chang, J.-K., M.-T. Lee, and W.-T. Tsai, In situ Mn K-edge X-ray absorption spectroscopic studies of anodically deposited manganese oxide with relevance to

supercapacitor applications. *Journal of Power Sources*, 2007. **166**(2): p. 590-594.

77. Hu, C.-C. and T.-W. Tsou, Ideal capacitive behavior of hydrous manganese oxide prepared by anodic deposition. *Electrochemistry Communications*, 2002. **4**(2): p. 105-109.

78. Messaoudi, B., et al., Anodic behaviour of manganese in alkaline medium. *Electrochimica Acta*, 2001. **46**(16): p. 2487-2498.

79. Raymundo-Piñero, E., et al., Performance of manganese oxide/CNTs composites as electrode materials for electrochemical capacitors. *Journal of The Electrochemical Society*, 2005. **152**(1): p. A229-A235.

80. Ye, C., Z.M. Lin, and S.Z. Hui, Electrochemical and capacitance properties of rod-shaped MnO₂ for supercapacitor. *Journal of The Electrochemical Society*, 2005. **152**(6): p. A1272-A1278.

81. Lee, M.-T., J.-K. Chang, and W.-T. Tsai, Effects of iron addition on material characteristics and pseudo-capacitive behavior of Mn-oxide electrodes. *Journal of The Electrochemical Society*, 2007. **154**(9): p. A875-A881.

82. Kim, H. and B.N. Popov, Synthesis and characterization of MnO₂-based mixed oxides as supercapacitors. *Journal of The Electrochemical Society*, 2003. **150**(3): p. D56-D62.

83. Chang, J.-K., et al., Physicochemical factors that affect the pseudocapacitance and cyclic stability of Mn oxide electrodes. *Electrochimica Acta*, 2009. **54**(12): p. 3278-3284.

84. Hsieh, Y.-C., et al., Investigation on capacity fading of aqueous MnO₂ nH₂O electrochemical capacitor. *Journal of Power Sources*, 2008. **177**(2): p. 660-664.

85. Zheng, H., et al., Multilayered films of cobalt oxyhydroxide nanowires/manganese oxide nanosheets for electrochemical capacitor. *Journal of Power Sources*, 2010. **195**(2): p. 680-683.
86. Patake, V.D., C.D. Lokhande, and O.S. Joo, Electrodeposited ruthenium oxide thin films for supercapacitor: Effect of surface treatments. *Applied Surface Science*, 2009. **255**(7): p. 4192-4196.
87. Yan, D., et al., MnO₂ film with three-dimensional structure prepared by hydrothermal process for supercapacitor. *Journal of Power Sources*, 2012. **199**(0): p. 409-412.
88. Zhi, M., et al., Nanostructured carbon-metal oxide composite electrodes for supercapacitors: review. *Nanoscale*, 2012.
89. Lota, K., V. Khomenko, and E. Frackowiak, Capacitance properties of poly(3,4-ethylenedioxythiophene)/carbon nanotubes composites. *Journal of Physics and Chemistry of Solids*, 2004. **65**(2-3): p. 295-301.
90. Suematsu, S., et al., Conducting polymer films of cross-linked structure and their QCM analysis. *Electrochimica Acta*, 2000. **45**(22-23): p. 3813-3821.
91. Snook, G.A., P. Kao, and A.S. Best, Conducting-polymer-based supercapacitor devices and electrodes. *Journal of Power Sources*, 2011. **196**(1): p. 1-12.
92. Peng, C., D. Hu, and G.Z. Chen, Theoretical specific capacitance based on charge storage mechanisms of conducting polymers: comment on 'Vertically oriented arrays of polyaniline nanorods and their super electrochemical properties'. *Chemical Communications*, 2011. **47**(14): p. 4105-4107.

93. Snook, G.A. and G.Z. Chen, The measurement of specific capacitances of conducting polymers using the quartz crystal microbalance. *Journal of Electroanalytical Chemistry*, 2008. **612**(1): p. 140-146.
94. Ryu, K.S., et al., Redox supercapacitor using polyaniline doped with Li salt as electrode. *Solid State Ionics*, 2002. **152–153**(0): p. 861-866.
95. Faverolle, F., et al., Highly conducting and strongly adhering polypyrrole coating layers deposited on glass substrates by a chemical process. *Chemistry of Materials*, 1998. **10**(3): p. 740-752.
96. Sivakkumar, S.R. and R. Saraswathi, Performance evaluation of poly(N-methylaniline) and polyisothianaphthene in charge-storage devices. *Journal of Power Sources*, 2004. **137**(2): p. 322-328.
97. Ryu, K.S., et al., Symmetric redox supercapacitor with conducting polyaniline electrodes. *Journal of Power Sources*, 2002. **103**(2): p. 305-309.
98. Talbi, H., P.E. Just, and L.H. Dao, Electropolymerization of aniline on carbonized polyacrylonitrile aerogel electrodes: applications for supercapacitors. *Journal of Applied Electrochemistry*, 2003. **33**(6): p. 465-473.
99. Zhang, J., D. Shan, and S. Mu, A rechargeable Zn- poly(aniline-co-m-aminophenol) battery. *Journal of Power Sources*, 2006. **161**(1): p. 685-691.
100. Neves, S. and C. Polo Fonseca, Influence of template synthesis on the performance of polyaniline cathodes. *Journal of Power Sources*, 2002. **107**(1): p. 13-17.

101. Li, H., et al., Theoretical and experimental specific capacitance of polyaniline in sulfuric acid. *Journal of Power Sources*, 2009. **190**(2): p. 578-586.
102. Girija, T.C. and M.V. Sangaranarayanan, Polyaniline-based nickel electrodes for electrochemical supercapacitors-Influence of Triton X-100. *Journal of Power Sources*, 2006. **159**(2): p. 1519-1526.
103. Wu, M., et al., Electrochemical fabrication and capacitance of composite films of carbon nanotubes and polyaniline. *Journal of Materials Chemistry*, 2005. **15**(23): p. 2297-2303.
104. Dubal, D.P., et al., Porous polypyrrole clusters prepared by electropolymerization for a high performance supercapacitor. *Journal of Materials Chemistry*, 2012. **22**(7): p. 3044-3052.
105. Mastragostino, M., C. Arbizzani, and F. Soavi, Conducting polymers as electrode materials in supercapacitors. *Solid State Ionics*, 2002. **148**(3-4): p. 493-498.
106. Arbizzani, C., M. Mastragostino, and L. Meneghello, Characterization by impedance spectroscopy of a polymer-based supercapacitor. *Electrochimica Acta*, 1995. **40**(13-14): p. 2223-2228.
107. Arbizzani, C., et al., N- and P-doped Polydithieno[3,4-B:3',4'-D] thiophene: A narrow band gap polymer for redox supercapacitors. *Electrochimica Acta*, 1995. **40**(12): p. 1871-1876.
108. Shown, I., et al., Conducting polymer-based flexible supercapacitor. *Energy Science & Engineering*, 2015. **3**(1): p. 2-26.

109. Fan, L.Z., et al., High Electroactivity of Polyaniline in Supercapacitors by Using a Hierarchically Porous Carbon Monolith as a Support. *Advanced Functional Materials*, 2007. **17**(16): p. 3083-3087.
110. Zhang, H., et al., Tube-covering-tube nanostructured polyaniline/carbon nanotube array composite electrode with high capacitance and superior rate performance as well as good cycling stability. *Electrochemistry Communications*, 2008. **10**(7): p. 1056-1059.
111. Li, H., R. Wang, and R. Cao, Physical and electrochemical characterization of hydrous ruthenium oxide/ordered mesoporous carbon composites as supercapacitor. *Microporous and Mesoporous Materials*, 2008. **111**(1-3): p. 32-38.
112. Ruiz, V., et al., Effects of thermal treatment of activated carbon on the electrochemical behaviour in supercapacitors. *Electrochimica Acta*, 2007. **52**(15): p. 4969-4973.
113. Demarconnay, L., E. Raymundo-Piñero, and F. Béguin, A symmetric carbon/carbon supercapacitor operating at 1.6V by using a neutral aqueous solution. *Electrochemistry Communications*, 2010. **12**(10): p. 1275-1278.
114. Fic, K., et al., Novel insight into neutral medium as electrolyte for high-voltage supercapacitors. *Energy & Environmental Science*, 2012. **5**(2): p. 5842-5850.
115. Gao, Q., et al., Exploring the large voltage range of carbon/carbon supercapacitors in aqueous lithium sulfate electrolyte. *Energy & Environmental Science*, 2012. **5**(11): p. 9611-9617.
116. Tsuda, T. and C.L. Hussey, Electrochemical applications of room-temperature ionic liquids. *Electrochemical Society Interface*, 2007. **16**: p. 42-49.

117. Tan, Y. and K. Ghandi, Kinetics and mechanism of pyrrole chemical polymerization. *Synthetic Metals*, 2013. **175**(0): p. 183-191.
118. Malinauskas, A., Chemical deposition of conducting polymers. *Polymer*, 2001. **42**(9): p. 3957-3972.
119. Wencheng, S. and J.O. Iroh, Electrodeposition mechanism of polypyrrole coatings on steel substrates from aqueous oxalate solutions. *Electrochimica Acta*, 2000. **46**(1): p. 1-8.
120. Hamer, W.J., L. Koene, and J.H.W. de Wit, Formation and electrochemical behaviour of poly(pyrrole) coatings on steel substrates. *Materials and Corrosion*, 2004. **55**(9): p. 653-658.
121. Tallman, D.E., et al., Direct electrodeposition of polypyrrole on aluminum and aluminum alloy by electron transfer mediation. *Journal of the Electrochemical Society*, 2002. **149**(3): p. C173-C179.
122. Håkansson, E., et al., The effects of dye dopants on the conductivity and optical absorption properties of polypyrrole. *Synthetic Metals*, 2006. **156**(18–20): p. 1194-1202.
123. Mitchell, G.R., F.J. Davis, and C.H. Legge, The effect of dopant molecules on the molecular order of electrically-conducting films of polypyrrole. *Synthetic Metals*, 1988. **26**(3): p. 247-257.
124. Wang, P.-C. and J.-Y. Yu, Dopant-dependent variation in the distribution of polarons and bipolarons as charge-carriers in polypyrrole thin films synthesized by oxidative chemical polymerization. *Reactive and Functional Polymers*, 2012. **72**(5): p. 311-316.

125. Sultana, I., et al., Electrodeposited polypyrrole (PPy)/para (toluene sulfonic acid) (pTS) free-standing film for lithium secondary battery application. *Electrochimica Acta*, 2012. **60**(0): p. 201-205.
126. Han, M., et al., Fabrication and characterizations of oligopyrrole doped with dodecylbenzenesulfonic acid in reverse microemulsion. *Journal of Colloid and Interface Science*, 2006. **296**(1): p. 110-117.
127. Qie, L., et al., Revisit of polypyrrole as cathode material for lithium-ion battery. *Journal of the Electrochemical Society*, 2012. **159**(10): p. A1624-A1629.
128. Wang, Y., C. Yang, and P. Liu, Acid blue AS doped polypyrrole (PPy/AS) nanomaterials with different morphologies as electrode materials for supercapacitors. *Chemical Engineering Journal*, 2011. **172**(2): p. 1137-1144.
129. Goel, S., N.A. Mazumdar, and A. Gupta, Synthesis and characterization of polypyrrole nanofibers with different dopants. *Polymers for Advanced Technologies*, 2010. **21**(3): p. 205-210.
130. Lang, X., et al., The role of anthraquinone sulfonate dopants in promoting performance of polypyrrole composites as pseudo-capacitive electrode materials. *Synthetic Metals*, 2010. **160**(15): p. 1800-1804.
131. Miller, J.R. and P. Simon, Electrochemical capacitors for energy management. *Science*, 2008. **321**(5889): p. 651-652.
132. Miller, J.R. and A. Burke, Electrochemical capacitors: challenges and opportunities for real-world applications. *Electrochemical Society Interface*, 2008. **17**(1): p. 53-57.

133. Kötz, R. and M. Carlen, Principles and applications of electrochemical capacitors.

Electrochimica Acta, 2000. **45**(15–16): p. 2483-2498.

Chapter 3 Problem statement and objective

3.1 Problem statement

(i) Challenges of electropolymerization of PPy on non-noble metal substrates

Electropolymerization is widely used for the fabrication of PPy films[1-3]. The choice of the dopant is of particular importance for electropolymerization since film adhesion, conductivity and microstructure are influenced by the dopant molecules. It was shown that anionic dopants can passivate the surface of non-noble electrodes and prevent their oxidation and dissolution during anodic electropolymerization of PPy[4]. Adherent films were obtained on stainless steel from aqueous oxalate solutions[4]. However, the formation of the non-conductive and non-capacitive iron oxalate layer[5] can result in increasing charge transfer resistance and reduced electrochemical capacitance of the PPy electrodes (shown in fig. 3.1).

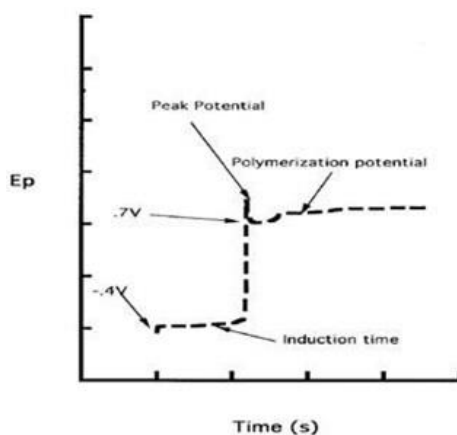


Figure 3.1 Induction time during electropolymerization of pyrrole on steel using aqueous electrolyte contains oxalic acid.[5]

Another strategy which is recently under investigation is based on mussel-inspired surface chemistry[6], using aromatic molecules from catechol[3, 7-10], salicylic acid[1, 2, 11] and chromotropic acid[12] families as dopants. Such molecules have potential to provide complexation of metal atoms on the substrate surface and may allow for better adhesion of PPy films. Various molecules from catechol family were investigated, such as Tiron[3], pyrocatechol violet[7], alizarin red[8]. However, the electrochemical properties and capacitive performance of PPy films synthesised by this strategy are still under investigation.

(ii) Problems related to electropolymerized PPy electrodes

The interest in polypyrrole (PPy) is attributed to high specific capacitance, high electrical conductivity and low cost of this polymer. However, it is challenging to achieve good electrochemical performance for PPy electrodes with active mass loadings of 10-20 mg cm⁻², which are required for many practical applications[13]. The increase in PPy mass loading resulted in decreasing specific capacitance and increasing impedance of PPy electrodes[14]. Therefore, high specific capacitance value can only be achieved in relatively thin film (less than 1 mg cm⁻²) using electropolymerization method. Another problem, limiting the application of PPy in ES, is poor cycling stability[15]. It was found that swelling, caused by the anion exchange between PPy and electrolyte during cycling has a detrimental effect on cycling stability[15, 16]. The material swelling usually results in the loss of film adhesion during cycling, increasing interface resistance and reduced capacitance.

In order to address those problems, an alternative fabrication method (like pulse

electropolymerization or chemical polymerization) as well as the design of composite electrode (such as PPy-carbon nanotubes composite) need to be investigated to fabricate PPy or composite electrodes with practical materials loading, acceptable cycle stability, good capacitive performance and high porosity microstructure.

(iii) Problems related to the formation of PPy-CNTs composite electrodes

The development of composite electrodes is a good way to solve capacitance reduction problem of PPy when increased materials loading and fast charge-discharge rate are applied. PPy-carbon nanotube (CNT) with improved conductivity are gaining attention for the ECs applications[15, 17, 18]. The fabrication of composites by chemical solution methods requires efficient dispersion of carbon nanotubes[19, 20]. Therefore, the methods of carbon nanotube dispersion and co-deposition of PPy-CNTs are of critical importance for the manufacturing of PPy-carbon nanotube composites for ECs applications. Additionally, the specific capacitance of CNT is significantly lower, compared to that of PPy. Therefore, the amount of CNT in the composites must be optimized and CNT must be well dispersed in the PPy matrix.

Chemically functionalized CNT showed improved dispersion and were used for the formation of PPy-CNT composites [21]. However, the functionalization strategies introduce defects on the CNT sidewalls and reduce the electronic conductivity of CNT. It was found [22] that the use of long chain surfactants for CNT dispersion generates problems related to PPy deposition on CNT and coating formation. Despite the impressive progress achieved in this area, there is a need in the development of new dopants and

advanced techniques for the fabrication of PPy coated CNT.

(iv) Discover multifunctional additives as dopants and dispersants

The development of anionic dopants for PPy polymerization has been the focus of significant research activity, due to the influence of dopants on microstructure, conductivity and capacitance of PPy[1, 23, 24]. With a desire to increase the capacitance, conductivity and cyclic stability of PPy, there is a growing interest in polycharged and polyaromatic dopants for the PPy polymerization[15, 24].

It was found that polycharged dopants created links between individual PPy molecules and facilitated charge transfer[25]. The polyaromatic dopants provided orientation of PPy molecules and improved electrical conductivity[26]. It was demonstrated that charge/mass ratio of the anionic dopants is an important factor, controlling the size of PPy particles and specific capacitance.

The anionic dopant also showed significant influence on the size and shape of particles and electrochemical performance of PPy, prepared by chemical polymerization method[27, 28]. It was found that PPy nanoparticles, nanofibers and nanorods can be obtained by the variation of dopant concentration[29]. Improved thermal stability of PPy nanofibers was achieved using aromatic dopants[29, 30].

In this case, an important task is the development of advanced dopants and analysis of influence of the dopant structure on PPy polymerization and properties of PPy electrodes, since the mechanism of such influence is still not well understood. Moreover, the use of polyaromatic dopants may offer additional benefits for the fabrication of PPy-CNTs

composites due to the π - π interaction between carbon rings and aromatic rings. Efficient dispersion of CNTs in the PPy matrix can be expected.

3.2 Objective and approach

The objective of this research is the fabrication and testing of PPy and PPy-CNTs composite formed EC electrodes and devices. The specific goals of this research include:

- (i) Investigation of new dopants for electropolymerization of PPy and PPy-CNTs composite films on non-noble metal substrates.
- (ii) Development of pulse electropolymerization of PPy films with porous microstructure.
- (iii) Investigation of the difference of electrochemical properties and capacitive performances between PPy electrodes fabricated through different polymerization methods.
- (iv) Study of new dopants and dispersants for PPy and PPy-CNTs composite fabricated through chemical polymerization.
- (v) Development of one-step synthesis method for the fabrication of PPy-CNTs composite electrodes using multifunctional dopants.
- (vi) Fabrication and testing of PPy and PPy-CNTs electrodes and symmetric EC devices, investigation of their capacitance and cyclic stability under different charge-discharge rates.

References

1. Li, X. and I. Zhitomirsky, Capacitive behaviour of polypyrrole films prepared on stainless steel substrates by electropolymerization. *Materials Letters*, 2012. **76**(0): p. 15-17.
2. Li, X., et al., Effect of 5-sulfosalicylic acid and poly[2,5-bis(3-sulfonatopropoxy)-1,4-ethynylphenylene-alt-1,4-ethynylphenylene] on electrodeposition of polypyrrole carbon nanotube films on stainless steel. *Materials Letters*, 2012. **68**(0): p. 24-27.
3. Tallman, D.E., et al., Direct electrodeposition of polypyrrole on aluminum and aluminum alloy by electron transfer mediation. *Journal of the Electrochemical Society*, 2002. **149**(3): p. C173-C179.
4. Wencheng, S. and J.O. Iroh, Electrodeposition mechanism of polypyrrole coatings on steel substrates from aqueous oxalate solutions. *Electrochimica Acta*, 2000. **46**(1): p. 1-8.
5. Hamer, W.J., L. Koene, and J.H.W. de Wit, Formation and electrochemical behaviour of poly(pyrrole) coatings on steel substrates. *Materials and Corrosion*, 2004. **55**(9): p. 653-658.
6. Lee, H., et al., Mussel-inspired surface chemistry for multifunctional coatings. *Science*, 2007. **318**(5849): p. 426-430.
7. Li, X. and I. Zhitomirsky, Electrodeposition of polypyrrole-carbon nanotube composites for electrochemical supercapacitors. *Journal of Power Sources*, 2013. **221**(0): p. 49-56.
8. Chen, S. and I. Zhitomirsky, Influence of dopants and carbon nanotubes on polypyrrole electropolymerization and capacitive behavior. *Materials Letters*, 2013. **98**: p. 67-70.

9. Shi, K., Y. Su, and I. Zhitomirsky, Characterization of Ni plaque based polypyrrole electrodes prepared by pulse electropolymerization. *Materials Letters*, 2013. **96**: p. 135-138.
10. Shi, C. and I. Zhitomirsky, Electrodeposition of composite polypyrrole-carbon nanotube films. *Surface Engineering*, 2011. **27**(9): p. 655-661.
11. Hermelin, E., et al., Industrial polypyrrole electrodeposition on zinc-electroplated steel. *Journal of Applied Electrochemistry*, 2001. **31**(8): p. 905-911.
12. Ariyanayagamkumarappa, D.K. and I. Zhitomirsky, Electropolymerization of polypyrrole films on stainless steel substrates for electrodes of electrochemical supercapacitors. *Synthetic Metals*, 2012. **162**(9-10): p. 868-872.
13. Gogotsi, Y. and P. Simon, True performance metrics in electrochemical energy storage. *Science*, 2011. **334**(6058): p. 917-918.
14. Shi, K. and I. Zhitomirsky, Influence of current collector on capacitive behavior and cycling stability of Tiron doped polypyrrole electrodes. *Journal of Power Sources*, 2013. **240**(0): p. 42-49.
15. Snook, G.A., P. Kao, and A.S. Best, Conducting-polymer-based supercapacitor devices and electrodes. *Journal of Power Sources*, 2011. **196**(1): p. 1-12.
16. Pyo, M., et al., Long-term redox switching stability of polypyrrole. *Synthetic Metals*, 1994. **68**(1): p. 71-77.
17. Fu, H., et al., Carbon nanotube reinforced polypyrrole nanowire network as a high-

- performance supercapacitor electrode. *Journal of Materials Chemistry A*, 2013.
18. Chang, H.-H., et al., Electrochemically synthesized graphene/polypyrrole composites and their use in supercapacitor. *Carbon*, 2012. **50**(6): p. 2331-2336.
 19. Fu, L., et al., Nanocomposite coating of multilayered carbon nanotube–titania. *Materials and Manufacturing Processes*, 2014. **29**(9): p. 1030-1036.
 20. Ata, M.S. and I. Zhitomirsky, Preparation of MnO₂ and composites for ultracapacitors. *Materials and Manufacturing Processes*, 2013. **28**(9): p. 1014-1018.
 21. Wang, J., et al., Capacitance properties of single wall carbon nanotube/polypyrrole composite films. *Composites Science and Technology*, 2007. **67**(14): p. 2981-2985.
 22. Qian, T., et al., Highly dispersed carbon nanotube/polypyrrole core/shell composites with improved electrochemical capacitive performance. *Journal of Materials Chemistry. A*, 2013. **1**(48): p. 15230-15234.
 23. Ariyanayagamkumarappa, D.K. and I. Zhitomirsky, Electropolymerization of polypyrrole films on stainless steel substrates for electrodes of electrochemical supercapacitors. *Synthetic Metals*, 2012. **162**(9–10): p. 868-872.
 24. Zhu, Y. and I. Zhitomirsky, Influence of dopant structure and charge on supercapacitive behavior of polypyrrole electrodes with high mass loading. *Synthetic Metals*, 2013. **185–186**(0): p. 126-132.
 25. Weng, B., et al., Gemini surfactant doped polypyrrole nanodispersions: an inkjet printable formulation. *Journal of Materials Chemistry*, 2011. **21**(6): p. 1918-1924.

26. Mitchell, G.R., F.J. Davis, and C.H. Legge, The effect of dopant molecules on the molecular order of electrically-conducting films of polypyrrole. *Synthetic Metals*, 1988. **26**(3): p. 247-257.
27. Han, M., et al., Fabrication and characterizations of oligopyrrole doped with dodecylbenzenesulfonic acid in reverse microemulsion. *Journal of Colloid and Interface Science*, 2006. **296**(1): p. 110-117.
28. Qie, L., et al., Revisit of polypyrrole as cathode material for lithium-ion battery. *Journal of the Electrochemical Society*, 2012. **159**(10): p. A1624-A1629.
29. Wang, Y., C. Yang, and P. Liu, Acid blue AS doped polypyrrole (PPy/AS) nanomaterials with different morphologies as electrode materials for supercapacitors. *Chemical Engineering Journal*, 2011. **172**(2): p. 1137-1144.
30. Goel, S., N.A. Mazumdar, and A. Gupta, Synthesis and characterization of polypyrrole nanofibers with different dopants. *Polymers for Advanced Technologies*, 2010. **21**(3): p. 205-210.

Chapter 4 Experimental procedures

4.1 Starting materials

Pyrrrole, alizarin red (AR), anthraquinone-2-sulfonic acid sodium salt (AQ), indigo carmine (IC), pyrocatecholsulfonphthalein (PS), tartrazine (TR), brilliant yellow (BY), benzyldimethylhexadecylammonium chloride (BAC), sodium dodecyl sulfate (SDS), sodium cholate (SCH), sodium benzene-1,3-disulfonate (SB), 1,3,(6,7)-naphthalenetrisulfonic acid trisodium salt hydrate (NAT), potassium indigotrisulfonate (TRI), potassium indigotetrasulfonate (TETRA), Na_2SO_4 are purchased from Aldrich. Sulfanilic acid azochromotrop (SPADNS) (Alfa Aesar), multi-walled carbon nanotubes (Bayer), ammonium peroxydisulfate (APS, Fisher Scientific), Ni plaque, Ni foams (porosity 95% and thickness 1.5 mm, Vale) were also used.

4.2 Materials synthesis

4.2.1 Electropolymerized PPy and composite films

Electropolymerization of PPy was performed using electrochemical cells as shown in fig. 4.1. Stainless steel foils or Ni plaque substrates work as the anode and two connected platinum foils work as the cathode. The distance between anode and cathode was set to be 20 mm.

(i) Galvanostatic deposition of PPy films

Electropolymerization was performed galvanostatically at a current density of 1 mA cm^{-2}

or potentiodynamically at a scan rate of 20 mV s^{-1} from an aqueous 0.1 M pyrrole solution containing different concentrations of dopants. All the deposition experiments were performed from freshly prepared solutions. After deposition, the working electrodes were rinsed with deionized water and then dried in air. Deposition yield was studied for the films deposited galvanostatically at different deposition durations. A minimum of 3 samples were prepared in each deposition experiment. The deposition yield measurements were repeatable and the error was less than 5%.

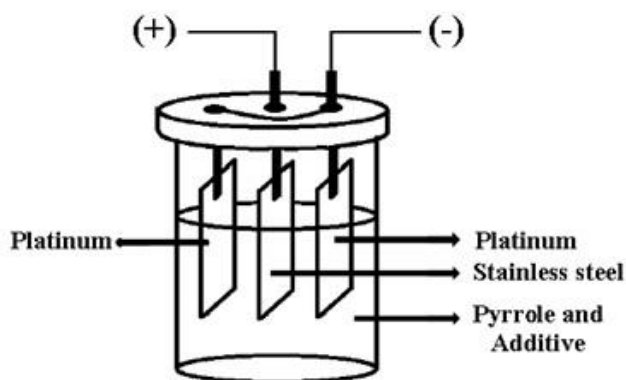


Figure 4.1 Electropolymerization set-up diagram

Solution for electropolymerization of PPy was prepared through several steps. 0.1 M pyrrole was dissolved in deionized water and stirred until fully dissolved. Then a dopant of appropriate concentration was added into the solution and stirred for 15 min. The complete procedures are shown in fig. 4.2.

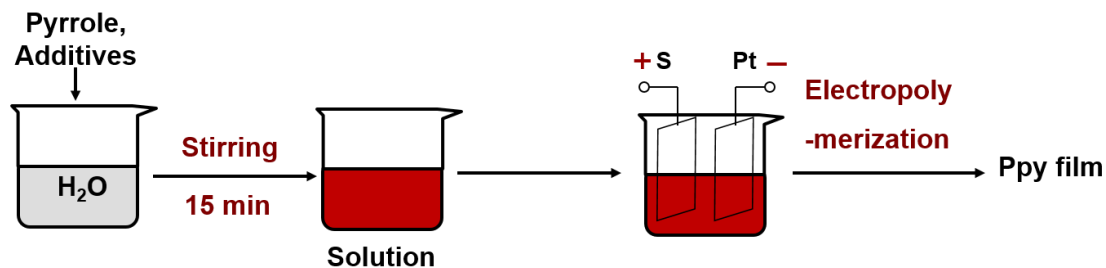


Figure 4.2 Electropolymerization of PPy films

(ii) Galvanostatic deposition of PPy-MWCNTs films

Galvanostatic deposition of PPy-MWCNTs films was conducted in a similar way as for pure PPy films, only the solution preparation was slightly different. 0.1 M pyrrole and dopant with proper concentration were added into deionized water and stirred for 15 min until dissolved. After that, 0.1-1 g L⁻¹ MWCNTs were added and ultrasonicated in such solution for 30 min until dispersed. The procedures are shown in fig. 4.3.

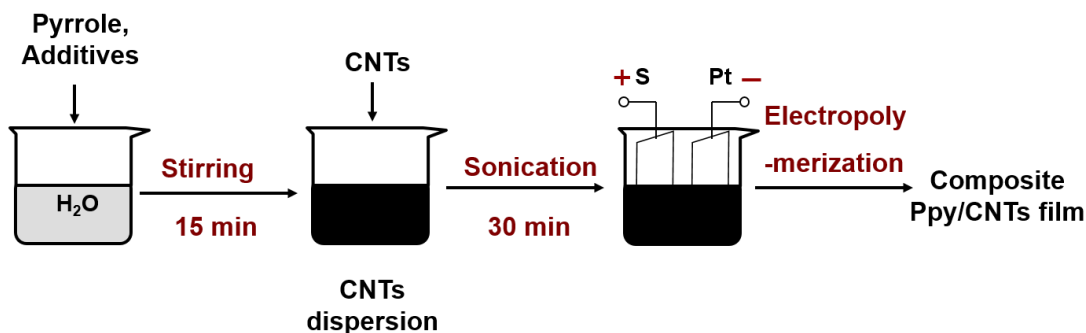


Figure 4.3 Electropolymerization of PPy-MWCNTs films

(iii) Pulse deposition of PPy films

Electropolymerization was conducted by pulse deposition at a current density of 1 mA cm⁻² and the ON and OFF times are 0.5 s from a freshly prepared aqueous solution containing 0.1 M pyrrole and 5 mM PS. The pulse currents are shown in fig. 4.4.

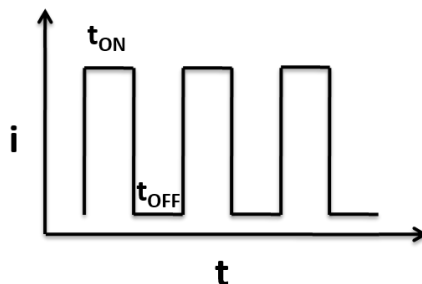


Figure 4.4 Pulse currents

4.2.2 Chemically polymerized PPy and composite powders

(i) Chemical polymerization of PPy

PPy powder was fabricated by a chemical polymerization in aqueous solutions using ammonium peroxydisulfate as an oxidant. Aqueous solutions, containing 0.1 M pyrrole and 5 mM dopant was stirred for 30 min, then 50 mM ammonium peroxydisulfate solution was added. After ultrasonication in ice bath for 3 h, obtained PPy was filtered, washed with deionized water and ethanol and then dried in air. The dried powders were stored in desiccator before use. The full process is schematically shown in fig. 4.5.

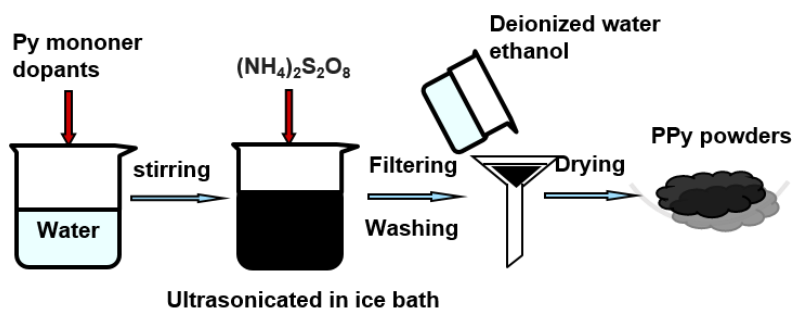


Figure 4.5 Full process of chemical polymerization of PPy

(ii) Fabrication of PPy-MWCNTs using dopants and dispersants

The synthesis of PPy-MWCNTs is slightly different from the fabrication of PPy powders. Carbon nanotubes (1 g L^{-1}) were dispersed using BAC, SDS and SCH (0.25 g L^{-1}) dispersants and ultrasonicated until uniformly dispersed and stabilized. Then 0.1 M pyrrole, 0.01 M TR or BY dopants were added into MWCNTs suspension and stirred until fully dissolved. Polymerization of PPy was performed from such aqueous solutions using 0.05 M APS as an oxidant for the manufacturing of PPy-MWCNTs composites. The polymerization was conducted in ice bath (at $0 \text{ }^\circ\text{C}$) for 3-4 hours. The PPy-MWCNTs composites were washed with water and ethanol and filtered, then dried in air at $60 \text{ }^\circ\text{C}$. The full procedures are shown in fig. 4.6.

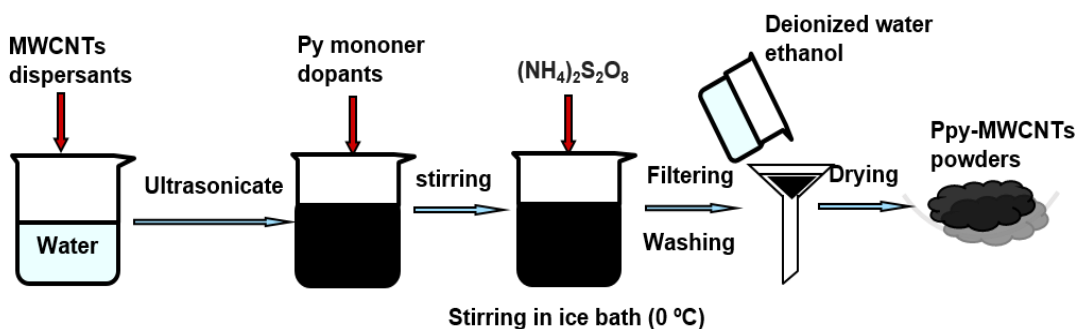


Figure 4.6 Full process of chemical polymerization of PPy-MWCNTs using dopants and dispersants

(iii) Fabrication of PPy coated MWCNTs using multifunctional dopants

A new synthesis procedure was developed for the fabrication of PPy-MWCNT composites using multifunctional dopants IC. This procedure start with the dispersion of MWCNTs (various concentration) in 10 mM IC solutions, the suspension was ultrasonicated until MWCNT were uniformly dispersed. Then 0.1 M pyrrole and 50 mM APS were added to the suspensions and stirred for 3-4 hours. The MWCNTs content in the suspensions was

varied in order to obtain composites, containing 10, 20 and 30 wt% of MWCNT. Obtained PPy-MWCNTs composites were filtered, washed with deionized water and ethanol, and then dried in air at 60 °C (see fig. 4.7).

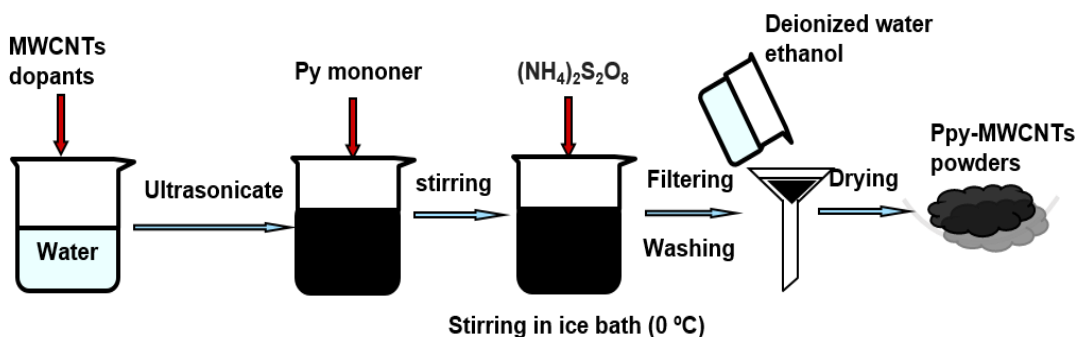


Figure 4.7 Synthesis PPy-MWCNTs using multifunctional dopants

4.3 Fabrication of electrodes and EC devices using impregnation

The obtained PPy or PPy-MWCNTs powders were fabricated into electrode using slurry impregnation. The procedure started with the powder grinding in ethanol to make slurry. The obtained slurry was then impregnated into Ni foam current collector (95% volume porosity) with area of 1 × 1 cm². The materials loading varied from 10 to 30 mg cm⁻². After drying in air at 60 °C, the electrode was pressed to 30% of original thickness to enhance the contact between electrode materials and current collectors (see fig. 4.8).

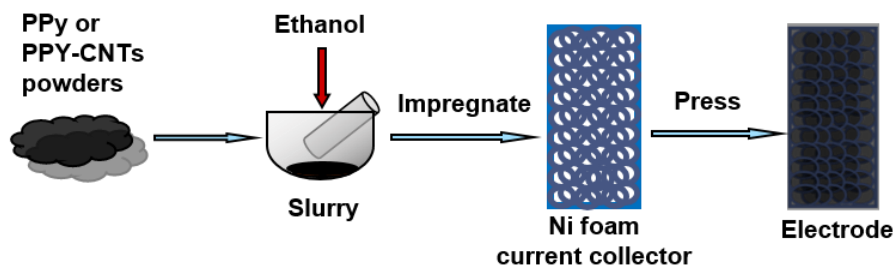


Figure 4.8 Fabrication process of electrodes

The obtained electrodes were combined for the fabrication of EC devices. Two impregnated electrodes were put in a coin cell (CR2032 type, MTI Corporation, USA) and separated by a porous polyethylene membrane (mean pore size 0.4 μm , Vale, Canada). After the injection of electrolyte (0.5 M Na_2SO_4), the device was sealed using a hydraulic crimping machine (MSK-110, MTI Corporation, USA). Fig. 4.9 shows the construction of EC devices.

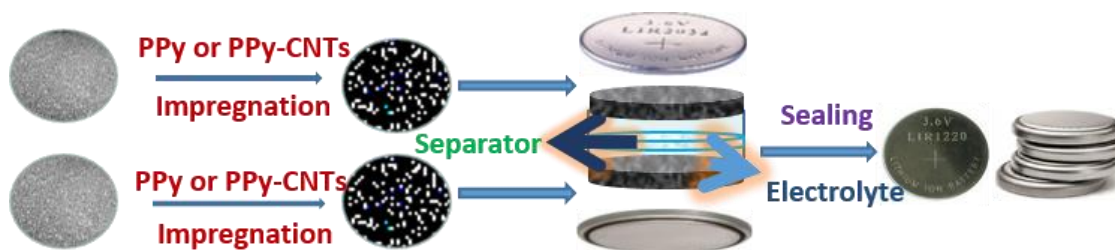


Figure 4.9 Construction of EC devices

4.4 Morphology characterization

The surface morphology of PPy and PPy-MWCNTs powders or films was investigated using a JEOL JSM-7000F scanning electron microscope (SEM). The samples were attached to the sample holder using copper paste. After that, the sample holder was stored in desiccator.

4.5 Adhesion test

The adhesion of deposited PPy films was characterized according to the ASTM D3359 standard. To start with, six cuts with 1mm apart were required in the x and y direction on the film. Pressure-sensitive tape (Elcometer 1539) was applied over the cutting area and then removed. Adhesion was evaluated by the comparison between different patterns on

the tapes. The adhesion classification was performed using a table (ASTM D3359) shown in fig. 4.10.

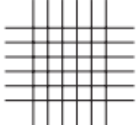
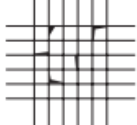
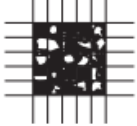
Classification for percentage of area removed	Surface of crosscut area (six each horizontal and vertical parallel cuts) where flaking has occurred: adhesion range by percent.*
5B – 0% None	
4B – Less than 5%	
3B – 5% to 15%	
2B – 15% to 35%	
1B – 35% to 65%	
0B – Greater than 65%	

Figure 4.10 Classification of adhesion test results

4.6 Electrochemical characterization of electrodes

Electrochemical tests of PPy and PPy-MWCNTs electrodes were carried out in three-electrode system (see fig. 4.11) using a potentiostat (PARSTAT 2273, Princeton Applied

Research). Surface area of the working electrode was 1 cm². The counter electrode was a platinum gauze, and the reference electrode was a standard calomel electrode (SCE).

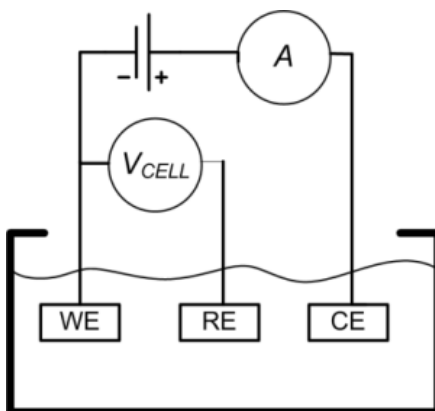


Figure 4.11 Three-electrode system

4.6.1 Cyclic voltammetry study

Cyclic voltammetry (CV) studies were performed within a potential range of -0.5 to +0.4 V versus SCE at scan rates of 2-100 mV s⁻¹ in 0.1 or 0.5M Na₂SO₄ aqueous solutions. The total capacitance was calculated using the following expression

$$C = \frac{Q}{\Delta V} \quad (\text{Eq. 4.1})$$

where Q is charge obtained by half the integrated area of the CV curve and ΔV is the width of the potential window. The mass normalized specific capacitance $C_m=C/m$ (m-sample mass) and area-normalized specific capacitance $C_s=C/S$ (S-geometric sample area), calculated from the CV data, were investigated versus mass loading, scan rate and cycle number.

4.6.2 Impedance spectroscopy study

The measurement of complex electrochemical impedance was conducted within a frequency range of 10 mHz to 100 kHz with AC signal amplitude of 5 mV in 0.1 or 0.5 M Na₂SO₄ aqueous solutions. The obtained complex impedance data (eq. 4.2) plotted in Nyquist graph was simulated using ZSimpWin software (Princeton Applied Research) and appropriate equivalent circuit was selected and applied to such simulation[1].

$$Z^* = Z' - iZ'' \quad (\text{Eq. 4.2})$$

The area normalized complex AC capacitance (Eq. 4.3) was calculated[1] from the complex impedance data using Eq. 4.4 and Eq. 4.5, where $\omega=2\pi f$ (f -frequency). The relaxation times (Eq. 4.6) were calculated from the relaxation frequencies f_m , corresponding to the C_s'' maxima.

$$C_s^* = C_s' - iC_s'' \quad (\text{Eq. 4.3})$$

$$C_s' = \frac{Z''}{\omega S Z^2} \quad (\text{Eq. 4.4})$$

$$C_s'' = \frac{Z'}{\omega S Z^2} \quad (\text{Eq. 4.5})$$

$$\tau = \frac{1}{f_m} \quad (\text{Eq. 4.6})$$

4.7 Characterization of capacitive performance for EC devices

The capacitive performance as well as cyclic stability of EC devices were characterized through the study of charge-discharge behavior using a battery analyzer (BST8, MTI Corporation, USA).

The charge-discharge tests were conducted at constant current varying from 1 mA to 40 mA with voltage limits (ΔU) of 0.9 V. The total stored charge (Q) was calculated by the product of applied current and discharge times. The capacitance (C) can be calculated according to Eq.4.1. The energy density (E_m) and power density (P_m) of EC device were obtained from Eq.4.7 and Eq.4.8, where m represent the mass of electrode materials and t was the corresponding discharging time.

$$E_m = \frac{\int_0^t UI dt}{m} \quad (\text{Eq. 4.7})$$

$$P_m = \frac{E_m}{t} \quad (\text{Eq. 4.8})$$

References

1. Taberna, P.L., P. Simon, and J.F. Fauvarque electrochemical characteristics and impedance spectroscopy studies of carbon-carbon supercapacitors. *Journal of The Electrochemical Society*, 2003. **150**(3): p. A292-A300.

Chapter 5 Influence of dopants and carbon nanotubes on polypyrrole electropolymerization and capacitive behavior

5.1 Electropolymerization of PPy thin films

Fig. 5.1 shows potential versus time curves for the galvanostatic deposition of PPy on stainless steel substrates from the 0.1 M pyrrole solutions containing 5 mM anthraquinone-2-sulfonic acid sodium salt (AQ) or alizarin Red (AR). The results indicated that there is no induction time for the electropolymerization of PPy on the stainless steel substrates. In contrast, deposition of PPy on stainless steel from the solutions containing oxalic acid revealed the presence of an induction period, related to the anodic dissolution of the substrates and formation of a passive layer[1]. The formation of the non-conductive and non-capacitive passive layer must be avoided, because it results in increasing charge transfer resistance and reduced capacitance.

At the beginning of the electropolymerization process, the potential difference between the working and reference electrode increased and then decreased. The deposition potential of PPy from the solutions, containing AR, was significantly lower than that for AQ. The reduced deposition potential is beneficial for suppressing anodic oxidation of the substrate. The comparison of the chemical structures of AQ and AR (Fig. 5.1) indicated that OH groups of AR were beneficial for the application of this material as a dopant for the electropolymerization of PPy. Similar to other aromatic molecules from the catechol family, the structure of AR includes two OH groups bonded to the adjacent carbon atoms of the

aromatic ring. It is known that materials from catechol family exhibit strong adhesion to various inorganic materials[2, 3]. The chemisorption mechanism involves the deprotonation of the phenolic hydroxyl groups of the catechol and chelation of metal ions on the material surface. It is important to note that catecholate bonding facilitated charge transfer between inorganic and organic materials[4, 5]. Therefore, the difference in experimental data for AQ and AR can be attributed to chelation of metal ions by OH groups of AR, which facilitated charge transfer and reduced the electropolymerization potential.

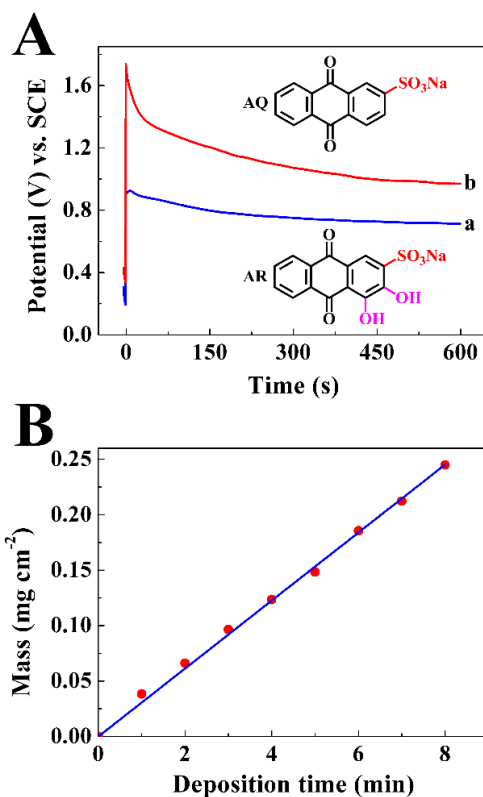


Figure 5.1 (A) Chemical structures of AQ and AR and potential versus time curves for galvanostatic deposition of PPy from 0.1 M pyrrole solution containing (a) 5 mM AR and (b) 5 mM AQ at a current density of 1 mA cm⁻², (B) film mass versus time for PPy films prepared at a current density of 1 mA cm⁻² from 0.1 M pyrrole solution containing 5 mM AR.

The measurements of film adhesion for AR doped films according to the ASTM D3359 standard showed that adhesion strength corresponded to the 4B classification. Turning again to the results of investigation of strong adhesion of catecholates to inorganic surfaces[2, 3], it can be suggested that chelating properties of AR promoted film adhesion. Due to the advantages of AR as a dopant material, further investigations were focused on the AR doped films. The film mass increased linearly with increasing deposition time at a constant current density, indicating the possibility of deposition of films with different mass (Fig. 5.1B).

5.2 Morphology study of PPy and PPy-MWCNTs films

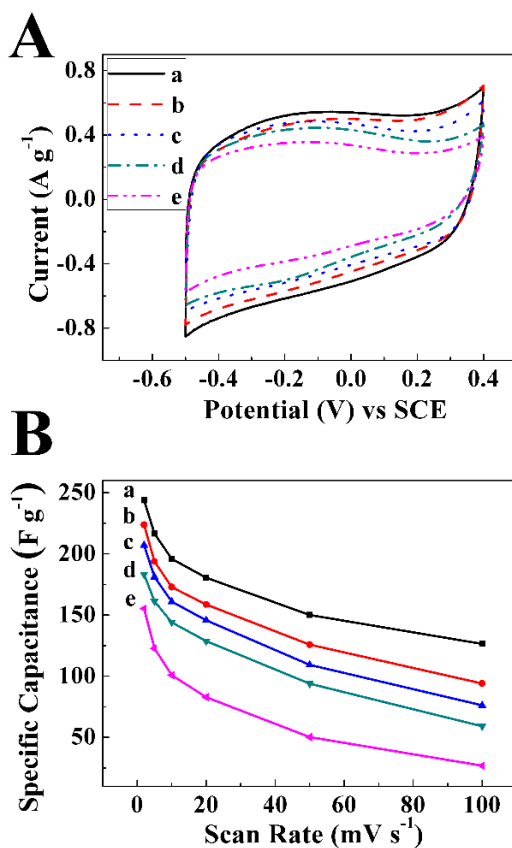


Figure 5.2 (A) CVs at a scan rate of 2 mV s^{-1} and (B) SCs versus scan rate for films of different mass: (a) 0.13, (b) 0.18, (c) 0.23, (d) 0.32 and (e) 0.52 mg cm^{-2} , prepared from 0.1 M pyrrole solutions containing 5 mM AR.

The PPy films showed capacitive behaviour, as indicated by nearly box shape CVs, shown in Fig. 5.2A. The SC, calculated from the CV data, decreased with increasing scan rate and film mass (Fig. 5.2B).

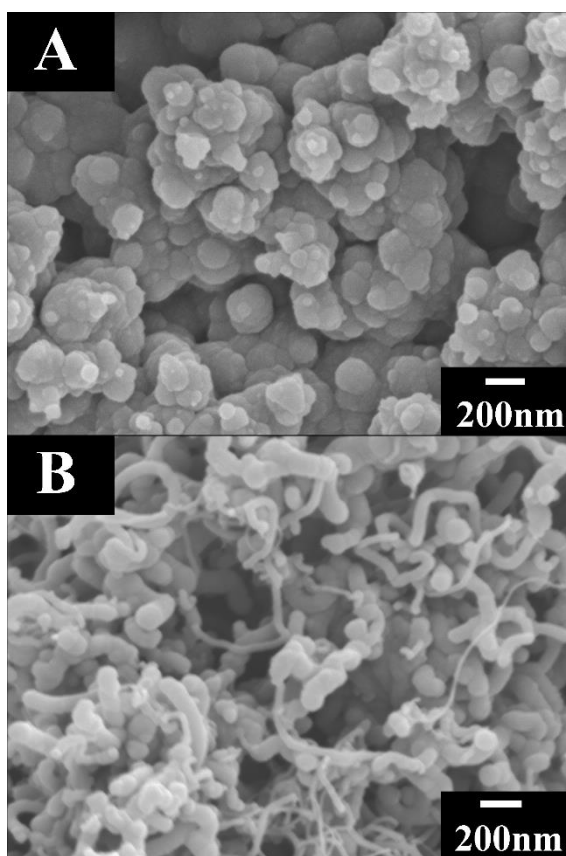


Figure 5.3 SEM images for films prepared from 0.1 M pyrrole solutions, containing 5 mM AR and (A) 0 and (B) 0.3 gL^{-1} MWCNT.

Further improvement in capacitive behaviour was achieved by the use of MWCNT additives. It was found that AR allowed dispersion of MWCNT in aqueous solutions. The anionic AR molecules adsorbed on MWCNT and provided electrostatic stabilization of

MWCNT and electric charge for electrodeposition. SEM data confirmed the formation of composite PPy-MWCNT films. Fig. 5.3(A, B) compares the SEM images of pure PPy and composite PPy-MWCNT films. Pure PPy films (Fig. 5.3A) were porous, the typical size of PPy particles was 100-200 nm. The film porosity and small particle size are beneficial for applications of such films in ES, because they allow improved electrolyte access to the active material. Fig. 5.3B shows that MWCNT were co-deposited with PPy. Moreover, the SEM image indicates that most of the MWCNT were coated with PPy.

5.3 Capacitive performance of PPy and PPy-MWCNTs films

Fig. 5.4A compares SC calculated from the CV data in a voltage window of 0.9 V for pure PPy and PPy-MWCNT films. The composite films showed higher capacitance, compared to pure PPy films.

The results indicated improved SC retention of PPy-MWCNT films with increasing film mass, compared to pure PPy films. The highest SC of 274 F g^{-1} was achieved for PPy-MWCNT films. The beneficial effect of MWCNT was also confirmed by measurements of AC capacitance.

Fig. 5.4B showed significantly higher C' for PPy-MWCNT films. The C' decreased with increasing frequency. The corresponding data for C'' showed significantly higher C'' values for PPy-MWCNT films. This is attributed to lower impedance $|Z|$ of the composite films. Therefore, the incorporation of MWCNT into the PPy films allowed reduced impedance and improved capacitive behaviour. The PPy-MWCNT films, prepared by electropolymerization using AR dopant, are promising electrode materials for ES.

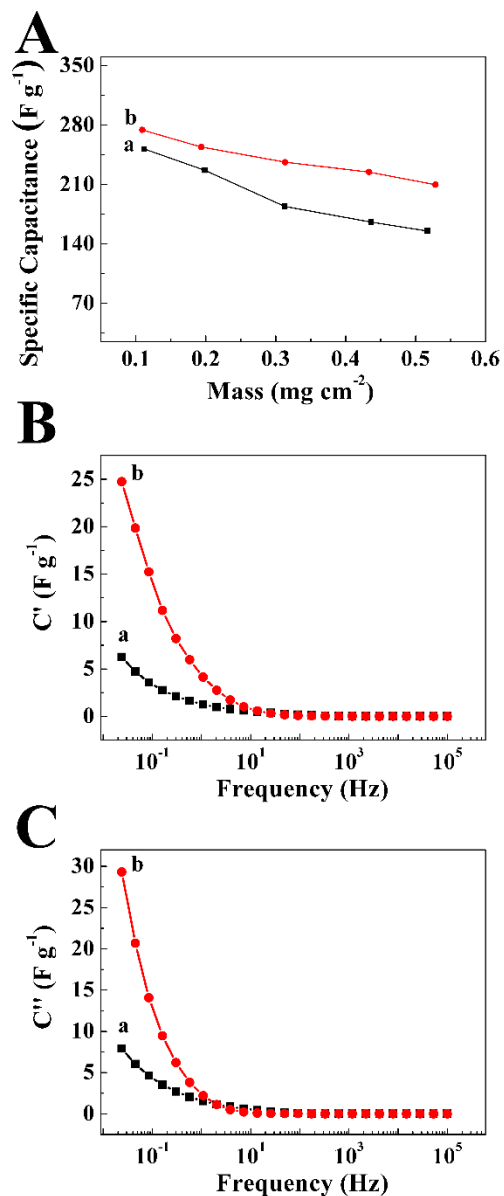


Figure 5.4 (A) SC calculated from CV data versus film mass and (B) C', (C) C'' components of complex capacitance, calculated from AC impedance data, versus frequency for films prepared from 0.1 M pyrrole solutions, containing 5 mM AR and (a) 0 and (b) 0.3 g L⁻¹ MWCNT.

5.4 Conclusions

PPy films were prepared by electropolymerization on stainless steel substrates using AR and AQ as anionic dopants. The comparison of the experimental data for AR and AQ and chemical structures of the organic molecules revealed the importance of OH groups of AR, which provided chelation of metal ions on substrate surface and allowed for the formation of adherent films at reduced electropolymerization potential. The use of AR allowed dispersion, charging and anodic deposition of MWCNT. Anodic electropolymerization of PPy and electrodeposition of MWCNT was combined for the fabrication of composite films. The composite PPy-MWCNT films showed higher SC and improved SC retention with increasing film mass, compared to pure PPy films. The highest SC of 274 F g⁻¹ was achieved for PPy-MWCNT films at a scan rate of 2 mVs⁻¹. The SC was higher than that reported for galvanostatically deposited PPy films (227 F g⁻¹ and 240 F g⁻¹), tested in metal salt electrolytes. The films prepared in this investigation are promising for applications in electrodes of ES.

References

1. Su, W. and J.O. Iroh, Formation of polypyrrole coatings onto low carbon steel by electrochemical process. *Journal of Applied Polymer Science*, 1997. **65**(3): p. 417-424.
2. Lee, H., et al., Mussel-inspired surface chemistry for multifunctional coatings. *Science*, 2007. **318**(5849): p. 426-430.
3. Sun, Y. and I. Zhitomirsky, Electrophoretic deposition of titanium dioxide using organic acids as charging additives. *Materials Letters*, 2012. **73**(0): p. 190-193.
4. Wang, G.-L., J.-J. Xu, and H.-Y. Chen, Dopamine sensitized nanoporous TiO₂ film on electrodes: Photoelectrochemical sensing of NADH under visible irradiation. *Biosensors and Bioelectronics*, 2009. **24**(8): p. 2494-2498.
5. Tallman, D.E., et al., Direct electrodeposition of polypyrrole on aluminum and aluminum alloy by electron transfer mediation. *Journal of the Electrochemical Society*, 2002. **149**(3): p. C173-C179.

Chapter 6 Polypyrrole electrodes doped with sulfanilic acid azochromotrop for electrochemical supercapacitors

6.1 Electrodeposition of PPy films doped by SPADNS

Fig. 6.1A shows a chemical structure of sulfanilic acid azochromotrop (SPADNS) used as an anionic dopant for electropolymerization and chemical polymerization of PPy. SPADNS is a polyaromatic molecule, containing anionic sulfonic groups. As pointed out before, the large polyaromatic molecules containing sulfonic groups are of special interest for the development of PPy films and powders with high conductivity and high capacitance. Moreover, SPADNS belongs to the chromotropic acid family of materials, the chemical structure of SPADNS includes two OH groups, bonded to carbon atoms of fused aromatic rings. Such adjacent OH groups of chromotropic acid and SPADNS provide strong complexing properties[1, 2].

In the previous investigations[1] it was found that complexation of metal atoms on the substrate surface by chromotropic acid reduced electropolymerization potential of PPy, facilitated charge transfer during electropolymerization and allowed for the formation of adherent PPy films on stainless steel substrates. Therefore, SPADNS molecules with a similar structure can be beneficial for the fabrication of PPy films by electropolymerization. It is important to note that compared to chromotropic acid, the SPADNS molecules have larger size and charge. According to previous study[3-6], the large charge and size of SPADNS can be beneficial for the fabrication of electrodes with improved conductivity and cycling stability.

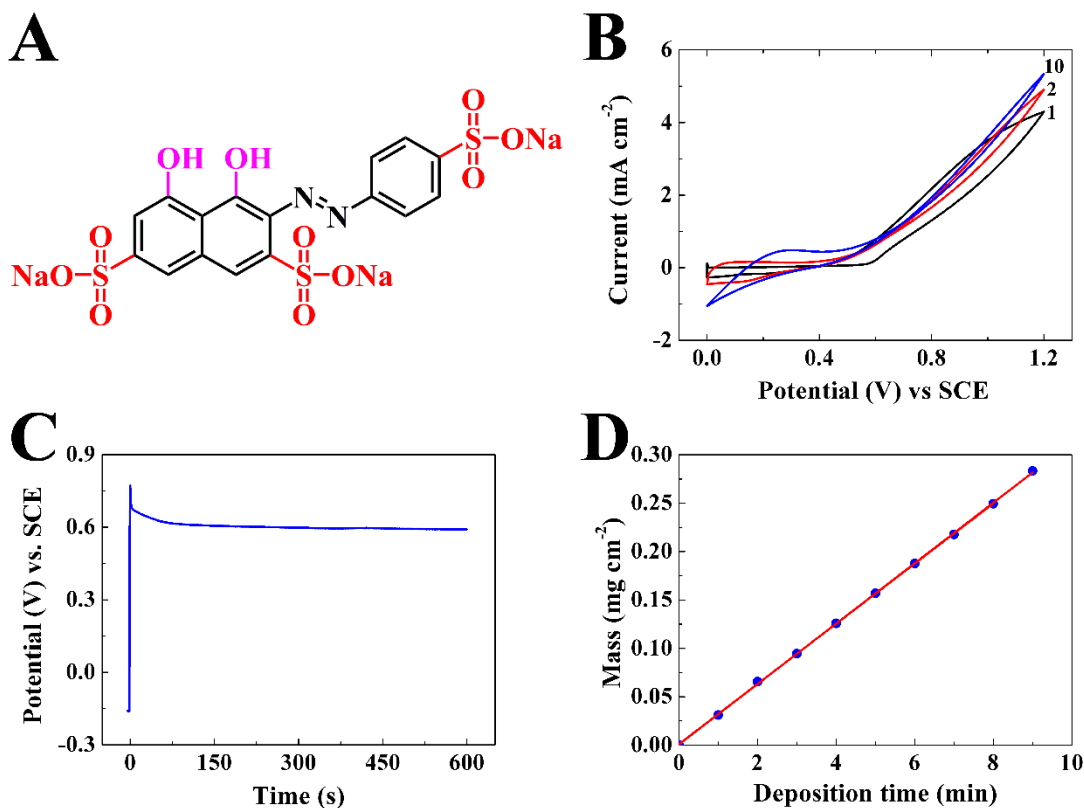


Figure 6.1 (A) chemical structure of SPADNS, (B) CVs at a scan rate of 20 mV s^{-1} for cycles 1, 2 and 10, (C) electrode potential versus time at a current density of 1 mA cm^{-2} , (D) deposit mass versus deposition time at a current density of 1 mA cm^{-2} for (B,C,D) stainless steel electrodes in 0.1 M pyrrole solution, containing 5 mM SPADNS.

Electropolymerization of PPY was performed potentiodynamically and galvanostatically. The potentiodynamic CVs for stainless steel electrode in pyrrole solutions, containing SPADNS, were presented in Fig. 6.1B. During the first scan, the increase in electrode potential above 0.6 V resulted in increasing current, attributed to electropolymerization of PPy. Indeed, PPy films were formed at the stainless steel electrode at higher potentials. In the subsequent scans, a slight progressive increase of current was observed, indicating the continuous growth of conductive film without oxidation of the substrate[7-10]. Such behavior also indicates that the electronic conductivity of the film is sufficiently high to

consider the ohmic potential drop inside the film as negligible[11, 12]. In contrast, the formation of a passivation layer usually results in the reduction of current with increasing cycle number[13].

PPY films were also formed galvanostatically. At the beginning of the electrodeposition process, the potential difference between the working and reference electrode increased (Fig. 6.1C) and then slightly decreased to a steady value of about 0.6V versus SCE. The potential versus time dependence did not show any induction period for the electropolymerization of PPy using SPADNS as anionic dopant. In contrast, literature data[14, 15] on electropolymerization of PPy from solutions, containing oxalic acid, revealed an induction period, related to the dissolution of iron and formation of an iron oxalate layer. The deposit mass versus time dependence presented in Fig. 6.1D was nearly linear and indicated continuous film growth without induction time. The measurements of film adhesion according to the ASTM D3359 standard showed that adhesion strength corresponded to the 4B classification for film mass 0.1- 0.3 mg cm⁻². However, the increase in film mass above 0.3 mg cm⁻² resulted in significant decrease in adhesion strength.

6.2 Electrochemical properties of electropolymerized PPy films

SEM studies revealed the formation of relatively dense films (Fig. 6.2A), which showed capacitive behaviour in 0.5 M Na₂SO₄ electrolyte. Fig. 6.2B shows typical CVs for films of different mass. C_m and C_s for the same films were plotted versus scan rate in Fig. 6.2C,D. It was found that for 0.187 mg cm⁻² PPy film, the C_m value decreased from 199 to 126 F g⁻¹ in the range of 2-100 mV s⁻¹. The decrease in C_m with increasing film mass (Fig. 6.2C(b))

was attributed to diffusion limitation of electrolyte in the bulk of the PPy film. The C_s increased with increasing film mass, however the C_s at 2 mV s^{-1} was only 45.6 mF g^{-1} for 0.283 mg cm^{-2} PPy films.

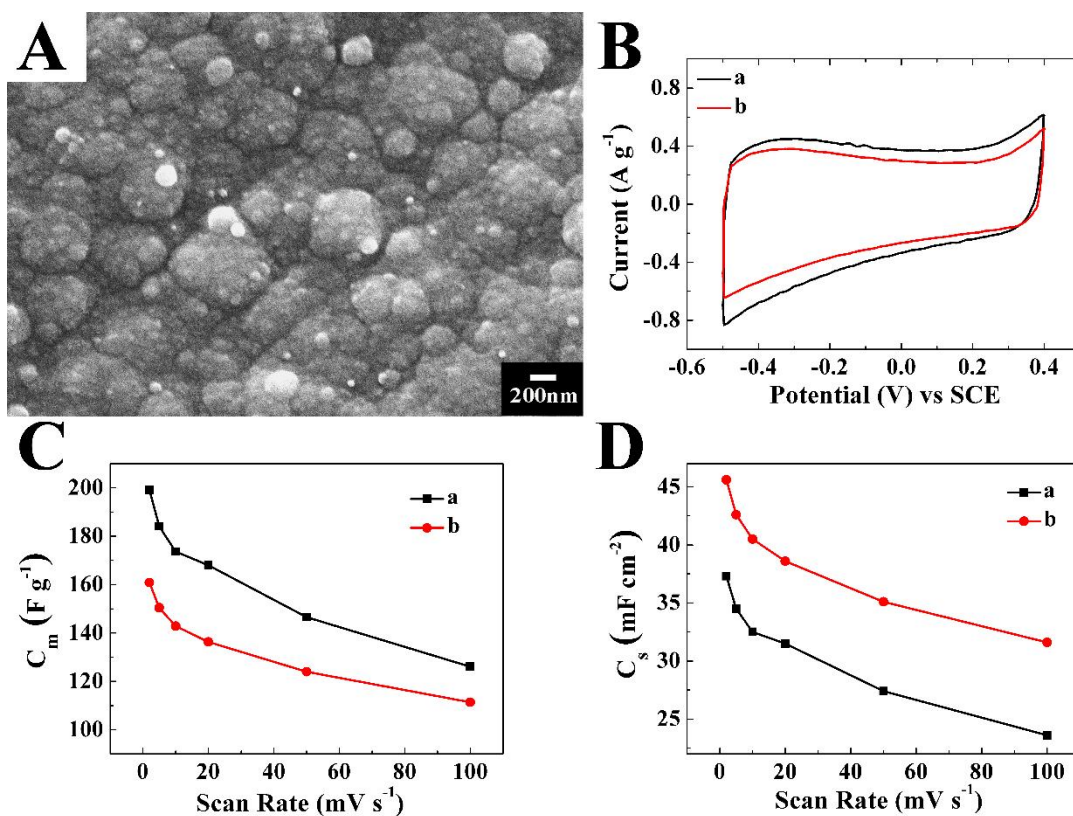


Figure 6.2 (A) SEM image of a PPy film on a stainless steel substrate and (B,C,D) testing results for the films in the $0.5 \text{ M Na}_2\text{SO}_4$ electrolyte: (B) CVs at a scan rate of 2 mV s^{-1} , (C) C_m and (D) C_s versus scan rate for (a) 0.187 and (b) 0.283 mg cm^{-2} PPy films.

Fig. 6.3 shows C_s' and C_s'' data for the PPy films. The C_s' and C_s'' values decreased significantly with increasing frequency in the range above 1 mHz . The C_s' values at low frequencies were comparable with C_s values obtained from the CV measurements. It is important to note that obtained capacitance values, measured by different methods, depend on the scan rate or frequency.

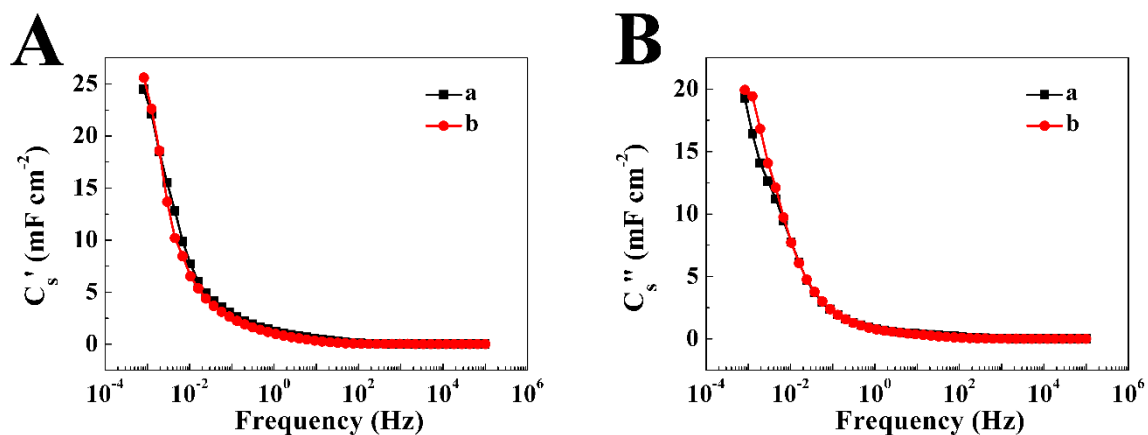


Figure 6.3 (A) C_s' and (B) C_s'' versus frequency for (a) 0.187 and (b) 0.283 mg cm⁻² PPY films on stainless steel substrates in 0.5 M Na₂SO₄ electrolyte.

6.3 Characterization of chemical polymerized porous PPY electrodes

The PPY electrodes were also formed using PPY powders, prepared by chemical polymerization. The SEM images of the PPY powders (Fig. 6.4) showed that typical particle size was less than 200 nm, however the particles formed agglomerates.

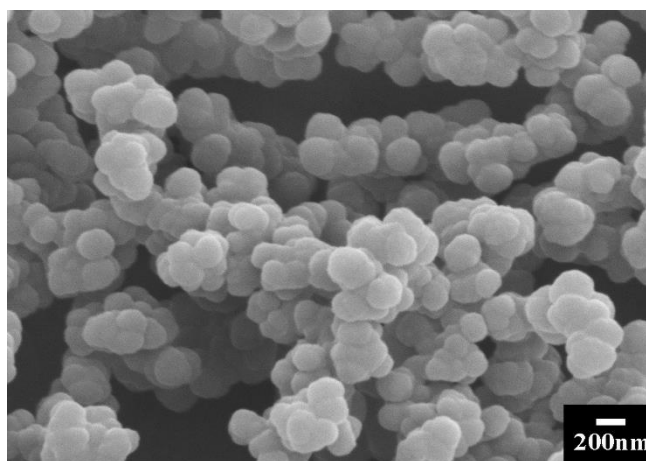


Figure 6.4 SEM image of PPY powder, prepared by a chemical polymerization method

The PPy particles were impregnated into Ni foam. The SEM image of the impregnated foam (fig. 6.5A) showed porous microstructure, which is beneficial for good electrolyte access to the PPy surface. Testing results showed that good electrochemical performance can be achieved at materials loading of 15.3-35.4 mg cm⁻². The electrodes showed box shape CVs (Fig. 6.5B). The C_m values for Ni foam based PPy electrodes with mass of 15.3-35.4 mg cm⁻² were comparable with the C_m values for thin film electrodes with mass loadings of 0.2-0.3 mg cm⁻². However, due to the high materials loading, significantly higher C_s values were obtained. The C_s of 5.43 F cm⁻² was obtained at materials loading of 35.4 mg cm⁻² at a scan rate of 2 mV s⁻¹. The volume normalized capacitance was 93.6 F cm⁻³. The C_s decreased with increasing scan rate and decreasing materials loading.

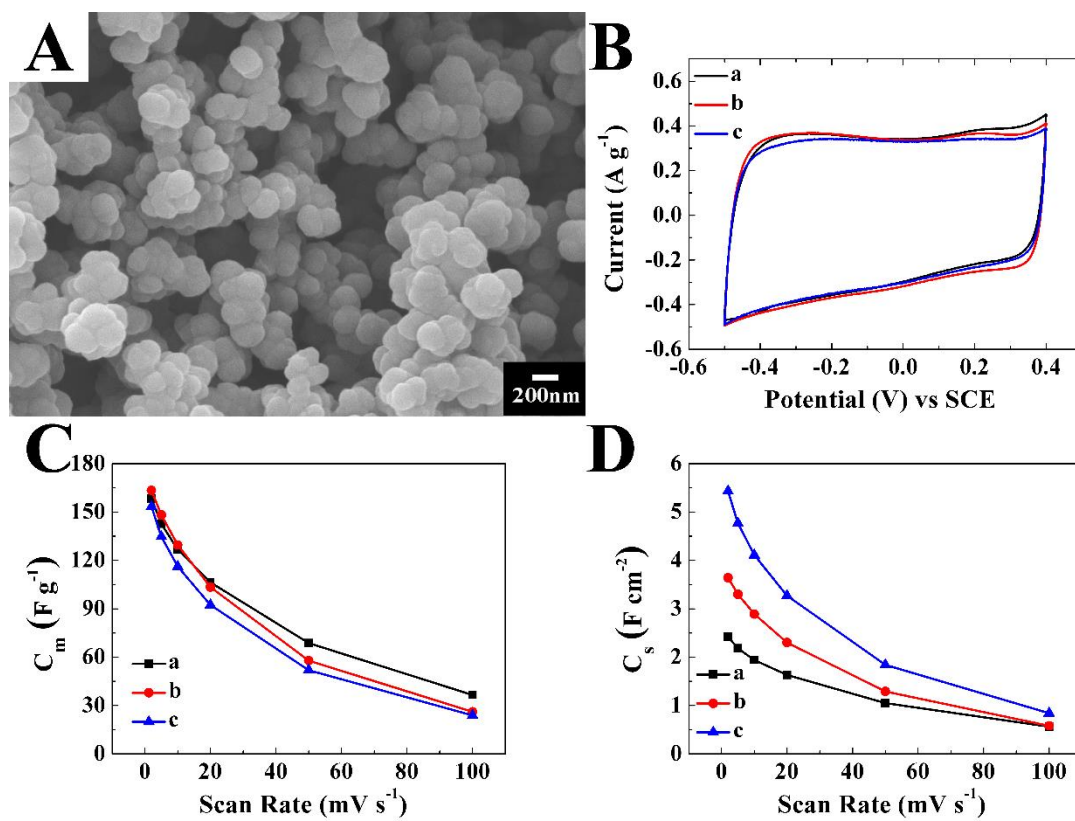


Figure 6.5 (A) SEM image of an electrode, fabricated by impregnation of a Ni foam with

PPy powder, prepared by a chemical polymerization method and (B,C,D) testing results for the electrodes in 0.5 M Na₂SO₄ electrolyte:(B) CVs at a scan rate of 2 mV s⁻¹, (C) C_m and (D) C_s versus scan rate for PPy loadings of (a) 15.3, (b) 22.3, (c) 35.4 mg cm⁻².

Fig. 6.6 shows that C_m, measured at a scan rate of 2 mV s⁻¹, was practically independent on materials loading in the range of 15.3-35.4 mg cm⁻², as a result, nearly linear increase in C_s with increasing materials loading was observed. The linear increase in C_s indicated that the use of Ni foam current collectors allowed good utilization of PPy material.

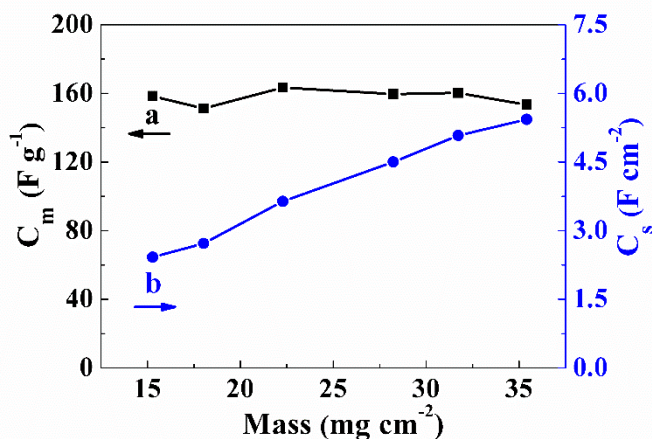


Figure 6.6 (a) C_m and (b) C_s at a scan rate of 2 mV s⁻¹ in 0.5 M Na₂SO₄ electrolyte versus PPy mass loading of Ni foam with PPy powder, prepared by a chemical polymerization method.

It is known[16] that high C_m values of electrode materials do not necessarily indicate good capacitive behavior. It was shown that reporting gravimetric characteristics (such as C_m) alone cannot provide realistic picture of material performance, especially at high material loadings. It is in this regard that for commercialization of ES, the mass loading of electrodes with active material must be higher than 10 mg cm⁻²[16]. The C_m data presented above did not exceed the literature C_m data for PPy electrodes, reported for the electrodes with

materials loading of 0.1-2.8 mg cm⁻²[1, 17-19]. However, significantly higher mass loadings were achieved in our investigation and obtained C_s of 5.43 F cm⁻² was higher than the literature C_s data[18, 20] for PPy electrodes, which were in the range of 0.38-0.95 F cm⁻² for materials loadings of 1.0-2.8 mg cm⁻².

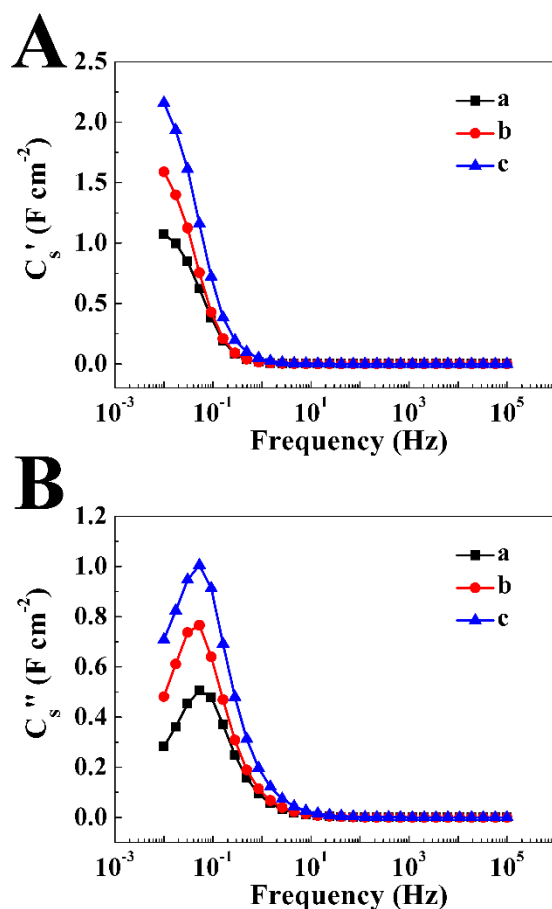


Figure 6.7 (A) C_s' and (B) C_s'' versus frequency for electrodes with PPy loading of (a) 15.3, (b) 22.3 and (c) 35.4 mg cm⁻², fabricated by impregnation of Ni foam with PPy powder, prepared by a chemical polymerization method and tested in 0.5 M Na₂SO₄ electrolyte.

Fig. 6.7 shows C_s' and C_s'' data for the Ni foam based PPy electrodes. The C_s' increased with increasing film mass (Fig. 6.7a-c) and decreased with increasing frequency. The C_s' of Ni foam based PPy electrode (Fig. 6.7A(a-c)) was by 2 order of magnitude higher,

compared to C_s' of PPy films (Fig. 6.3A). It is important to note that Ni foam based electrodes showed lower energy dissipation factor C_s''/C_s' , especially at frequencies below 0.1 Hz. The C_s'' showed relaxation maxima at ~ 0.1 Hz, corresponding to relaxation times of $\tau \cong 10$ s (Fig. 6.7B(a-c)). However, such maxima were not observed in the frequency dependences of C_s'' for PPy films (Fig. 6.3B), indicating higher relaxation times. Turning again to the SEM image of PPy film, shown in Fig. 6.2A, it should be noted that diffusion limitations of electrolyte in such relatively dense films can result in high relaxation times. It is important to note that electrode porosity showed a strong influence on the frequency dependence of capacitance of porous electrodes[21]. It was found that cut-off frequency[21] increased with increasing pore size and decreasing electrode thickness.

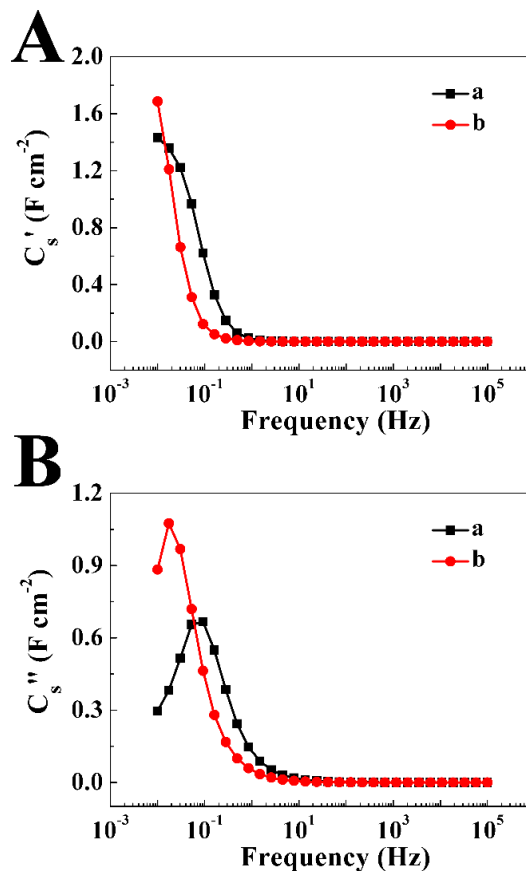


Figure 6.8 (A) C_s' and (B) C_s'' versus frequency for electrodes with PPy loading of 20.8 mg cm^{-2} , fabricated by impregnation of Ni foam with PPy powder, prepared by a chemical polymerization method and tested in (a) 0.5 and (b) 0.1 M Na_2SO_4 electrolyte.

Fig. 6.8 shows the influence of electrolyte concentration on C_s^* . It was found that the reduction in electrolyte concentration resulted in reduced relaxation frequency. Indeed, the maximum in C_s'' shifted from $\sim 0.1 \text{ Hz}$ ($\tau \cong 10 \text{ s}$) for 0.5 M Na_2SO_4 electrolyte to 0.05 Hz ($\tau \cong 20 \text{ s}$) for 0.1 M Na_2SO_4 electrolyte. The results indicated that relaxation mechanism was governed by electrolyte diffusion in electrode material.

Fig. 6.9 compares cycling behaviour of 0.187 mg cm^{-2} thin film and 23 mg cm^{-2} Ni foam based PPy electrodes. The thin film electrode showed continuous reduction in capacitance, the capacitance retention after 1000 cycles was only 45.1%. In contrast, the Ni foam based electrode showed small increase in the capacitance during the first 600 cycles and then capacitance decreased. The capacitance retention after 1000 cycles was found to be 91.5%.

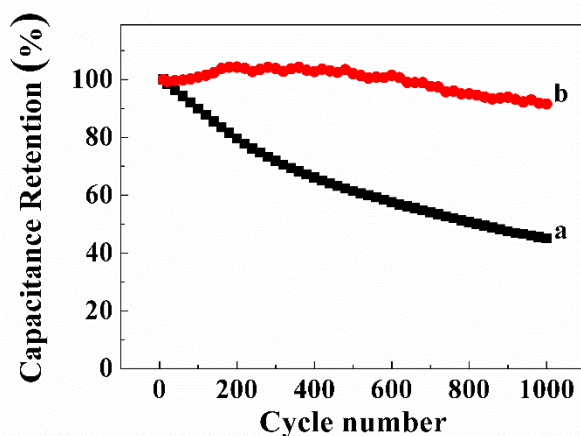


Figure 6.9 Capacitance retention in 0.5 M Na_2SO_4 electrolyte versus cycle number for 0.187 mg cm^{-2} PPy film, prepared by electropolymerization on a stainless steel substrate

and 23 mg cm^{-2} PPy electrode, prepared by impregnation of Ni foam with PPy powder, prepared by a chemical polymerization method.

The results indicated that the electrodes, formed by impregnation of Ni foams with PPy, prepared by chemical polymerization, offer advantages compared to electrodes prepared by electropolymerization. The use of Ni foam based electrodes allowed improved capacitive behaviour at high materials loading, high C_s and improved cycling stability. The results of this investigation indicated that problems limiting applications of PPy in ES, such as low materials loading and poor cycling stability, can be addressed by the use of SPADNS as a new anionic dopant and Ni foam current collectors. The use of SPADNS was beneficial for the fabrication of fine particles. The fine particle size allowed efficient impregnation of Ni foam current collectors and high materials loading was achieved. The comparison of the cycling stability data for PPy films and Ni foam based PPy electrodes indicated that the use of Ni foam was the major factor, which allowed good cycling stability. It is suggested that Ni foam prevented swelling of the polymer during cycling and allowed good contact of Ni foam current collector and PPy. As pointed out above, the large size and charge of the aromatic dopant molecules are important in order to achieve high conductivity, high capacitance and good cycling stability of PPy electrodes[3-6, 22]. Therefore relatively large size and charge of SPADNS provided additional benefits for the fabrication of efficient PPy electrodes. Thin PPy films prepared by electropolymerization on stainless steel can be used for thin film capacitors, whereas the Ni-foam based bulk PPy electrodes with high materials loadings can be fabricated using PPy particles prepared by chemical polymerization. The PPy electrodes, prepared in this investigation are promising for the fabrication of ES.

6.4 Conclusions

Electropolymerization and chemical polymerization of PPy were performed using SPADNS as a new anionic dopant. The chelating properties of SPADNS allowed for the fabrication of adherent films by electropolymerization on stainless steel substrates. The high charge and mass of SPADNS were beneficial for the fabrication of PPy electrodes with good capacitive behaviour.

The PPy films were obtained galvanostatically or potentiodynamically and the amount of the deposited material was well controlled by the variation of deposition time at the galvanostatic mode. The fabrication of fine PPy powders by chemical polymerization allowed for efficient impregnation of Ni foam current collectors and fabrication of porous electrodes with high materials loading in the range of 15.3-35.4 mg cm⁻². The PPy films and Ni foam based PPy electrodes showed good capacitive behaviour in the Na₂SO₄ electrolyte. The Ni foam based PPy electrodes offered advantages of high materials loading, improved capacitive behaviour and good cycling stability. The area normalized and volume normalized specific capacitances were as high as 5.43 F cm⁻² and 93.6 F cm⁻³, respectively, for materials loading of 35.4 mg cm⁻². The capacitance retention of Ni foam based electrodes was 91.5% after 1000 cycles. The Ni foam based PPy electrodes are promising for application in ES.

References

1. Ariyanayagamkumarappa, D.K. and I. Zhitomirsky, Electropolymerization of polypyrrole films on stainless steel substrates for electrodes of electrochemical supercapacitors. *Synthetic Metals*, 2012. **162**(9-10): p. 868-872.
2. Wang, Y. and I. Zhitomirsky, Effect of phenolic molecules on electrophoretic deposition of manganese dioxide-carbon nanotube nanocomposites. *Colloids and Surfaces A*, 2010. **369**(1-3): p. 211-217.
3. Mitchell, G.R., F.J. Davis, and C.H. Legge, The effect of dopant molecules on the molecular order of electrically-conducting films of polypyrrole. *Synthetic Metals*, 1988. **26**(3): p. 247-257.
4. Han, M., et al., Fabrication and characterizations of oligopyrrole doped with dodecylbenzenesulfonic acid in reverse microemulsion. *Journal of Colloid and Interface Science*, 2006. **296**(1): p. 110-117.
5. Qie, L., et al., Revisit of polypyrrole as cathode material for lithium-ion battery. *Journal of the Electrochemical Society*, 2012. **159**(10): p. A1624-A1629.
6. Lang, X., et al., The role of anthraquinone sulfonate dopants in promoting performance of polypyrrole composites as pseudo-capacitive electrode materials. *Synthetic Metals*, 2010. **160**(15): p. 1800-1804.
7. Martins dos Santos, L.M., et al., Electrochemical synthesis of polypyrrole films on copper electrodes in acidic and neutral aqueous media. *Journal of Electroanalytical*

Chemistry, 2006. **587**(1): p. 67-78.

8. Gonzalez, M.B. and S.B. Saidman, Electrodeposition of polypyrrole on 316L stainless steel for corrosion prevention. *Corrosion Science*, 2011. **53**(1): p. 276-282.

9. Annibaldi, V., A.D. Rooney, and C.B. Breslin, Corrosion protection of copper using polypyrrole electrosynthesised from a salicylate solution. *Corrosion Science*, 2012. **59**(0): p. 179-185.

10. Bazzaoui, M., et al., Electrochemical synthesis of polypyrrole on ferrous and non-ferrous metals from sweet aqueous electrolytic medium. *Thin Solid Films*, 2005. **485**(12): p. 155-159.

11. Correia, J.P., et al., Polypyrrole films functionalized with pendant titanocene dichloride complexes: Ellipsometric study of the electropolymerization process. *Electrochimica Acta*, 2007. **53**(3): p. 1195-1205.

12. Mabrouk, P.A., Oxidative electropolymerization of pyrrole from neat monomer solution. *Synthetic Metals*, 2005. **150**(1): p. 101-105.

13. Redondo, M.I. and C.B. Breslin, Polypyrrole electrodeposited on copper from an aqueous phosphate solution: Corrosion protection properties. *Corrosion Science*, 2007. **49**(4): p. 1765-1776.

14. Hamer, W.J., L. Koene, and J.H.W. de Wit, Formation and electrochemical behaviour of poly(pyrrole) coatings on steel substrates. *Materials and Corrosion*, 2004. **55**(9): p. 653-658.

15. De Bruyne, A., J.L. Delplancke, and R. Winand, Comparison between polypyrrole films obtained on mild steel by electropolymerization from oxalic acid and sodium sulphate aqueous solutions. *Surface and Coatings Technology*, 1998. **99**(12): p. 118-124.
16. Gogotsi, Y. and P. Simon, True performance metrics in electrochemical energy storage. *Science*, 2011. **334**(6058): p. 917-918.
17. Snook, G.A., P. Kao, and A.S. Best, Conducting-polymer-based supercapacitor devices and electrodes. *Journal of Power Sources*, 2011. **196**(1): p. 1-12.
18. Shi, K. and I. Zhitomirsky, Influence of current collector on capacitive behavior and cycling stability of Tiron doped polypyrrole electrodes. *Journal of Power Sources*, (0): p. in press.
19. Zhang, J., et al., Synthesis of polypyrrole film by pulse galvanostatic method and its application as supercapacitor electrode materials. *Journal of Materials Science*, 2010. **45**(7): p. 1947-1954.
20. Dong, Z.H., et al., Characterisation of doped polypyrrole/manganese oxide nanocomposite for supercapacitor electrodes. *Materials Chemistry and Physics*, 2011. **131**(12): p. 529-534.
21. Kötz, R. and M. Carlen, Principles and applications of electrochemical capacitors. *Electrochimica Acta*, 2000. **45**(15–16): p. 2483-2498.
22. Wang, P.-C. and J.-Y. Yu, Dopant-dependent variation in the distribution of polarons and bipolarons as charge-carriers in polypyrrole thin films synthesized by oxidative chemical polymerization. *Reactive and Functional Polymers*, 2012. **72**(5): p. 311-316.

Chapter 7 Capacitive behaviour of polypyrrole, prepared using pyrocatecholsulfonphthalein by electrochemical and chemical methods

7.1 Electropolymerization of PPy using PS

The interest in pyrocatecholsulfonphthalein (PS) (Fig. 7.1A) as a new polyaromatic anionic dopant for PPy polymerization was based on the literature data, which indicated that PPy doped with polyaromatic dopants showed reduced particles size, high conductivity and improved electrochemical performance[1-3]. Preliminary experiments showed that adherent films can be obtained on Ni foil substrates by electrodeposition (Fig. 7.1B).

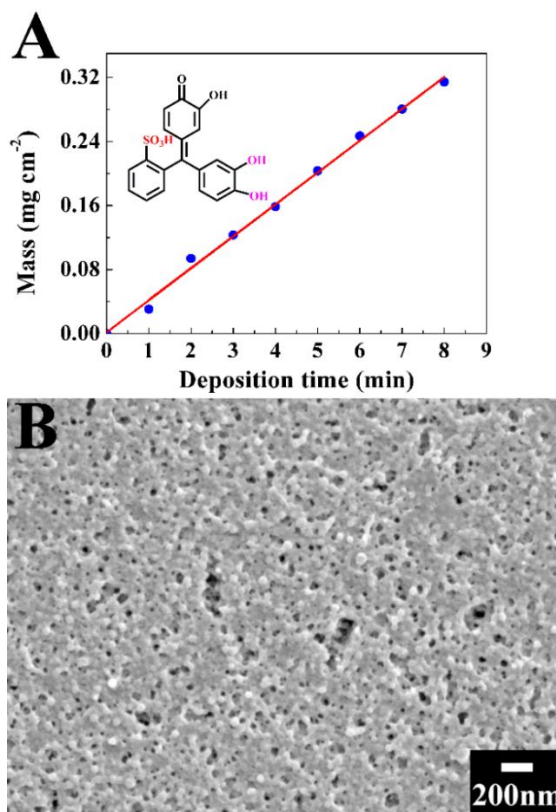


Figure 7.1 (A) The mass-time curve and chemical structure of PS (inset), (B) SEM image of PPy fabricated by galvanostatic deposition using PS under 1 mA cm⁻² on Ni foil.

The film adhesion measurement according to the ASTM D3359 standard indicated that the adhesion strength corresponded to 4B classification for film mass of $0.1\text{-}0.3\text{ mg cm}^{-2}$. The film showed capacitive behaviour according to its CV curve and specific capacitance. The impedance spectroscopy data was simulated by corresponding equivalent circuit involved following circuit elements: solution resistance R_1 , faradaic resistance R_2 , double layer capacitance Q_1 and pseudocapacitance Q_2 . The cycle stability test indicated that the capacitance reduced by 50% after 500 cycles (Fig. 7.2).

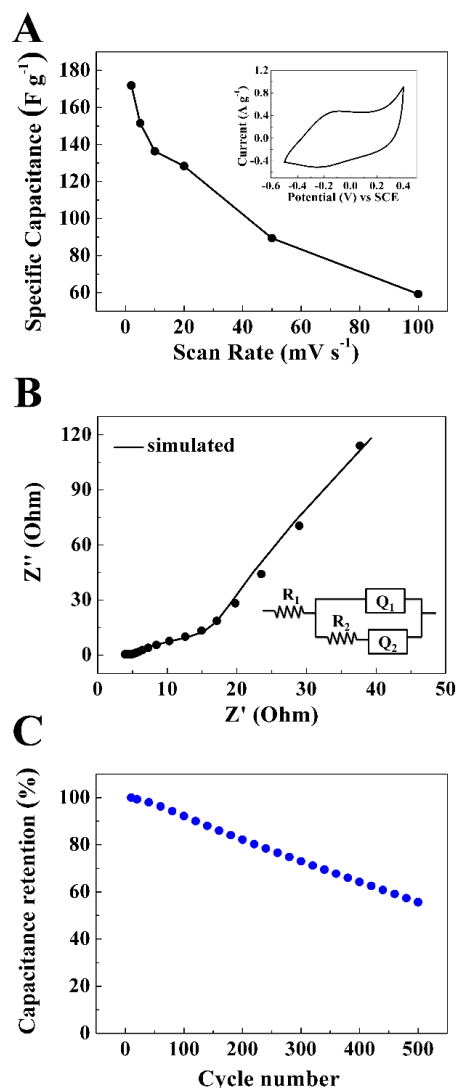


Figure 7.2 (A) specific capacitance at scan rates from 2 to 100 mV s^{-1} and CV at a scan rate of 2 mV s^{-1} (inset), (B) electrochemical impedance spectroscopy data and corresponding equivalent circuit (inset), and (C) cyclic stability of PPy fabricated by galvanostatic deposition using PS dopant.

The increase in the PS concentration in the range of 2.6-5.0 mM resulted in increasing capacitance and decreasing impedance, but no significant variations in capacitance and impedance was observed at higher PS concentrations (Fig. 7.3). The optimum amount of PS was found to be 5 mM.

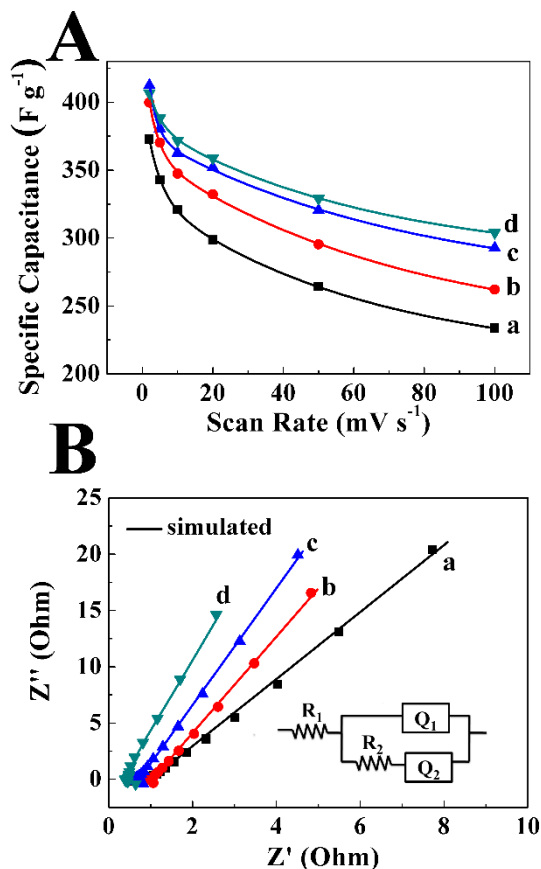


Figure 7.3 (A) SC versus scan rate curves of PPy fabricated by galvanostatic deposition in solution contains different concentration of PS (B) Corresponding Nyquist plots for complex impedance and corresponding equivalent circuit (inset).

7.2 Comparison between galvanostatic and pulse deposited PPy

Fig. 7.4(A,B) shows deposition yield as a function of deposition time for galvanostatic and pulse electropolymerization of PPy. The deposition yield increased nearly linearly with increasing deposition time. Therefore, the amount of the deposited material can be varied and controlled.

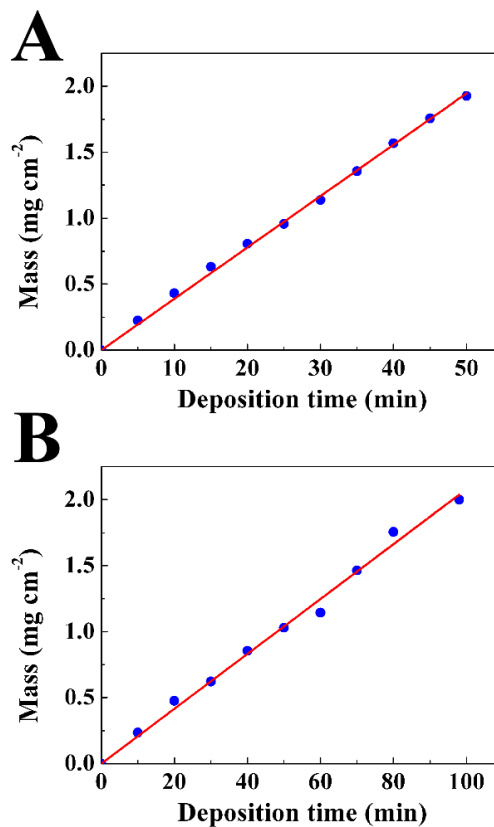


Figure 7.4 Deposit mass versus deposition time for (A) galvanostatic electropolymerization and (B) pulse electropolymerization.

Fig. 7.5 compares the SEM images of as-received and electrochemically impregnated Ni plaques. The as-received plaques (Fig. 7.5(A,B)) were porous, the typical size of pores and Ni particles was in the range of 1-20 and 1-3 μm , respectively. The SEM image of the plaques after galvanostatic deposition (Fig. 7.5(C,D)) showed that porosity was closed by

the PPy material. However, the PPy layer showed cracks. It is suggested that voids in the porous plaque substrate below the PPy layer promoted crack formation. It is in this regard that cracks were not observed for galvanostatically deposited films on Ni foils (Fig. 7.1B). The analysis of SEM images of PPy plaques after pulse electropolymerization (Fig. 7.5(E,F)) showed that individual Ni particles were coated with PPy. The size of individual PPy particles was on the nanometric scale (Fig. 7.5F). Small pores of Ni plaques were closed with PPy material, whereas larger pores remained open.

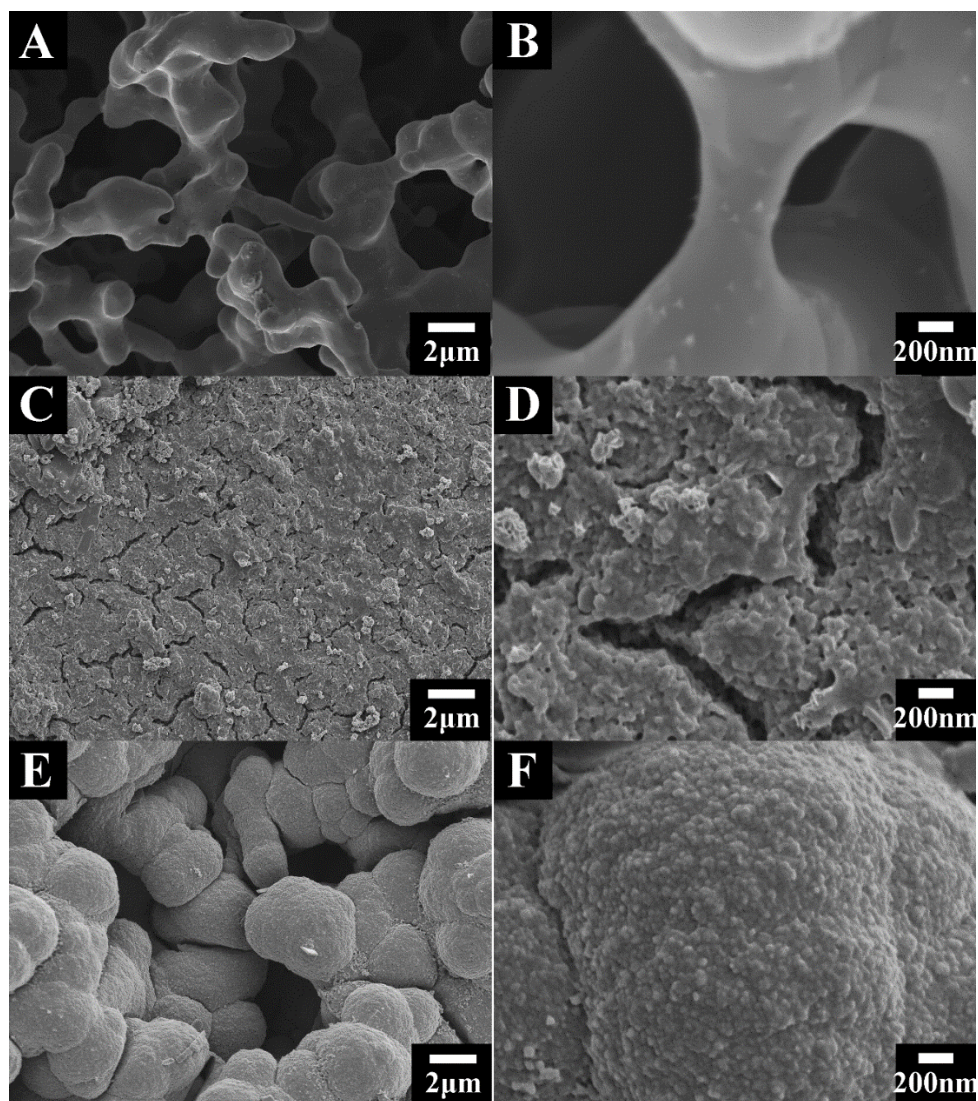


Figure 7.5 SEM images of Ni plaques at different magnifications: (A,B) as-received, (C,D) impregnated with PPy by galvanostatic electropolymerization, (E,F) impregnated with PPy by pulse electropolymerization.

Such pores were beneficial for the ES electrodes, because they allowed for good electrolyte access to the bulk of PPy active material.

7.3 Morphology and capacitive behaviour of PPy synthesized by different methods

The analysis of SEM images at different magnifications for the electrodes, impregnated with chemically polymerized PPy (Fig. 7.6), showed porous microstructures, containing PPy particles with typical size of 100-200 nm. However, such particles formed agglomerates.

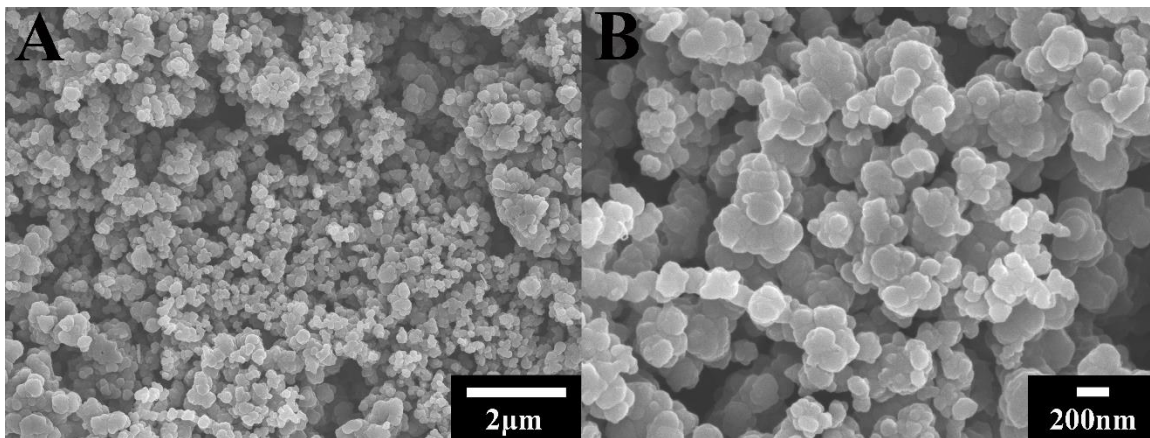


Figure 7.6 (A,B) SEM images at different magnifications of Ni plaques, impregnated with PPy, using slurry of PPy powder, prepared by a chemical polymerization method.

Testing results showed nearly box shape CVs (Fig. 7.7A) for the electrodes, prepared by different methods. The electrodes, prepared by the electrochemical methods showed higher capacitance, compared to the electrodes prepared using PPy powders, prepared by chemical

polymerization (Fig. 7.7B). Pulse electropolymerization allowed for the fabrication of electrodes with higher capacitance and improved capacitance retention at high charge-discharge rates, compared to galvanostatic deposition (Fig. 7.7B). The highest capacitance of 320 F g^{-1} (0.64 F cm^{-2}) was obtained at a scan rate of 2 mV s^{-1} for the PPy electrodes, prepared by pulse electropolymerization. The electrodes showed capacitance retention of 58% at a scan rate of 100 mV s^{-1} .

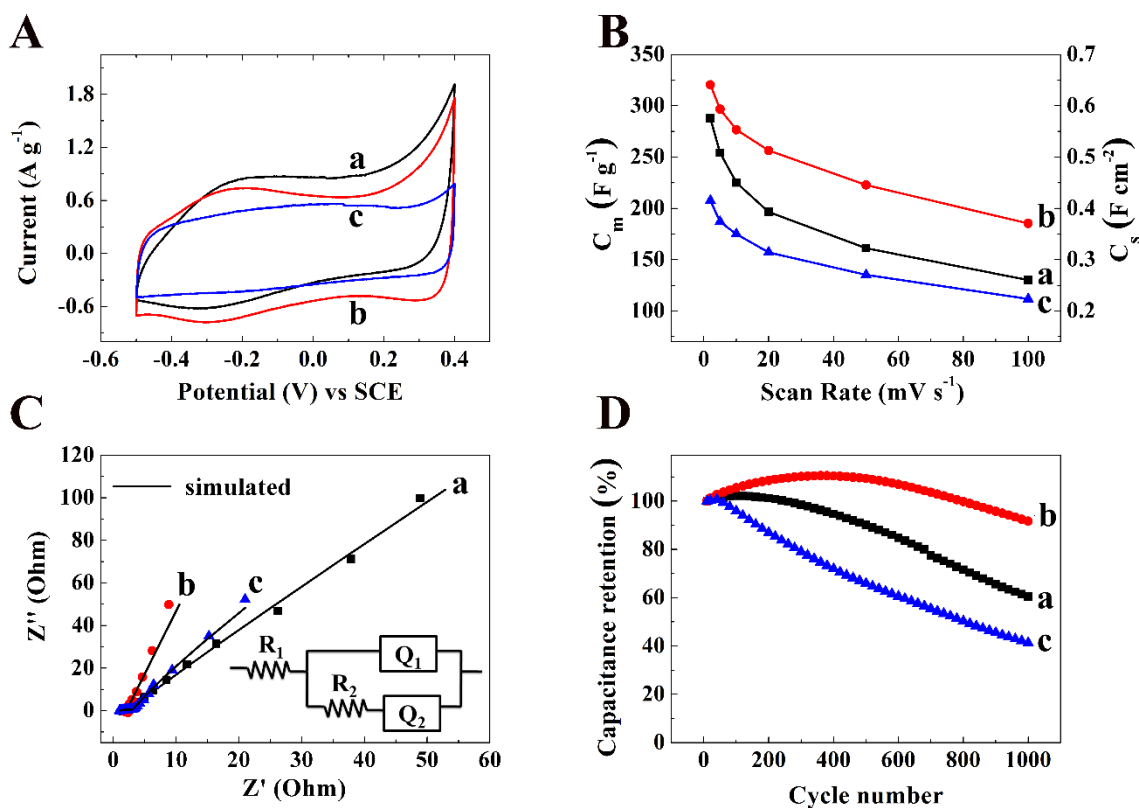


Figure 7.7 (A) CVs at a scan rate of 2 mV s^{-1} , (B) specific capacitance versus scan rate, (C) Nyquist plot of complex impedance, inset shows equivalent circuit used for simulation, (D) capacitance retention versus cycle number at a scan rate of 50 mV s^{-1} for Ni plaque based electrodes, impregnated with PPy: (a) by galvanostatic electropolymerization, (b) by pulse electropolymerization and (c) using slurry of a PPy powder, prepared by chemical polymerization.

The results of impedance measurements presented in the Nyquist plot (Fig. 7.7C) showed that the electrodes, prepared by pulse electropolymerization exhibited lower resistance $R=Z'$, compared to the electrodes prepared using galvanostatic and chemical polymerization methods. The lower resistance can explain higher capacitance of the electrodes prepared by pulse electropolymerization. The results of impedance measurements are in good agreement with the simulation data, obtained using the equivalent circuit shown in Fig. 7.7C(inset). This circuit included electrolyte resistance R_1 and charge transfer resistance R_2 . Constant phase elements Q_1 and Q_2 represent double layer capacitance and pseudocapacitance, respectively. The electrodes, prepared using pulse electropolymerization showed improved cycling stability, compared to the electrodes prepared by galvanostatic polymerization and chemical polymerization (Fig. 7.7D). The increase in capacitance during the first 400 cycles (Fig. 7.7D(b)) can be attributed to morphological changes in PPy layers during cycling, the capacitance retention after 1000 cycles was 92%. The use of Ni plaque current collectors offered the advantage of higher materials loadings, improved electrochemical performance and stability during cycling (Fig. 7.7), compared to Ni foil current collectors (Fig. 7.2).

7.4 Conclusions

PPy electrodes for ES were prepared by galvanostatic electropolymerization, pulse electropolymerization and chemical polymerization methods using PS as an anionic dopant. Pulse electropolymerization allowed improved impregnation of Ni plaque current collectors and formation of nanostructured PPy coatings on individual Ni particles. The

higher porosity and small particle size of PPy electrodes, prepared by pulse electropolymerization and higher electrode porosity allowed for higher capacitance, lower electrical resistance, improved capacitance retention at high charge-discharge rates and improved cycling stability. The use of Ni plaque current collectors allowed for good electrochemical performance at high PPy mass loading. The highest capacitance of 320 F g⁻¹ was achieved at a scan rate of 2 mV s⁻¹.

References

1. Snook, G.A., P. Kao, and A.S. Best, Conducting-polymer-based supercapacitor devices and electrodes. *Journal of Power Sources*, 2011. **196**(1): p. 1-12.
2. Ariyanayagamkumarappa, D.K. and I. Zhitomirsky, Electropolymerization of polypyrrole films on stainless steel substrates for electrodes of electrochemical supercapacitors. *Synthetic Metals*, 2012. **162**(9–10): p. 868-872.
3. Mitchell, G.R., F.J. Davis, and C.H. Legge, The effect of dopant molecules on the molecular order of electrically-conducting films of polypyrrole. *Synthetic Metals*, 1988. **26**(3): p. 247-257.

Chapter 8 Influence of tartrazine and brilliant yellow dopants and new dispersants on performance of polypyrrole–carbon nanotube supercapacitors

8.1 Chemical structures of dopants and dispersants

The chemical structures of polyaromatic tartrazine (TR) and brilliant yellow (BY) molecules are shown in Fig. 8.1. The electrical charge of TR is related to two SO_3^- and CO_2^- ligands, whereas the charge of BY is attributed to two SO_3^- ligands. As pointed out above, the polycharged and polyaromatic anionic molecules are promising for their application as dopants for PPy polymerization. TR and BY (Fig. 8.1) are azo dyes, containing redox active $-\text{N}=\text{N}-$ groups, which can be converted to $-\text{NH}-\text{NH}-$ hydrazo groups[1, 2] in an electrochemical reaction, involving two electrons. The redox-active dopants are of particular interest for the supercapacitor applications because such dopants can make a contribution to the charge storage properties of PPy.

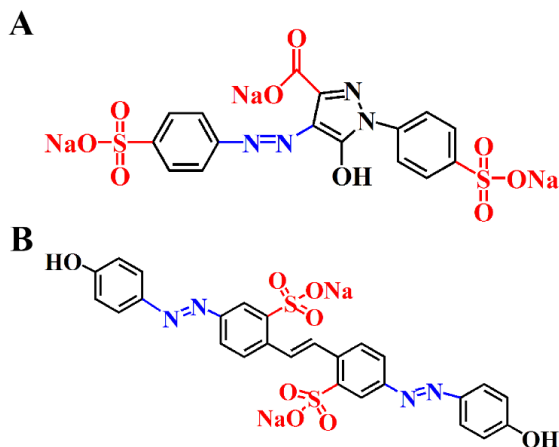


Figure 8.1 Chemical structures of (A) TR and (B) BY dopants.

The structures of dispersants, used in this investigation, are shown in Fig. 8.2. Benzyltrimethylhexadecylammonium chloride (BAC) and sodium dodecyl sulfate (SDS) are long chain surfactants, containing cationic and anionic groups, respectively. The mechanisms of BAC and SDS adsorption on MWCNT are related to hydrophobic interactions between long chain hydrophobic tails of the surfactants and MWCNT. The structure of sodium cholate (SCH) is different from the structure of conventional head-tail surfactants. The SCH structure is characterized by hydrophobic convex and hydrophilic concave surfaces[3]. The hydrophilic surface is created by OH and CO_2^- groups. It is known that anionic SCH molecules wrap around carbon nanotubes in aqueous suspensions to form charged SCH rings[4, 5]. Such mechanism allows for superior carbon nanotube dispersion, compared to head-tail surfactants and other commercial dispersants.

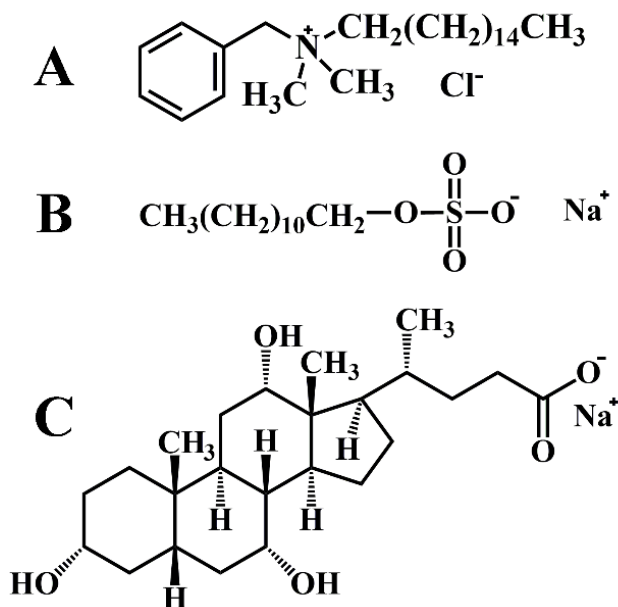


Figure 8.2 Chemical structures of BAC, SDS and SCH dispersants.

8.2 Capacitive performance of PPy doped by TR and BY

Fig. 8.3A compares CVs for PPy electrodes, prepared using TR and BY. The larger area of the CV, obtained using TR dopant indicated higher capacitance. The PPy electrodes, prepared using TR showed nearly ideal box shape CV in 0.9 V voltage window (-0.5 - +0.4 V vs SCE). Similar CVs were observed in 1.1 V voltage window (-0.6 - +0.5 V vs SCE). However, the increase in the voltage window above 0.9 V resulted in reduced capacitance and poor cycling stability. Therefore, further investigations were performed in the optimized 0.9 V window.

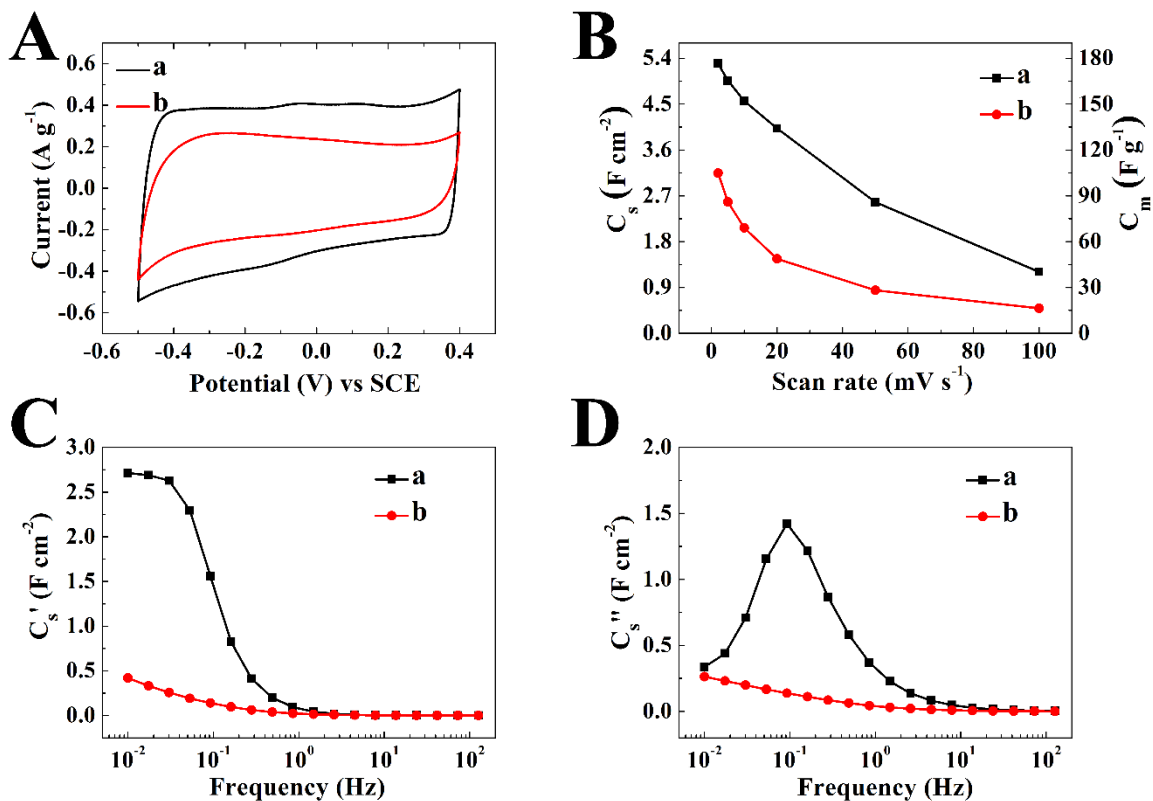


Figure 8.3 (A) CVs at a scan rate of 2 mV s^{-1} , (B) specific capacitance, derived from the CV data, versus scan rate, (C) real and (D) imaginary parts of capacitance, derived from the impedance data, versus frequency for the PPy electrodes with the active mass of 30 mg

cm^{-2} , prepared using (a) TR and (b) BY dopants.

Fig. 8.3B presents capacitances for the PPy electrodes, calculated from the CV data at various charge-discharge rates. The use of TR allowed for significantly higher capacitance of PPy, compared to that, achieved using BY as a dopant. The specific capacitance of the TR doped electrode was 5.3 F cm^{-2} (176.54 F g^{-1}) at a scan rate of 2 mV s^{-1} for mass loading of 30 mV s^{-1} . However, the PPy electrodes showed poor capacitance retention with increasing charge-discharge rate. The capacitance retention of 22.6% was obtained at a scan rate of 100 mV s^{-1} . The CV data provided integral capacitance in a voltage window of 0.9 V. The differential capacitance was derived from the impedance data. The PPy electrodes, prepared using TR showed significantly higher differential capacitance (Fig. 8.3C) at low frequencies, compared to the capacitance of the PPy electrodes, containing BY. The frequency dependence of the capacitance of the PPy electrodes, prepared using TR, showed a dispersion of a relaxation type[6]. Such dispersion is characterized by the decrease in the real part (Fig. 8.3C(a)) of specific capacitance with increasing frequency and corresponding maximum (Fig. 8.3D(a)) in the imaginary part.

The increase in the mass loading resulted in increasing areal capacitance, derived from the CV data, at low scan rates (Fig. 8.4A). The highest capacitance of 6.3 F cm^{-2} was obtained at mass loading of 36 mg cm^{-2} . However, we did not observe an increase in areal capacitance with increasing electrode mass at a scan rate of 100 mV s^{-1} . The gravimetric capacitance (Fig. 8.4B) at 2 mV s^{-1} was practically unchanged with increasing mass loading in the range of $22\text{-}36 \text{ mg cm}^{-2}$. However, it decreased slightly with increasing mass loading at a scan rate of 100 mV s^{-1} . The areal and gravimetric capacitances, derived from the CV

data, decreased with increasing scan rate (Fig. 8.4A, B). The areal capacitance, derived from the impedance data at low frequencies (Fig. 8.4C), increased with increasing electrode mass in the range of 22-36 mg cm^{-2} . However, the capacitance decreased with increasing frequency, showing relaxation type frequency dependence (Fig. 8.4C, D). The analysis of testing results for PPy based electrodes showed poor capacitance retention and low capacitance at high charge-discharge rates. This problem was addressed by the use of PPy-MWCNT composites.

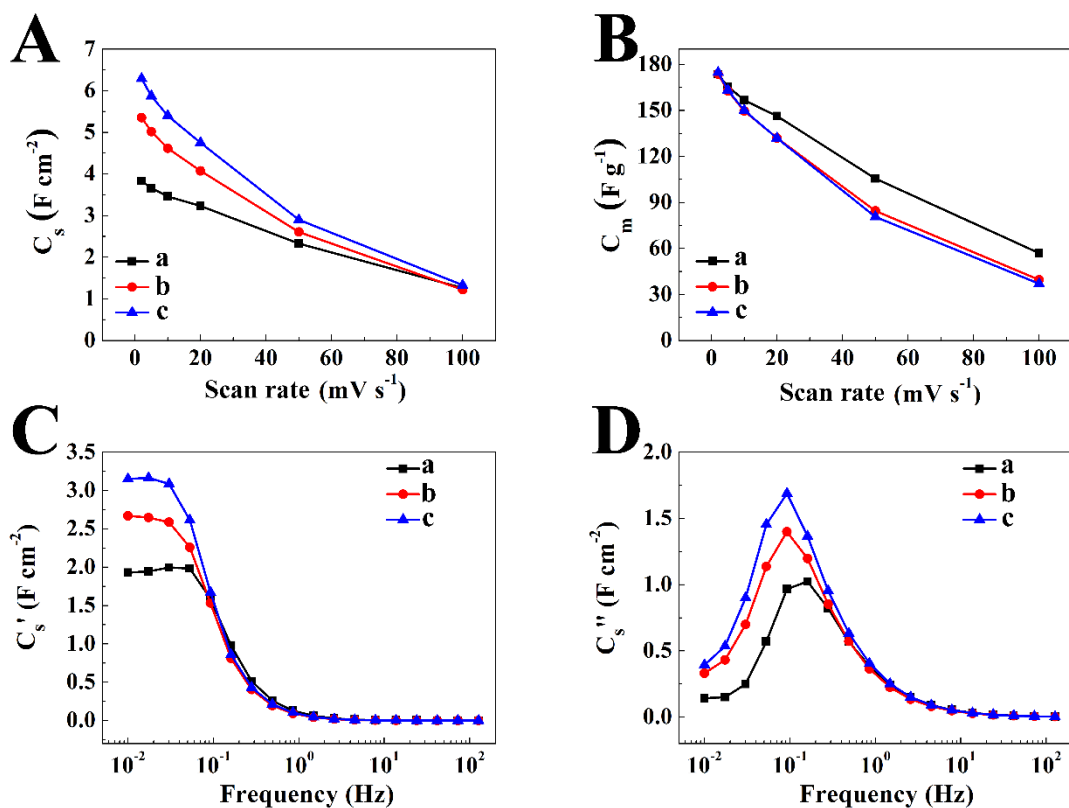


Figure 8.4 (A) Areal and (B) gravimetric capacitances, derived from the CV data versus scan rate and (C) real and (D) imaginary parts of differential capacitances, derived from impedance spectroscopy data, versus scan rate for PP electrodes with mass loadings of (a) 22, (b) 30 and (c) 36 mg cm^{-2} .

8.3 Characterization of PPy-MWCNT composites, prepared using different dispersants

Fig. 8.5A shows CVs at a scan rate of 5 mV s^{-1} for the PPy-MWCNT electrodes, prepared at different conditions. The electrodes, prepared using TR dopant and BAC dispersant showed larger CV area, compared to the electrodes, developed using TR and other dispersants and for the electrodes, prepared using BY and BAC (Fig. 8.5A).

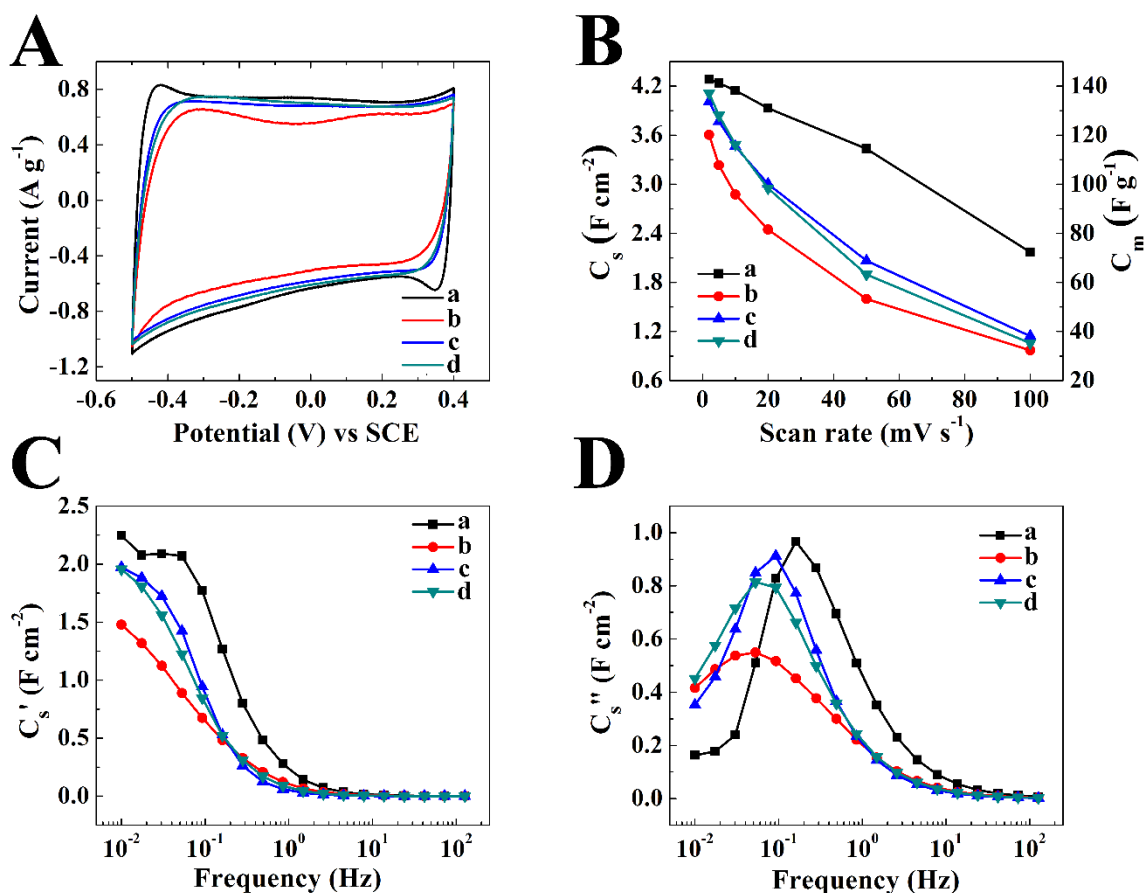


Figure 8.5 (A) CVs at a scan rate of 5 mV s^{-1} , (B) specific capacitance, derived from the CV data, versus scan rate, (C) real and (D) imaginary parts of capacitance, derived from the impedance data, versus frequency for the PPy-MWCNT electrodes with the active mass of 30 mg cm^{-2} , prepared using (a) TR and BAC (b) BY and BAC, (c) TR and SDS, (d) TR

and SCH.

The larger area of the CVs indicated improved capacitance. The PPy-MWCNT electrodes, prepared using TR dopant and BAC dispersant showed higher capacitance, compared to other electrodes (Fig. 8.5B). Such electrodes showed significant improvement in capacitance retention, compared to pure PPy electrodes, prepared using TR. The capacitance retention at 100 mV s^{-1} was found to be 51%. The PPy-MWCNT electrodes showed significantly higher capacitance (72.3 F cm^{-2}) at a scan rate of 100 mV s^{-1} , compared to the capacitance of PPy electrodes (57.0 F cm^{-2}), prepared using TR. The PPy-MWCNT electrodes, fabricated using TR dopant and BAC dispersant showed higher differential capacitance, compared to other electrodes (Fig. 8.5C).

The analysis of the frequency dependencies of components of complex capacitance, presented in Fig. 8.5C,D indicated that such electrodes showed relaxation type dispersion at higher frequencies, compared to other electrodes. The real component of the capacitance showed a decrease at higher frequencies (Fig. 8.5C) and corresponding relaxation maximum also shifted to higher frequencies, indicating improved capacitive properties. The difference in the capacitive behavior of PPy-MWCNT electrodes, prepared using TR and cationic BAC or anionic SDS and SCH, can be attributed to the positive charge of BAC. It is suggested that adsorbed BAC imparted a positive charge to MWCNT. The electrostatic interactions of cationic BAC and anionic dopants promoted MWCNT incorporation in PPy matrix. Such mechanism can result in improved MWCNT dispersion in the PPy matrix and improved electrochemical properties.

Fig. 8.6 shows capacitance retention as a function of a cycle number. The PPy-MWCNT

electrodes, prepared using TR and BAC, and PPy electrodes, prepared using TR, showed capacitance retention of 94.0 % and 78.1%, respectively after 1000 cycles. The increase in capacitance during the first 200-300 cycles can result from the microstructure changes during cycling and other factors discussed in the literature [6].

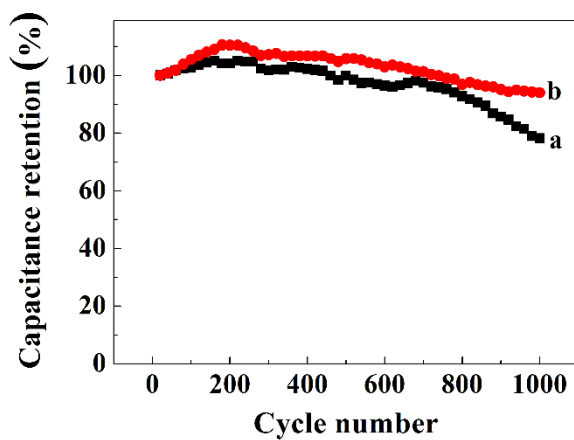


Figure 8.6 Cyclic stability of (a) PPy electrodes, prepared using TR and (b) PPy-MWCNT electrodes, prepared using TR and BAC with mass loading of 30 mA cm^{-2} .

Fig. 8.7 compares microstructures of PPy, prepared using TR and PPy-MWCNT, prepared using TR and BAC. The SEM image of the PPy powder shows agglomerates of PPy particles. The size of such agglomerates was about 200-500 nm. In contrast, the SEM image of the PPy-MWCNT showed a fibrous microstructure, containing PPy coated MWCNT. However, uncoated MWCNT were also observed in the SEM images. The formation mechanism of PPy coated MWCNT involved hydrophobic interactions of PPy and dispersed MWCNT. It allowed improved electrical contact of PPy and conductive MWCNT, which resulted in higher conductivity of the electrodes and higher capacitance.

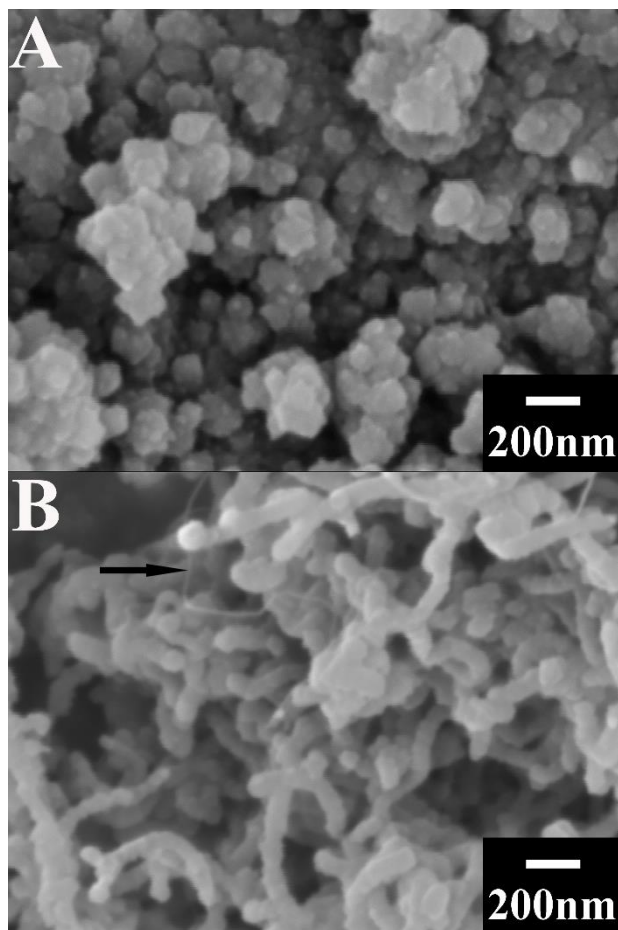


Figure 8.7 SEM images of (A) PPy electrodes, prepared using TR and (B) PPy-MWCNT electrodes, prepared using TR and BAC, arrow shows uncoated MWCNT.

The PPy-MWCNT prepared using TR and BAC were used for the manufacturing of coin cells. Fig. 8.8A shows capacitance, calculated from the cell discharge data at different current densities. The cell capacitance showed small changes in the range of 2-40 mA cm⁻². The charge-discharge curves were of nearly triangular symmetrical shape, indicating good capacitive behavior (Fig. 8.8B) Cycling stability test of the coin cell showed capacitance retention of 88.5% after 1000 cycles (Fig. 8.8C) at a current density of 10 mA cm⁻². The cells were used for powering of LED bulbs (Fig. 8.8D) with a nominal current

density of 20 mA cm^{-2} .

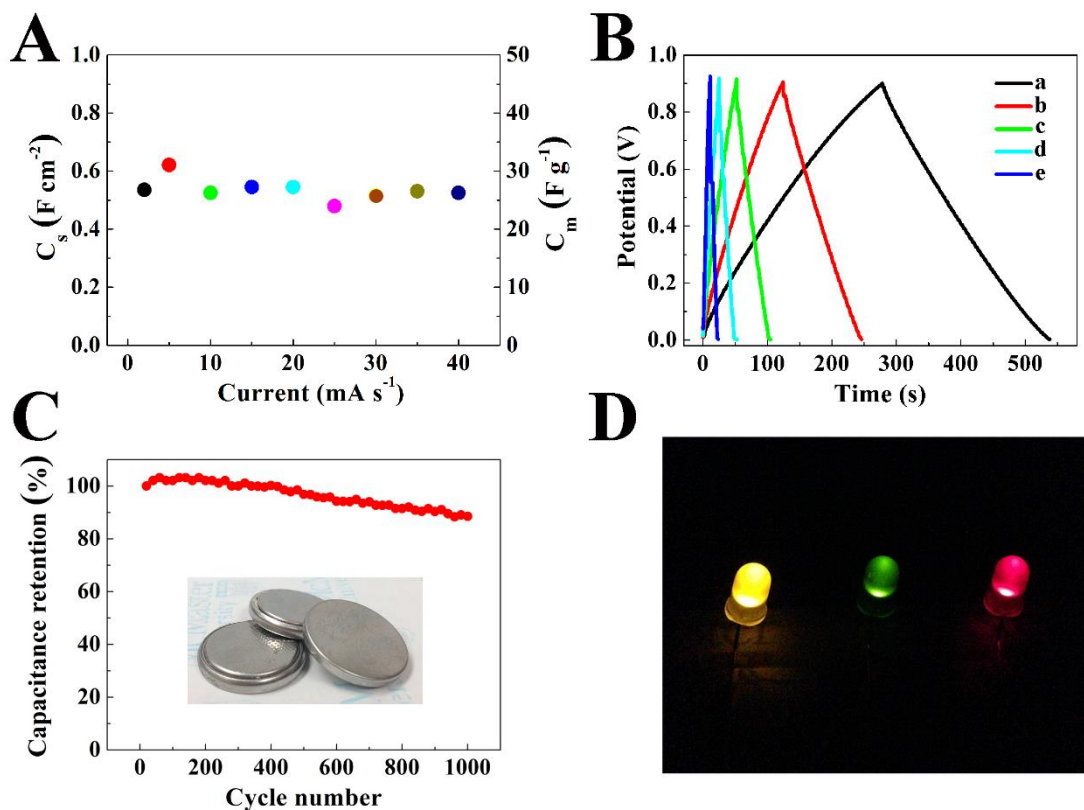


Figure 8.8 (A) Specific capacitance versus discharge current, (B) charge-discharge data at current densities of (a) 2, (b) 5, (c) 10, (d) 20 and (e) 40 mA cm^{-2} , (C) cyclic stability for coin cells, shown in the inset of (C), and (D) LED bulbs powered by the coin cells.

8.4 Conclusions

PPy and PPy-MWCNT composites were fabricated for charge storage application in electrodes of SC, using TR and BY as new dopants for PPy and cationic BAC or anionic SDS and SCH as dispersants for MWCNT. The highest capacitance of 6.3 F cm^{-2} was obtained at 2 mV s^{-1} for 36 mg cm^{-2} PPy electrodes, doped with TR. The use of MWCNT allowed improved capacitance retention of PPy-MWCNT composites at high charge-

discharge rates and improved cyclic stability. Good capacitive behavior was achieved at high active mass loadings using light weight commercial current collectors. New electrode materials were successfully used for the fabrication of SC cells, which showed promising electrochemical performance.

References

1. Jain, R., N. Sharma, and K. Radhapyari, Electrochemical treatment of pharmaceutical azo dye amaranth from waste water. *Journal of Applied Electrochemistry*, 2009. **39**(5): p. 577-582.
2. Dossi, N., et al., Rapid analysis of azo-dyes in food by microchip electrophoresis with electrochemical detection. *Electrophoresis*, 2007. **28**(22): p. 4240-4246.
3. Bogdanova, L.R., et al., Micellization in sodium deoxycholate solutions. *Colloid Journal*, 2012. **74**(1): p. 1-6.
4. Lin, S. and D. Blankschtein, Role of the bile salt surfactant sodium cholate in enhancing the aqueous dispersion stability of single-walled carbon nanotubes: a molecular dynamics simulation study. *The Journal of Physical Chemistry B*, 2010. **114**(47): p. 15616-15625.
5. Wenseleers, W., et al., Efficient isolation and solubilization of pristine single-walled nanotubes in bile salt micelles. *Advanced Functional Materials*, 2004. **14**(11): p. 1105-1112.
6. Shi, K. and I. Zhitomirsky, Influence of current collector on capacitive behavior and cycling stability of Tiron doped polypyrrole electrodes. *Journal of Power Sources*, 2013. **240**(0): p. 42-49.

Chapter 9 Polypyrrole coated carbon nanotubes for supercapacitors, prepared using indigo carmine as a dispersant and dopant

9.1 Morphology study of PPy-MWCNT using indigo carmine

Fig. 9.1A shows a chemical structure of indigo carmine (IC), used in this investigation. The anionic properties of IC are attributed to two SO_3^- groups. The aromatic rings of IC molecules were beneficial for IC adsorption on MWCNT through the π - π electron coupling mechanism [1].

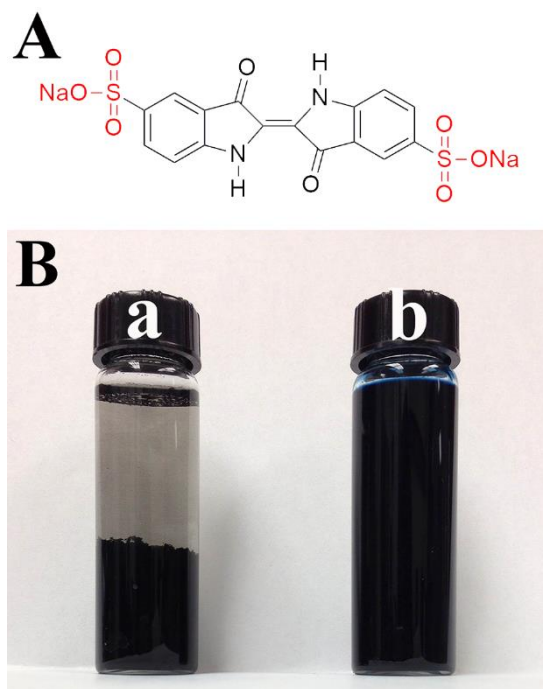


Figure 9.1 (A) Chemical structure of IC, (B) 0.2 g L⁻¹ MWCNT suspensions: (a) without IC and (b) containing 10 mM IC.

Moreover, the analysis of the literature data on adsorption of dyes [1], containing various functional groups, indicated that N-H and C=O groups of IC can enhance the IC adsorption on MWCNT. The anionic IC, adsorbed on the MWCNT surface promoted the formation of stable MWCNT suspensions (Fig. 9.1B), which were of critical importance for the formation of PPy coated MWCNT.

Another important finding was the possibility of the use of IC dye as an anionic dopant for PPy polymerization. Fig. 9.2A shows a scanning electron microscopy (SEM) image of the PPy powder. The powder contained agglomerates, which included primary PPy particles with a typical size of 100 nm. The size of the agglomerates was about 200-400 nm.

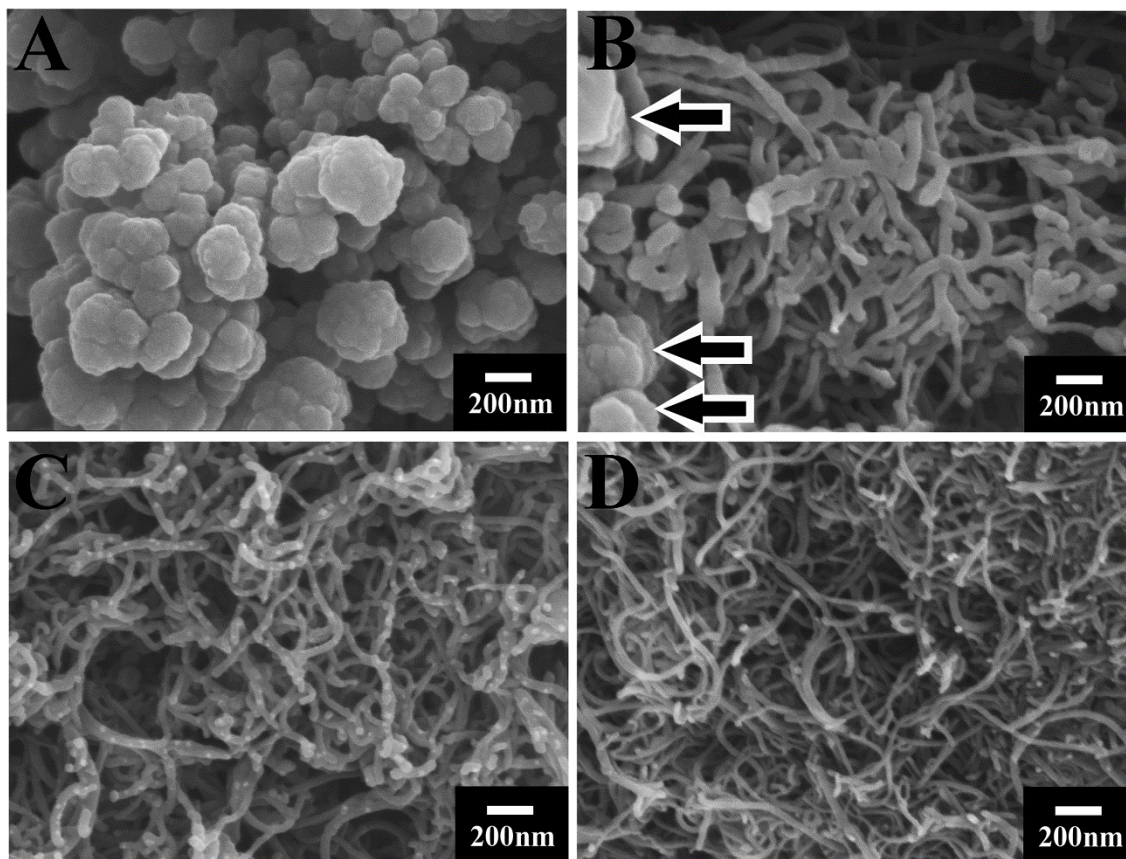


Figure 9.2 SEM images (A) PPy and (B-D) PPy-MWCNTs powders, containing (B) 10 (C) 20 (D) 30% MWCNT. Arrows (B) show PPy particles.

The possibility of MWCNT dispersion and PPy polymerization using IC as a dispersant and dopant paved the way for the fabrication of PPy coated MWCNT. In this approach, MWCNT were dispersed in IC solutions. The adsorbed IC was involved in the polymerization of PPy as an anionic dopant and promoted PPy nucleation and growth on the MWCNT surface (Fig. 9.3).

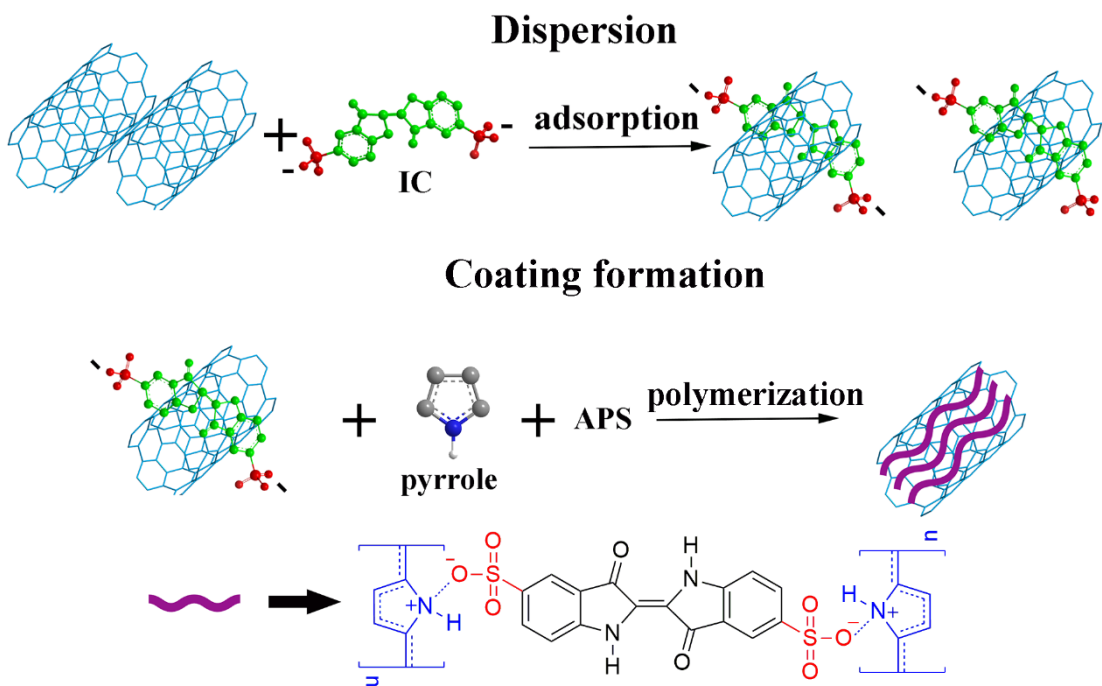


Figure 9.3 Synthesis of PPy-MWCNT composites

SEM studies (Fig. 9.2B,C and D) showed that the morphology of the prepared powders was influenced by MWCNT concentration. The SEM images of the powders, containing 10% MWCNT, showed PPy coated MWCNT and PPy particles. However, the powders, containing 20 or 30% MWCNT, included only coated MWCNT.

9.2 Capacitive behavior of PPy-MWCNT electrodes and devices

The electrodes, containing PPy or PPy coated MWCNT were fabricated and tested for ES applications. Cyclic voltammetry (CV) data (Fig. 9.4A) showed nearly box shapes of CVs at a scan rate of 2 mV s^{-1} , indicating good capacitive behavior. The box shape CV, obtained for pure PPy at materials loadings of 30 mg cm^{-2} (Fig. 9.4A(a)) indicated that IC is a promising dopant material for PPy polymerization. It is in this regard that PPy electrodes, prepared with other dopants, showed significant deviation from the ideal box shape CV even at much smaller active mass loadings [2]. The mass normalized C_m and area normalized C_s capacitances (Fig. 9.4B) were calculated from the CV data.

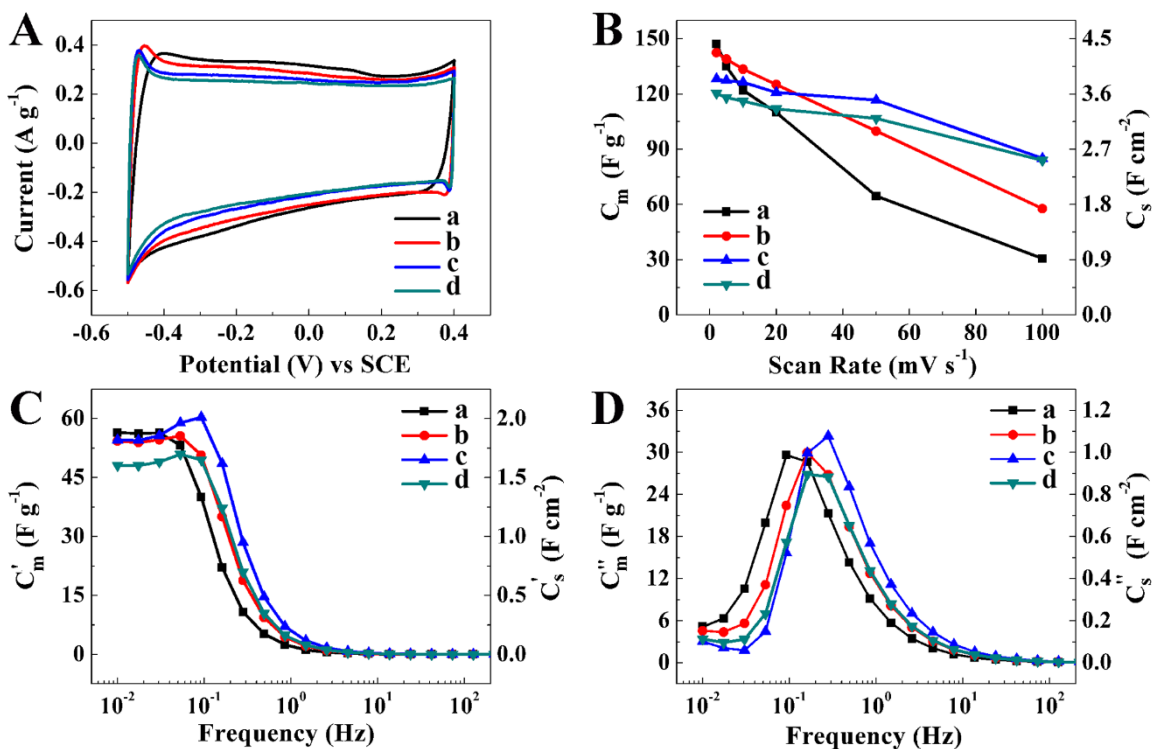


Figure 9.4 (A) CVs at a scan rate of 2 mV s^{-1} , (B) C_s and C_m , calculated from the CV data versus scan rate, (C) C'_s and (D) C''_s , calculated from the impedance data versus frequency

for (a) PPy and (b-d) PPy-MWCNTs electrodes, containing (b) 10, (c) 20 (d) 30% MWCNT for electrode mass of 30 mg cm^{-2} .

The PPy electrodes with active mass loading of 30 mg cm^{-2} showed a capacitance of 147.24 F g^{-1} (4.41 F cm^{-2}) at a scan rate of 2 mV s^{-1} . However, the capacitance decreased with increasing scan rate to the level of 30.65 F g^{-1} (0.92 F cm^{-2}) at a scan rate of 100 mV s^{-1} . The capacitance retention in the range of 2-100 mV s^{-1} was 20.8%. PPy-10%MWCNT electrodes showed capacitances 142.49 F g^{-1} (4.27 F cm^{-2}) and 57.74 F g^{-1} (1.73 F cm^{-2}) at scan rates of 2 and 100 mV s^{-1} , respectively, and capacitance retention was 40.5%. The lower capacitance of PPy-10%MWCNT electrodes, compared to pure PPy electrodes at 2 mV s^{-1} , was attributed to lower capacitance of MWCNT, compared to the capacitance of PPy. However, due to the improved conductivity and changes in microstructure, the PPy-10%MWCNT electrodes showed improved capacitance retention. The capacitance of PPy-20%MWCNT electrodes at 2 mV s^{-1} was found to be 128.18 F g^{-1} (3.85 F cm^{-2}). However, the PPy-20%MWCNT electrodes showed excellent capacitance retention of 66.4% and remarkably high capacitance of 85.05 F g^{-1} (2.55 F cm^{-2}) at a scan rate of 100 mV s^{-1} . The PPy-30%MWCNT electrodes showed lower capacitance, compared to that of PPy-20%MWCNT electrodes at scan rates in the range of 2-100 mV s^{-1} .

The presented C_m and C_s data indicated that PPy-20%MWCNT electrodes are promising for the development of efficient ES devices. The capacitive properties of materials are usually presented in the literature as C_m data. Recent studies [3] highlighted the importance of the fabrication of ES electrodes with high mass loading. It was shown that high C_m can be achieved for thin films with relatively low mass. However, the increase in material

loading usually results in increased resistance, limited electrolyte access to the bulk of active material and reduced capacitance. In this case the ES electrodes do not benefit from the increasing mass of the active material. The high C_s and C_m of the PPy-20%MWCNT, achieved at materials loading of 30 mg cm^{-2} , indicated good active material utilization.

Fig. 9.4D,C shows frequency dependences of components of complex capacitance $C^*=C'-iC''$, calculated from the AC impedance. The capacitance dependences showed typical relaxation type dispersions, as indicated by the decreasing C' and corresponding maxima in the frequency dependences of C'' . The PPy coated MWCNT showed dispersion at higher frequencies, compared to the pure PPy electrodes, indicating improved performance at higher charge-discharge rates.

Fig. 9.5A compares cycling behavior and columbic efficiency of PPy and PPy-20% MWCNT electrodes, measured in a three-electrode circuit at a scan rate of 50 mV s^{-1} . The capacitance of pure PPy after 1000 cycles was only 73% of the initial value. In contrast, the PPy-20% MWCNT electrodes did not show capacitance reduction after 1000 cycles.

The PPy-20% MWCNT electrodes were used for the fabrication of coin cells. Nearly linear charge-discharge behavior (Fig. 9.5B) at different currents was observed. The capacitance, measured at different currents (Fig. 9.5C) for the coin cells was varied in the range of 29-36 F g^{-1} . The coin cells showed good cycling stability and high columbic efficiency (Fig. 9.5D) measured at a charge-discharge current of 10 mA.

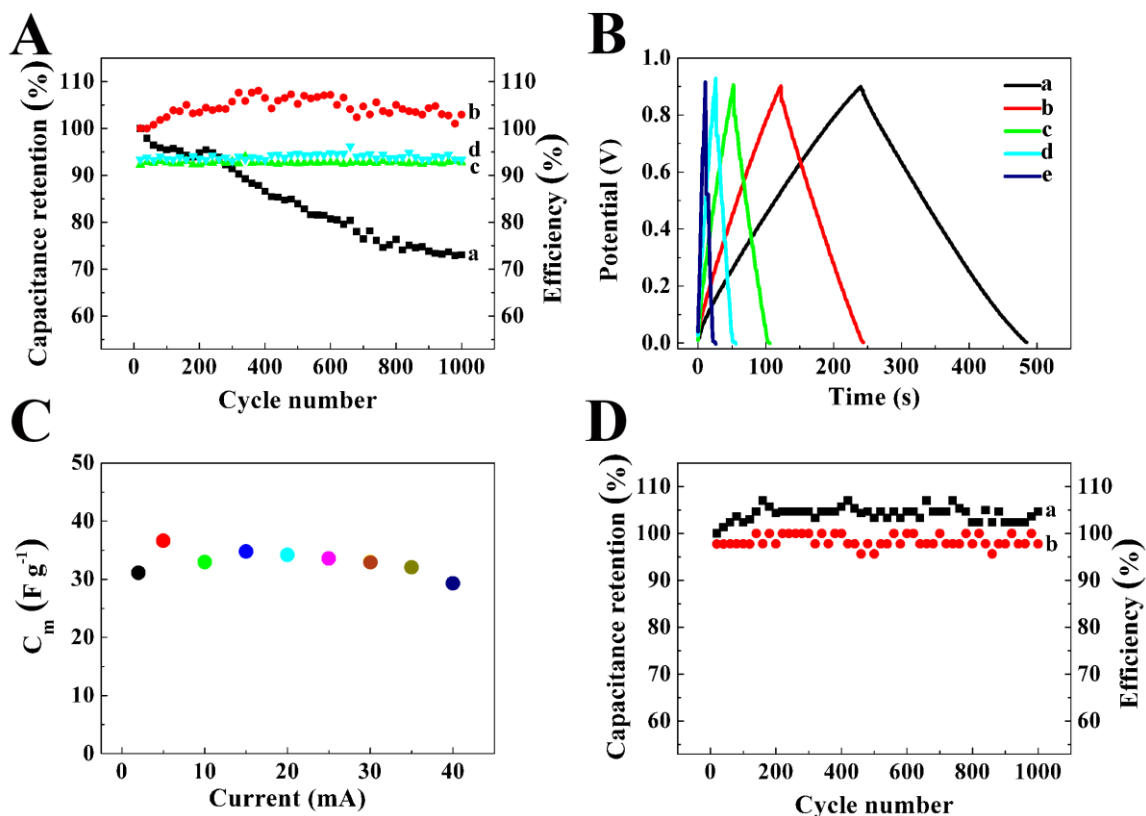


Figure 9.5 (A) Capacitance retention versus cycle number for (a) PPy and (b) PPy-20%MWCNT electrodes, with electrode mass of 30 mg cm^{-2} , (B) charge-discharge curves for two electrode PPy-20%MWCNT coin cell at currents of (a) 2, (b) 5, (c) 10, (d) 20 and (e) 40 mA, (C) C_m versus current for the coin cells, inset shows coin cells, (D) capacitance retention of a coin cell versus cycle number, inset shows LED bulbs powered by the coin cells.

9.3 Conclusions

PPy coated MWCNT were prepared by a novel approach, based on the use of IC as a dopant for PPy polymerization and a dispersant for MWCNT. The method is simple and suitable for mass production. The ES electrodes and devices showed high capacitance, good

capacitance retention and good cycling stability at high mass loadings. The ES electrodes showed a record high capacitance $C_s=2.55 \text{ F cm}^{-2}$ at a scan rate of 100 mV s^{-1} .

References

1. Gupta, V.K., et al., Adsorptive removal of dyes from aqueous solution onto carbon nanotubes: A review. *Advances in Colloid and Interface Science*, 2013. **193-194**(0): p. 24-34.
2. Shi, C. and I. Zhitomirsky, Electrodeposition of composite polypyrrole-carbon nanotube films. *Surface Engineering*, 2011. **27**(9): p. 655-661.
3. Gogotsi, Y. and P. Simon, True performance metrics in electrochemical energy storage. *Science*, 2011. **334**(6058): p. 917-918.

Chapter 10 Influence of multifunctional dopants on capacitive behavior of polypyrrole-carbon nanotube ECs

10.1 Chemical structures of multifunctional dopants

Fig. 10.1A-D shows the chemical structures of sodium benzene-1, 3-disulfonate (SB), 1, 3, (6, 7)-naphthalenetrisulfonic acid trisodium salt hydrate (NAT), potassium indigotrisulfonate (TRI) and potassium indigotetrasulfonate (TETRA) which are used in this investigation. Those dopants have different number of SO_3^- groups which related to their anionic properties. Such polycharged and polyaromatic molecules have potential to benefit the chemical polymerization of PPy with good electrochemical properties[1, 2].

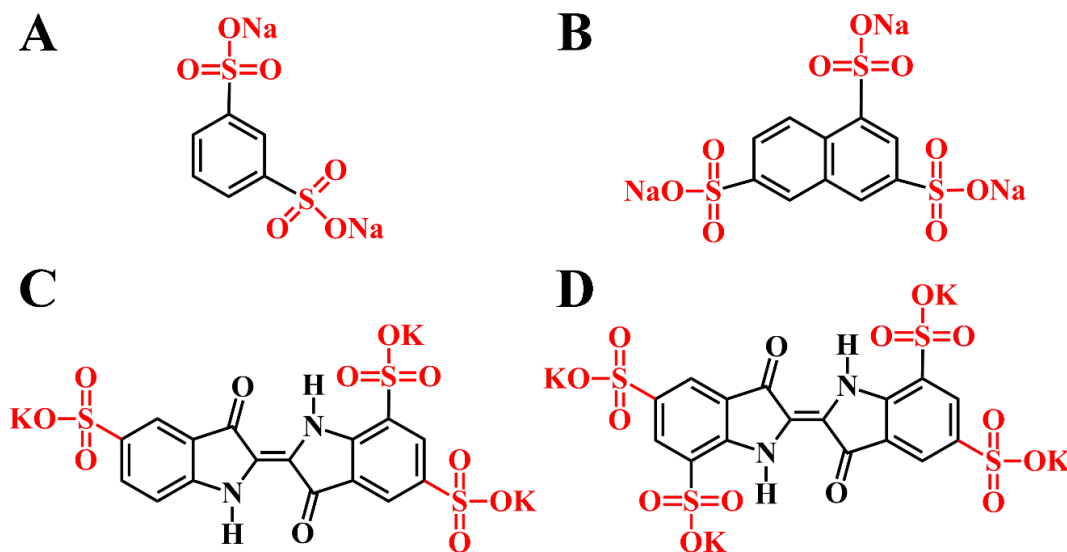


Figure 10.1 Chemical structures of different dopants (a) SB, (b) NAT, (c) TRI and (d) TETRA

The aromatic rings of those dopants can also promote their adsorption on MWCNT due to the π - π interaction[3]. According to literature, dopants containing N-H and C=O groups

can improve their adsorption on MWCNT and allow the formation of stable MWCNT suspension[3], which play a very important role in the fabrication of PPy coated MWCNT.

10.2 Capacitive performance of PPy and PPy-MWCNT

Fig 10.2 compares the capacitive performance of PPy and PPy-MWCNT electrodes using SB and NAT. All of them show box shape CV in the 0.9 voltage window (-0.5- +0.4 V vs SCE). However, compared to pure PPy electrodes, PPy-MWCNT electrodes present much smaller CV area at low scan rates, which indicates much lower capacitance.

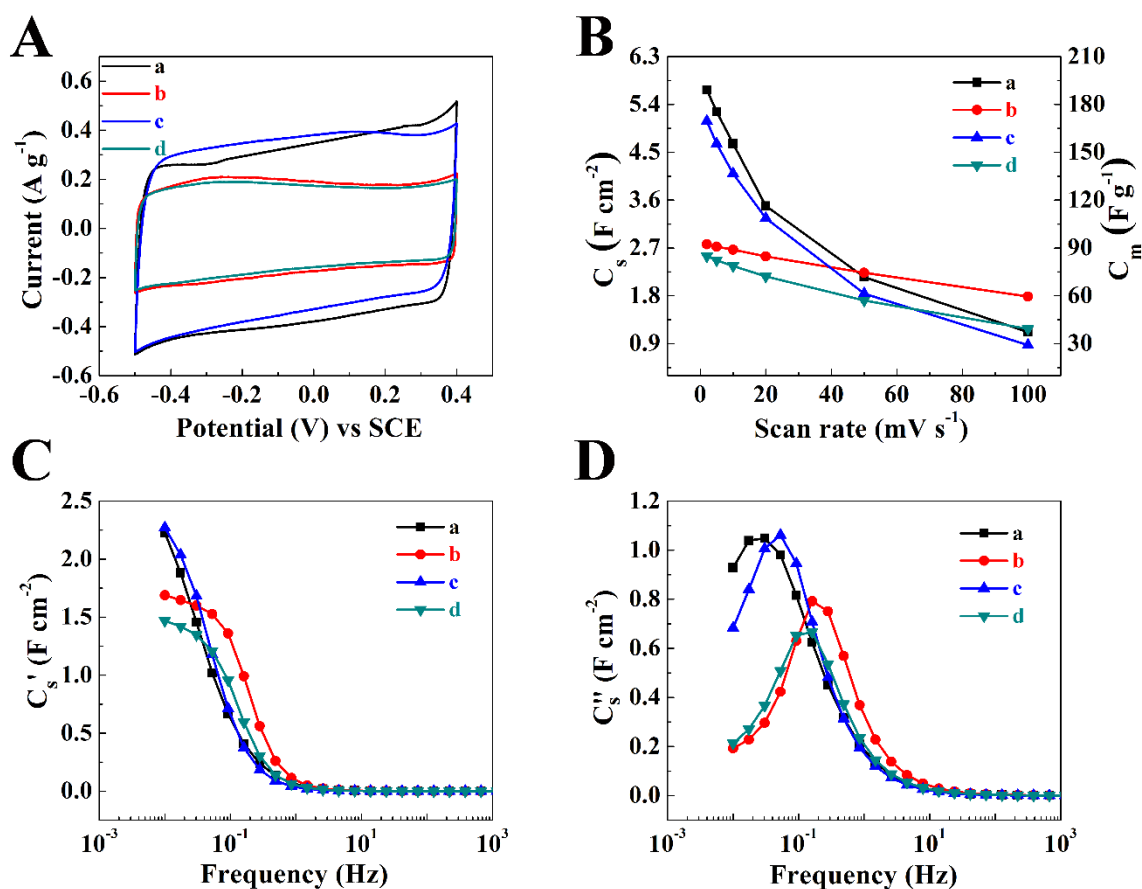


Figure 10.2 (A) CVs at a scan rate of 2 mV s⁻¹, (B) C_m and C_s calculated from the CV data versus scan rate, (C) C_s' and (D) C_s'' calculated from the impedance data versus frequency

for PPy electrodes with the active mass loading of 30 mg cm^{-2} , prepared using (a) SB, (b) SB with 20% MWCNT, (c) NAT and (d) NAT with 20% MWCNT.

In fig. 10.2B, C_s and C_m which are calculated from CVs data are presented. It is indicated that, pure PPy electrode doped by SB exhibits very high specific capacitance which is 189.1 F g^{-1} (5.67 F cm^{-2}) at scan rate of 2 mV s^{-1} . However, their capacitance decrease significantly as scan rate increased. At high scan rate of 100 mV s^{-1} only 19.7% capacitance retained. PPy-MWCNT electrodes improved capacitance retention at high charge-discharge rates. The results indicate that, although PPy-MWCNT prepared by SB shows better retention of nearly 65% at high scan rate, its capacitance is too low for application. It is implied that most of capacitance of such PPy-MWCNT electrodes comes from the CNT instead of PPy.

Fig. 10.2CD shows frequency dependences of components of complex capacitance, derived from the impedance data. The real part of the specific capacitance decreased with increasing frequency and corresponding maxima in the imaginary part were observed. Such capacitance dependences correspond to typical relaxation type dispersion[4]. Compared to pure PPy electrode, PPy-MWCNT electrode showed dispersion at higher frequencies, which indicates improved capacitive performance at higher charge-discharge rates.

Fig. 10.3 compares the capacitive behavior of PPy and PPy-MWCNT doped by TRI and TETRA. There's no significant difference of CV curves between electrodes doped by the two dopants. However, compare to pure PPy electrodes, PPy-MWCNT electrodes show nearly box shapes of CVs at scan rate of 2 mV s^{-1} indicating good capacitive behavior. The mass normalized C_m and area normalized C_s capacitance of PPy and PPy-MWCNT are

shown in Fig. 10.3B. Although pure PPy electrode doped by TETRA exhibit high capacitance of 179.88 F g^{-1} (5.4 F cm^{-2}) at low scan rate, the capacitance decreased with increasing scan rate to the level of 22.48 F g^{-1} (0.67 F cm^{-2}) at a scan rate of 100 mV s^{-1} . Therefore, the capacitance retention in the range of $2\text{-}100 \text{ mV s}^{-1}$ was only 12.5%. On the contrary, the PPy-MWCNT doped by TETRA, exhibited lower capacitance at 2 mV s^{-1} and showed excellent retention at high charge-discharge rates. The retained capacitance is 88.99 F g^{-1} (2.67 F cm^{-2}) at 100 mV s^{-1} indicating a 67% capacitance retention in the range of $2\text{-}100 \text{ mV s}^{-1}$. The lower capacitance of PPy-MWCNT electrodes at low scan rates compared to pure PPy electrodes was attributed to lower capacitance of CNT compared to the capacitance of PPy.

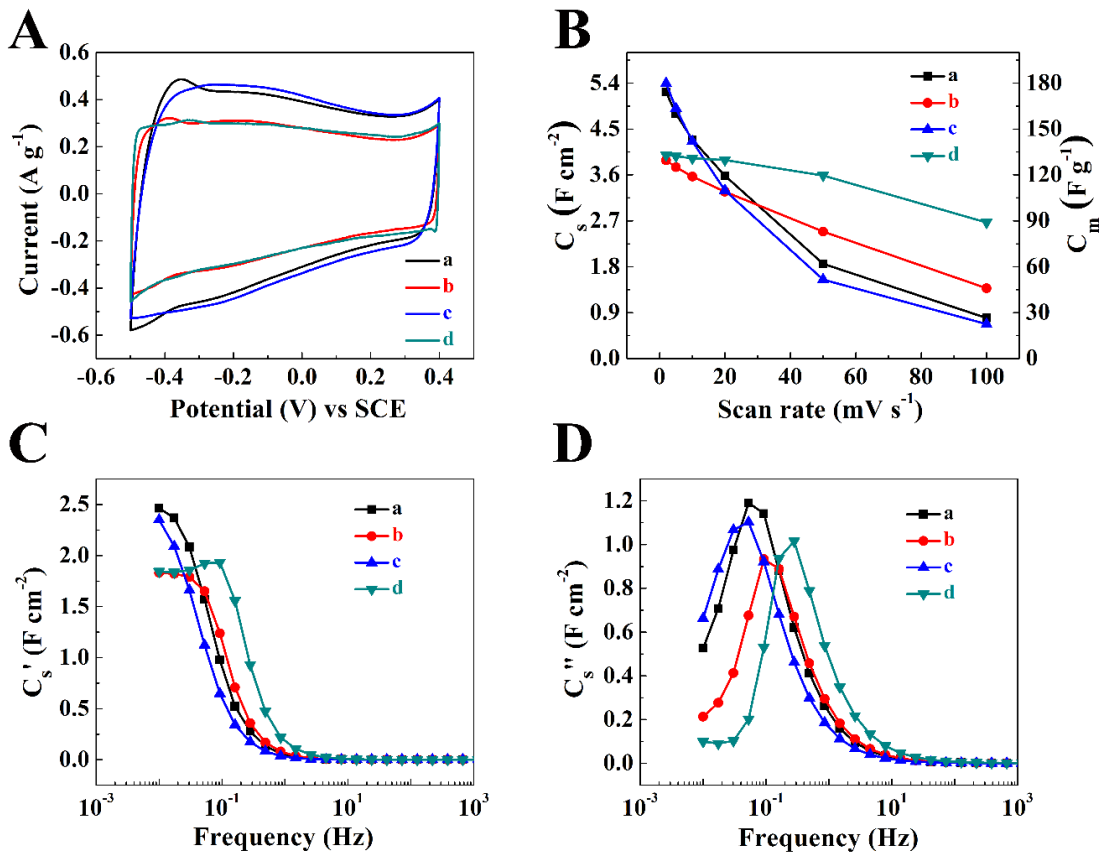


Figure 10.3 (A) CVs at a scan rate of 2 mV s^{-1} , (B) C_m and C_s calculated from the CV data versus scan rate, (C) C_s' and (D) C_s'' calculated from the impedance data versus frequency for PPy electrodes with the active mass of 30 mg cm^{-2} , prepared using (a) TRI, (b) TRI with 20% MWCNT, (c) TETRA and (d) TETRA with 20% MWCNT.

It is indicated that among those different dopants TETRA is the most promising dopant material for fabrication of PPy-MWCNT electrodes for the development of efficient EC devices. According to recent studies, the importance of the fabrication of EC electrode with high mass loading is emphasized.[5] Normally, high C_m can only be achieved for thin film electrode which has relatively low mass loading. And the increase in mass loading for such electrode usually results in the increase of resistance and reduced capacitance. The high C_m and C_s of the PPy-MWCNT doped by TETRA achieved at materials loading of 30 mg cm^{-2} at different charge-discharge rate indicated good active material utilization.

Fig. 10.3CD shows the differential capacitance derived from the impedance data. The results also show typical relaxation type dispersion[4]. The real part of the specific capacitance decreased with increasing frequency and corresponding maxima in the imaginary part were observed. Among those electrodes, PPy-MWCNT doped by TETRA showed dispersion at higher frequencies, as indicated by the real part capacitance decrease at higher frequency and corresponding relaxation maxima also shifted to higher frequency. Such result indicates that PPy-MWCNT doped by TETRA electrode exhibits improved capacitive performance at higher charge-discharge rate and is promising electrode materials for ECs.

The cycling behaviors of PPy and PPy-MWCNT doped by different dopants were compared in fig. 10.4. The pure PPy electrode showed continuous reduction in capacitance,

even the best one only has 85% of the initial value retained after 1000 cycles. In contrast, the PPy-MWCNT electrodes did not show capacitance reduction after 1000 cycles. The results indicated that cyclic stability problem limiting application of PPy in EC can be addressed by the formation of PPy-MWCNT electrodes. The use of TETRA allowed the fabrication of fine PPy particles and was beneficial for the synthesis of PPy-MWCNT electrodes with high capacitance and good cycling stability.

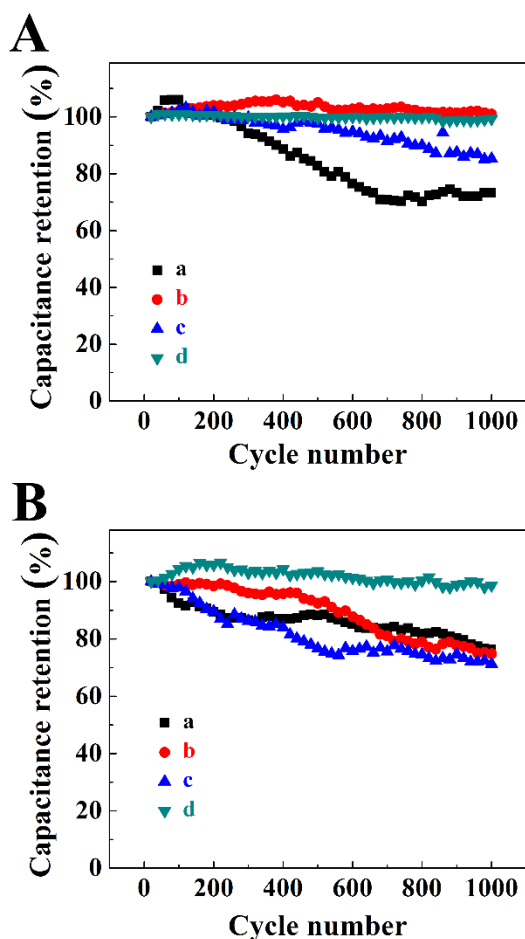


Figure 10.4 (A) Capacitance retention versus cycle numbers for (a) PPy doped by SB, (b) PPy-MWCNT doped by SB, (c) PPy doped by NAT and (d) PPy-MWCNT doped by NAT, (B) Capacitance retention versus cycle numbers for (a) PPy doped by TRI, (b) PPy-

MWCNT doped by TRI, (c) PPy doped by TETRA and (d) PPy-MWCNT doped by TETRA.

10.3 Morphology study of PPy and PPy-MWCNT

Fig. 10.4 shows scanning electron microscopy (SEM) images of PPy powders fabricated using SB (Fig. 10.5AB) and NAT (Fig. 10.5CD) as dopants. Typically, particle size of those powders is less than 200 nm. However, some of those particles formed agglomerates and result in larger size. Compare to PPy powders prepared by SB, PPy powder fabricated using NAT shows a microstructure with higher porosity and smaller particle size.

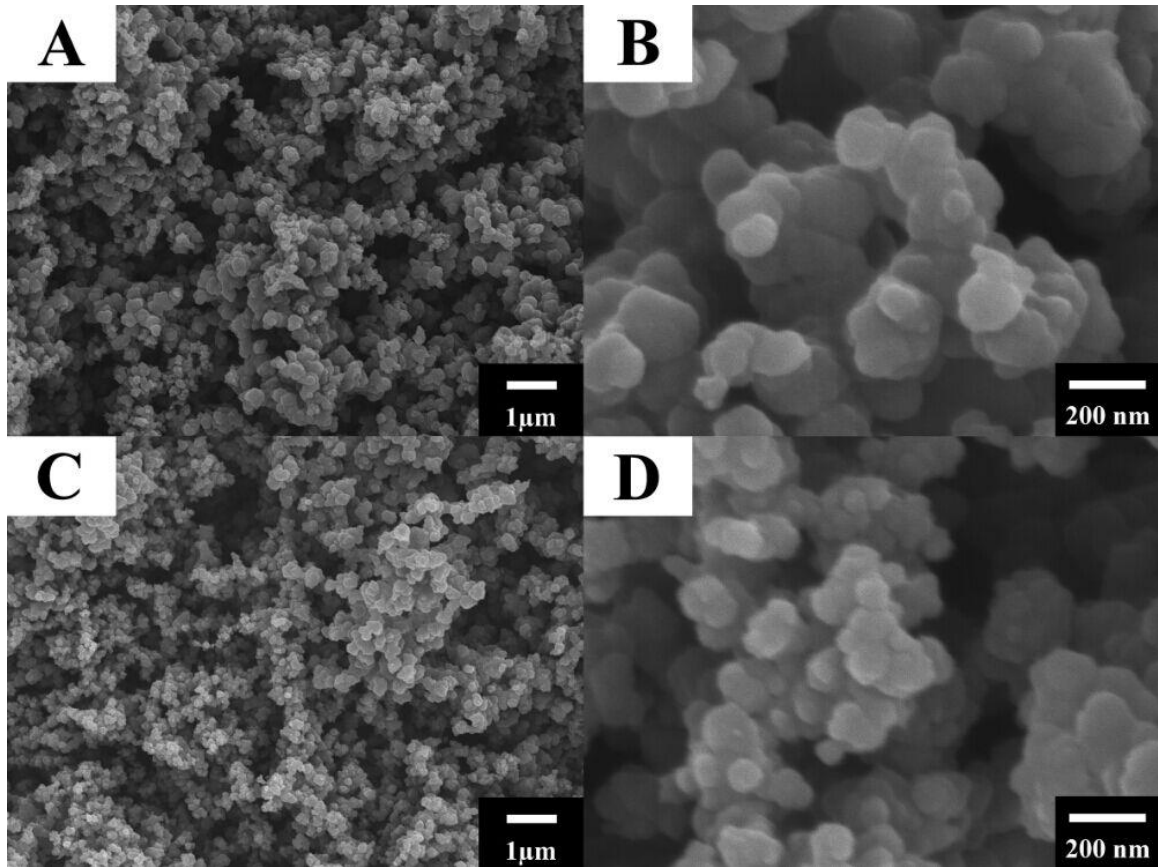


Figure 10.5 SEM image of polypyrrole powders (a) (b) doped by SB (c) (d) doped by NAT

The microstructures of PPy prepared using TRI and TETRA as dopants are shown in fig. 10.6. It is indicated that PPy powders with much smaller particle size which is less than 100 nm were successfully synthesized. Compare to TRI (fig. 10.6AB), TETRA (fig. 10.6CD) can help to reduce the particle size of PPy powders further. The significant difference of particle size of PPy prepared by different dopants can be attributed to different number of carbon rings and different number of SO_3^- groups. The PPy powders with smaller particle size can not only improve the surface area of electrode materials, but also benefit the formation of PPy coated MWCNT electrodes.

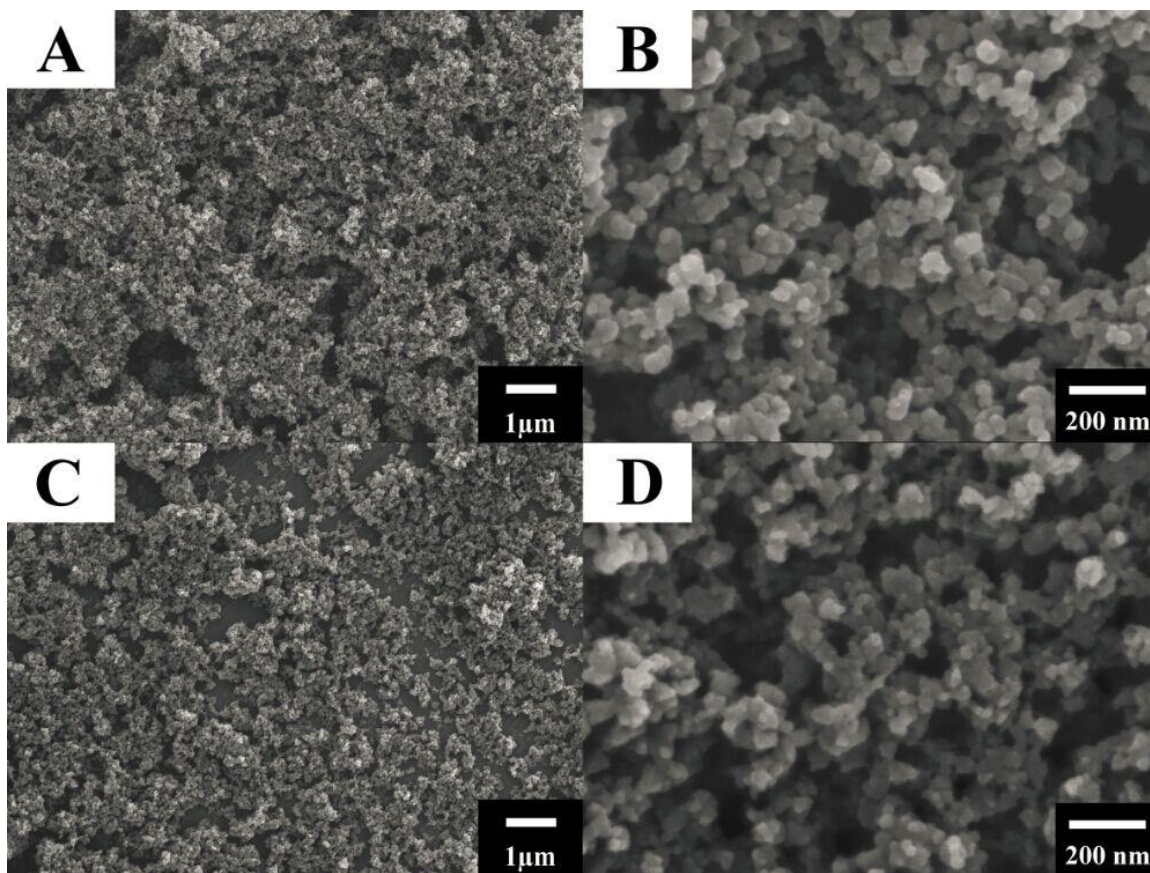


Figure 10.6 SEM images at different magnifications of PPy powders (a, b) doped by TRI and (c, d) doped by TETRA.

The microstructures of PPy-MWCNT doped by SB and TETRA are compared in fig. 10.7. The PPy-MWCNT powder doped by SB shows a simple mixture of PPy particles and carbon nanotubes. In contrast, the SEM image of PPy-MWCNT powder doped by TETRA indicates that the PPy have grown on the surface of carbon nanotubes and formed PPy coated MWCNT fibers. This microstructure allows improved electrical contact of PPy and conductive MWCNT, which results in higher conductivity of the electrodes and higher capacitance. The formation of such microstructure can be attributed to the using of TETRA as dispersant and dopant.

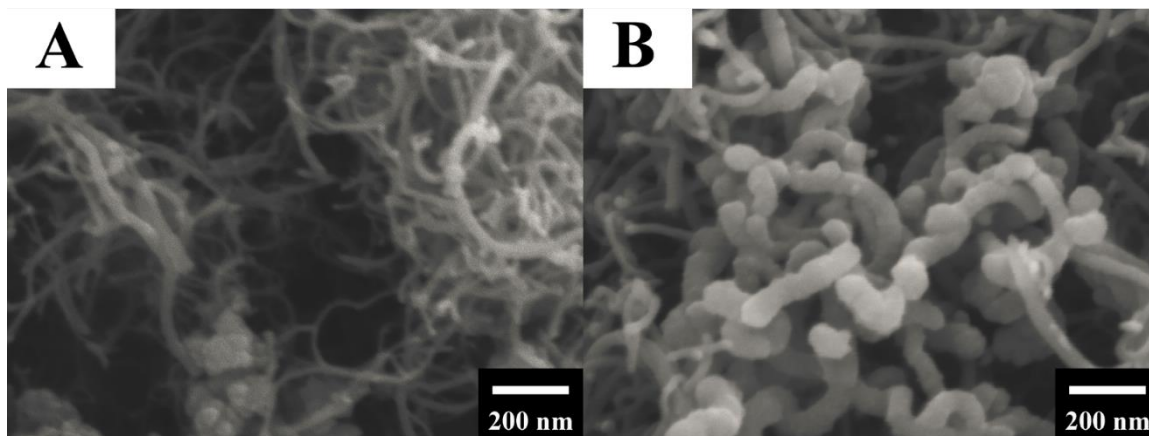


Figure 10.7 SEM image of PPy-MWCNT (a) doped by SB and (b) doped by TETRA

The PPy-MWCNT prepared using TETRA was used for the manufacturing of coin cells. Fig. 10.8A shows capacitance calculated from the cell discharge data at different current densities. The cell capacitances show small changes, varied from 35.18 to 30.86 F g⁻¹ in the range of 2-40 mA cm⁻². Nearly triangular symmetrical shape charge-discharge curves are obtained, indicating good capacitive behavior of cells (Fig. 10.8B). The corresponding Ragone plot indicates that high power and energy densities can be achieved using such cell

devices (Fig.10.8C). Cycling stability test of the coin cell showed capacitance retention of 90.47% after 1000 cycles (Fig. 10.8D) at a current density of 20 mA cm⁻².

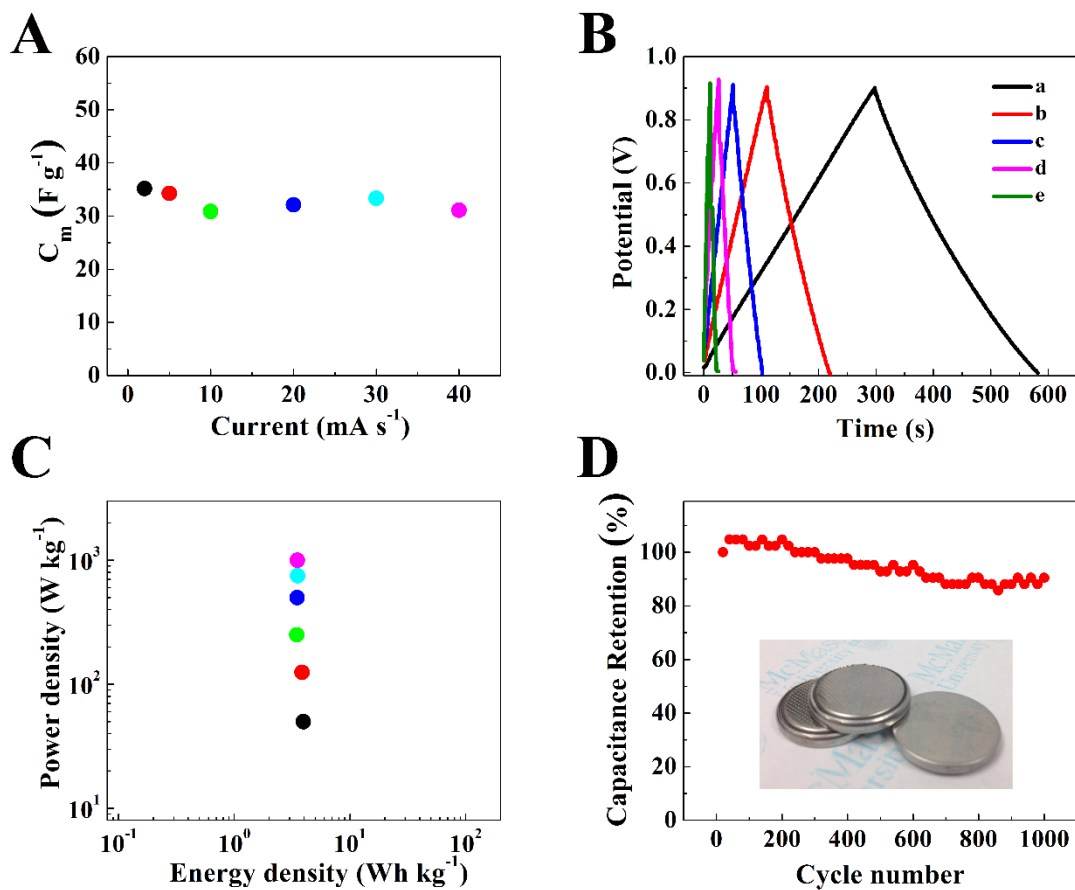


Figure 10.8 (A) Specific capacitance versus discharge current, (B) charge-discharge data at current densities of (a) 2, (b) 5, (c) 10, (d) 20 and (e) 40 mA, (C) ragone plot, (D) cyclic stability for coin cells

10.4 Conclusions

PPy and PPy-MWCNT materials were fabricated for energy storage application in electrodes of EC. SB, NAT, TRI and TETRA were used as anionic dopants for PPy polymerization and dispersants for carbon nanotubes. The highest capacitance of 189.1 F

g^{-1} (5.67 F cm^{-2}) was obtained at 2 mV s^{-1} for 30 mg cm^{-2} pure PPy electrodes, doped with SB. The use of MWCNT allowed for improved capacitance retention of PPy-MWCNT composites at high charge-discharge rates and improved cyclic stability, which was beneficial for their application in EC. The electrode made of PPy-MWCNT doped by TETRA showed the best capacitance retention and good cycling stability. A record of high capacitance 2.67 F cm^{-2} at a scan rate of 100 mV s^{-1} and nearly 100% capacitance retention after 1000 cycles were obtained.

References

1. Wang, P.-C. and J.-Y. Yu, Dopant-dependent variation in the distribution of polarons and bipolarons as charge-carriers in polypyrrole thin films synthesized by oxidative chemical polymerization. *Reactive and Functional Polymers*, 2012. **72**(5): p. 311-316.
2. Lang, X., et al., The role of anthraquinone sulfonate dopants in promoting performance of polypyrrole composites as pseudo-capacitive electrode materials. *Synthetic Metals*, 2010. **160**(15–16): p. 1800-1804.
3. Gupta, V.K., et al., Adsorptive removal of dyes from aqueous solution onto carbon nanotubes: A review. *Advances in Colloid and Interface Science*, 2013. **193–194**(0): p. 24-34.
4. Shi, K. and I. Zhitomirsky, Influence of current collector on capacitive behavior and cycling stability of Tiron doped polypyrrole electrodes. *Journal of Power Sources*, 2013. **240**(0): p. 42-49.
5. Gogotsi, Y. and P. Simon, True performance metrics in electrochemical energy storage. *Science*, 2011. **334**(6058): p. 917-918.

Conclusion

In this work, different aromatic dopants and surfactants were investigated in order to synthesis PPy and PPy-CNTs electrodes with high materials loading, high capacitance and improved cyclic stability. A series of experiments were done to study the influence of dopants and surfactants on the electrochemical properties and capacitance behavior of PPy and PPy-CNTs electrodes. The conclusion can be drawn as follows:

1. Aromatic dopants from catechol, salicylic acid and chromotropic acid families can provide complexation of metal atoms on the substrate surface and allowed strong adhesion of PPy films on non-noble metals. Using such dopants can also reduce electropolymerization potential and prevent dissolution of non-noble metal substrates.
2. Aromatic dopants with high charge/volume ratio can help to fabricate PPy electrode with enhanced electrical conductivity. Polyaromatic dopants can help to improve the cyclic stability of PPy electrode.
3. PPy electrodes with high materials loading and improved capacitance were synthesized through chemical polymerization method under 0 °C.
4. Among different surfactants, benzyldimethylhexadecylammonium chloride (BAC) can provide the best dispersion of CNTs and achieve the fabrication of PPy-CNTs electrodes. The use of MWCNT allowed improved capacitance retention of PPy-CNTs at high charge-discharge rates and improved cyclic stability.

5. New synthesis method of PPy-CNTs was developed using indigo carmine as a dopant for polymerization of PPy and a dispersant for MWCNT. The method is simple and suitable for mass production. Such electrodes and devices showed high capacitance, better capacitance retention at high charge-discharge rates and excellent stability at high mass loading.

In the future, recommended work is as follows:

1. Investigate the influence of other functional groups of dopants on the microstructure, electrochemical properties and capacitance behavior of PPy and PPy-CNTs electrodes for ECs.
2. Study the fabrication of composite electrodes using PPy and other advanced carbon materials such as graphene and carbon aerogel to achieve improved capacitance, capacitance retention and cyclic stability.
3. Study the mechanism of capacitive behavior of PPy-CNTs composite electrodes.
4. Study the synthesis of flexible electrochemical capacitor devices using PPy and carbon materials without metal current collectors.